PhD degree in Molecular Medicine

European School of Molecular Medicine (SEMM),

University of Milan and University of Naples "Federico II"

Faculty of Medicine

Settore disciplinare: BIO/10

FUNCTIONAL DISSECTION OF THE HISTONE LYSINE DEMETHYLASE JMJD3

Thomas Burgold

IFOM-IEO Campus, Milan

Matricola n. R06807

Supervisor: Dr. Giuseppe Testa

IFOM-IEO Campus, Milan

Added co-Supervisor: Dr. Bruno Amati

IFOM-IEO Campus, Milan

Anno accademico 2009-2010

Abstract

Epigenetic control of developmental genes has emerged as a key mechanism in the acquisition of developmental competence. In particular, patterns of methylation at lysine 4 and 27 of histone H3 have been associated, respectively, with states of gene activation and repression that are developmentally regulated and are thought to underlie the establishment of lineage specific gene expression programs. Recent studies have provided fundamental insight into the problem of lineage specification by comparing global changes in chromatin and transcription between embryonic stem cells (ESCs) and neural stems cells (NSCs), points of departure and arrival for neural commitment, respectively. With these maps of the differentiated state in place, a central task is now to unravel the chromatin dynamics that enable these differentiation transitions between pluripotent ESCs and multipotent NSCs. In particular, the observation that lineage-specific genes repressed in ESCs by Polycomb-mediated histone H3 lysine 27 trimethylation (H3K27me3) are demethylated and derepressed in differentiated cells posited the existence of a H3K27-specific demethylase. In order to gain insight into the epigenetic mechanisms that enable lineage specification, we investigated in the first part of this work the early stages of neural commitment using as a model system the neural differentiation of mouse ESCs. Using a comprehensive expression analysis of JmjC genes, we identified Jmjd3 as a H3K27me3 demethylase that is specifically upregulated at the onset of neural differentiation. This study revealed that Jmjd3 controls the expression of key regulators and markers of neurogenesis and is required for commitment to the neural lineage. In the second part of this work, we have used a genetic loss-of-function approach to characterise the role of Jmjd3 *in vivo*. Mice lacking Jmjd3 die at birth from respiratory failure. A detailed characterisation of this neurodevelopmental phenotype demonstrated that the defect in respiratory rhythmogenesis upon loss of Jmjd3 is due to an abnormal maturation of the

preBötzinger complex (preBötC), one of the two principal sites generating respiratory rhythm in mammals.

Some of the results presented in this thesis appear in the following publication:

Burgold T, Spreafico F, De Santa F, Totaro MG, Prosperini E, et al. (2008) The histone H3 lysine 27-specific demethylase Jmjd3 is required for neural commitment. PLoS One 3: e3034.

Table of Contents

Introduction

1 The role of epigenetics in the specification and maintenance of cell identity

1.1 Epigenetics

One of the intriguing questions that have fascinated scientists since decades is how in a complex multicellular organism a plethora of functionally distinct cell types can be determined by an invariant DNA sequence. During development, cell fate decisions are orchestrated by the integration of extracellular signals arriving to the cell and intrinsic programs unfolding within the cell. The regulation of this process is not yet fully understood. Recent studies on neocortical neurogenesis have shed some light on the importance of cell-intrinsic programs over cell-extrinsic cues in determining cell fate [1]. Isolated mouse cortical stem cells grown in clonal cultures were able to sequentially generate the main neuronal subtypes of the cortex, recapitulating to a significant extent the timing and sequence observed during cortical neurogenesis *in vivo*. Even the exposure of the developing clones to putative extrinsic cues such as secreted molecules did not have significant effects on the range of cell types that individual clones could generate, indicating that extrinsic cues could not override the intrinsic program. Therefore, it is believed that intrinsic mechanisms may control the responsiveness of cells to fate-regulating extracellular signals. One of the major players in the establishment of intrinsic programs underlying cell fate determination and maintenance is the epigenetic regulation of gene expression. The term “epigenetics” was first introduced by the embryologist and geneticist C. H. Waddington in 1942 to define all the causal processes during development by which a genotype gives rise to a phenotype [2]. Over time the meaning of epigenetics was refined in accordance with new findings and today the most rigorous flavour of

epigenetics includes all those phenomena, including changes in gene expression, that are inherited across generations independent of the underlying DNA sequence.

In mammals, epigenetic control of gene expression is mainly mediated through DNA methylation, posttranslational histone modifications, nucleosomal remodelling and small noncoding RNAs. These mechanisms are thought to establish signatures of gene expression states that can be propagated through cell division, thus contributing to the epigenetic inheritance of cellular states. However, the molecular processes that regulate the transmission of epigenetic marks are not entirely understood yet and to date only DNA methylation can be considered as a *bona fide* epigenetic mark since it has been demonstrated to be stably inherited during cell division from one generation to the next [3]. Recently, several findings have suggested models for the propagation of posttranslational histone modifications in proliferating cells that ensures the preservation of transcriptional programs and cellular identity [4-5]. In fact, these covalent modifications of the nucleosomal core histones H2A, H2B, H3 and H4 have been shown to be implicated in establishing, maintaining and propagating different gene expression patterns throughout developmental processes.

1.2 Histone lysine methylation

Histones, initially regarded as merely architectural components of chromatin, undergo a variety of posttranslational modifications and depending on the type and the site of the covalent mark, these modifications determine distinct biological outcomes by affecting processes such as chromatin organisation, transcriptional regulation, DNA repair and replication [6-9]. In particular, the amino-terminal tails of the histones are subject to a wide range of covalent modifications including acetylation, methylation, phosphorylation and ubiquitination as well as other modifications whose functional role is less well characterised (Figure 1).

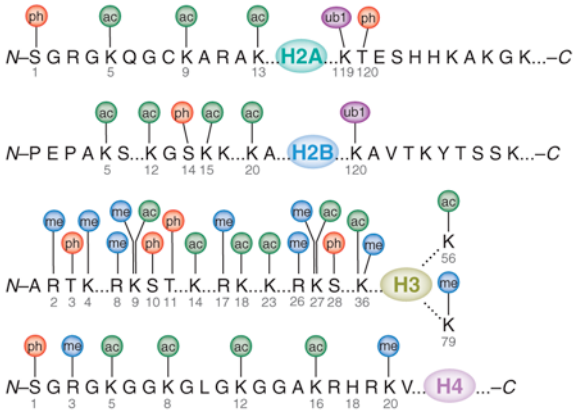

Figure 1. Posttranslational modifications of nucleosomal histones. Histones are subjected to a variety of covalent modifications, such as acetylation (ac), methylation (me), phosphorylation (ph) and ubiquitination (ub1). Most of the known modifications occur on residues in the amino-terminal tail. From [10].

Among the histone modifications, the methylation of histone lysine residues has been of special interest for many years, as studies have revealed that it is a key player in the maintenance of active and silent states of gene expression during development. So far, six lysine residues in histones H3 and H4 have been described to be sites of methylation, lysine (K) residues 4, 9, 27, 36 and 79 in histone H3 and lysine 20 in histone H4. Each of these lysine residues is present in one of four distinct states: un-, mono- (me1), di- (me2) or trimethylated (me3), which confers an additional layer of complexity and potential for the diversification of biological outputs. These methylation states result from the activity of histone lysine methyltransferases and are differentially recognised by effector proteins and chromatin modifiers that mediate a variety of functional outcomes such as transcriptional activation and repression [11-14]. In general, methylation of H3K4, H3K36 and H3K79 is linked to transcriptionally active regions of chromatin, whereas H3K9, H3K27 and H4K20 are found in transcriptionally repressed regions. There is, however, increasing evidence that a single modification does not dictate a single outcome with respect to the transcriptional state. For example, methyl marks such as H3K4me2/3 and H3K9me2/3, although enriched on active and silenced genes, respectively, are also found to be present

in the reciprocal state [15-16]. Therefore, it now seems that these modifications act rather in combination to determine specific transcriptional outputs.

Historically, histone methylation has been considered as a stable and irreversible epigenetic mark. This prevailing view was based on biochemical evidence indicating that the turnover rate of the histone methyl groups was comparable to that of histones themselves [17]. In turn, this stability led to posit a central role for histone lysine methylation in the establishment and maintenance of lineage-specific gene expression. However, a static methyl mark was not compatible with developmental and physiological processes in which rapid changes in gene expression occur in response to differentiation cues and environmental signals.

1.3 Histone lysine demethylation

The first demonstration that histone methylation is dynamic was obtained in human dendritic cells, in which specific tightly regulated and inducible inflammatory genes underwent a rapid loss of H3K9 methylation [18]. Yet, the underlying mechanism of demethylation was unclear and in absence of evidence for an active enzymatic demethylation, the removal of histone methyl marks was explained by several alternative mechanisms, including replacement of methylated histones by unmodified histones or cleavage of methylated histone tails [19-22]. This common view changed only in 2004 with the identification of lysine-specific demethylase 1 (LSD1, also known as Kdm1) as the first histone lysine demethylase [23]. LSD1 is an amine oxidase that catalyses the oxidative demethylation of mono- and dimethylated lysine residues 4 and 9 on histone H3 (H3K4me2/1 and H3K9me2/1) using flavin adenine dinucleotide (FAD) as cofactor [23-24]. Because this reaction mechanism requires a protonated nitrogen as hydrogen donor the trimethylated lysine cannot be demethylated by LSD1. Given the large number of known histone lysine methylation sites and the inability of LSD1 to demethylate trimethylated

lysine, it was hypothesised that other enzymes capable of catalysing histone lysine demethylation might exist [25].

1.4 Jumonji C (JmjC) domain-containing histone demethylases

The identification of the bacterial DNA repair demethylase AlkB showed that DNA could be demethylated in an iron- and α-ketoglutarate-dependent hydroxylation reaction [26-27]. Similarities between the catalytic domain of AlkB and the Jumonji C (JmjC) domain in eukaryotes led to the hypothesis that JmjC domain-containing proteins might be involved in the demethylation of modified lysine residues within histones by using the same oxidative demethylation mechanism, thus representing a second class of histone lysine demethylases. To isolate proteins with potential histone demethylase activity, Tsukada and colleagues designed a biochemical assay based on the reaction mechanism of AlkB-mediated demethylation [28]. In 2006 the same group reported the purification of a novel histone lysine demethylase from human cells, named JmjC domain-containing histone demethylase 1 (JHDM1a, also known as Fbxl11 and Kdm2a). JHDM1a was shown to possess substrate specificity towards H3K36me2/1 and it was further proven that its JmjC domain was critical for the enzymatic activity. This finding defined the JmjC domain as a signature motif for histone demethylases and over the next years several other JmjC domain-containing proteins with histone lysine demethylase activity were identified, each with a distinct specificity for methylated lysine residues in the amino-terminal tail of histone H3. JmjC domain-containing histone demethylases can demethylate all three histone lysine methylation states through an oxidative demethylation reaction that requires iron and α-ketoglutarate as cofactors. The cofactor-bound JmjC domain catalyses the direct hydroxylation of the methyl group, producing succinate and carbon dioxide as reaction products (Figure 2). The unstable hydroxymethyl group is then spontaneously released as formaldehyde.

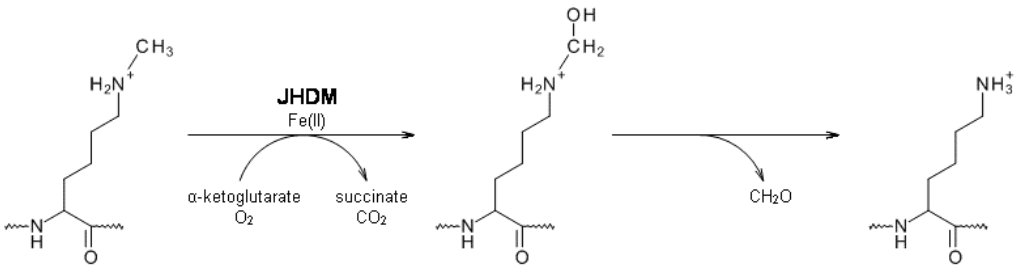

Figure 2. Reaction mechanism of histone lysine demethylation catalysed by JmjC domain-containing proteins. The reaction mechanism shows the removal of a methyl group from a monomethylated lysine residue catalysed by a JmjC domain-containing histone demethylase (JHDM). The JmjC domain requires Fe(II) and α-ketoglutarate as cofactors in an oxidative demethylation reaction that hydroxylates the methyl group. The unstable hydroxymethyl group is then spontaneously released as formaldehyde. JHDMs can demethylate mono-, di- and trimethylated lysine.

The discovery of histone lysine demethylases challenged the notion of the inherent stability of histone lysine methylation and therefore imposed a revision of the functional role of histone lysine methylation. Indeed, the reversibility of histone lysine methyl marks is consistent with the observation that histone lysine methylation at specific loci is responsive to environmental cues and is regulated during differentiation [18,29-30]. In fact, the combination of the tightly regulated process of addition and removal of the methyl mark with the stability it imparts ensures the integration of lineage-specific and environmental cues, suggesting a crucial role for histone lysine demethylation in lineage commitment.

1.5 Polycomb proteins and H3K27 methylation during differentiation

Regulation by Polycomb group (PcG) proteins has been shown to constitute one of the molecular mechanisms that are central to the epigenetic inheritance of cellular memory. First identified in *Drosophila melanogaster* through their function in stabilising transcriptional repression of homeotic (Hox) genes [31-33], PcG proteins belong to the key regulators of proper embryonic development and the maintenance of cell identity [34-36]. The demonstration that enhancer of zeste homolog 2 (Ezh2), a member of the PcG protein

family, has histone lysine methyltransferase activity for H3K27, suggested a central role for this histone methyl mark in the process of gene silencing that accompanies cell differentiation [37-40]. Indeed, H3K27 methylation and binding of PcG proteins are dynamically regulated during differentiation, and two main patterns have emerged from recent genome-wide studies in *Drosophila* [41-43] and mammals [44-47]. In both ESCs and neural progenitors several genes bound by PcG proteins and marked by H3K27me3 are transcriptionally repressed but become activated during differentiation. As many of these genes are key developmental regulators, the current model holds that PcG protein-mediated repression of these genes prevents inappropriate differentiation. Another group of PcG protein target genes however, appears to be actively expressed despite PcG protein binding and presence of the H3K27me3 mark [44-45]. This observation indicates that, as with many other posttranslational histone modifications, also the H3K27me3 mark needs to be 'read' and 'translated' into to the appropriate functional output and posits a more complex and nuanced set of functions for PcG proteins.

1.6 Bivalent chromatin domains

Furthermore, recent studies showed that several loci in both ESCs and adult stem cells, including those encoding key developmental regulators and components of critical signalling pathways, are characterised by the simultaneous presence of the activating H3K4me3 mark and the repressive H3K27me3 mark, a chromatin configuration that has been termed 'bivalent domain' [29-30,48]. In undifferentiated ESCs this unusual combination of opposing chromatin marks is thought to keep genes repressed or expressed at very low level but poised for later activation. Upon ESC differentiation, a large fraction of these bivalent domains appears to be resolved in a lineage-specific manner into transcriptionally active (H3K4me3) or transcriptionally silent (H3K27me3) chromatin regions. Thus, the observation that during differentiation of ESCs into neural stem cells

(NSCs) the resolution of the bivalent to the active state entails the removal of the repressive H3K27me3 mark from promoters of many neural determinant genes, implied the existence of a H3K27me3-specific histone lysine demethylase [48]. This assumption prompted us to investigate whether any of the JmjC domain-containing proteins is capable of catalysing the demethylation of H3K27me3 and to explore the relevance of histone lysine demethylation during the commitment of ESCs to the neural lineage.

2 Manipulating the mouse genome

2.1 Functional genomics in the mouse

The physiological and genetic similarities between mice and men make the laboratory mouse (*Mus musculus*) the premier model organism for studying embryonic development and behaviour, elucidating gene function and modelling human diseases. In the past few years, especially with the completion of the mouse genome sequence [49], the efforts to develop new efficient strategies that enable the analysis of gene function have made enormous progress. Currently, the most common approaches to manipulate and mutagenize the mouse genome are gene trapping, gene targeting, transgenesis and gene silencing by RNA-mediated interference (RNAi).

Gene trap mutagenesis belongs to the genotype-driven genetic techniques and is used to introduce randomly insertional mutations across the genome in mouse embryonic stem cells (ESCs) [50]. In general, gene trap vectors consist of a promoterless lacZ reporter gene and a selectable marker gene, such as neomycin phosphotransferase. The lacZ reporter is immediately flanked by an upstream splice acceptor site and the selectable marker is followed by a polyadenylation signal that truncates the nascent transcript. Upon transcriptional activation of the trapped gene, a fusion transcript is generated from the upstream coding sequence and the reporter gene, simultaneously mutating the trapped gene and reporting its expression pattern. Furthermore the inserted trap sequence acts as a tag from which the disrupted gene can be cloned and identified.

An alternative to random mutagenesis for pursuing functional genomics in the mouse is targeted mutagenesis by homologous recombination in ESCs, allowing the efficient alteration of genes in a specific and precise manner [51-52]. In the standard targeted mutation, homologous recombination is used to delete essential parts of the gene to generate a null allele. These knockouts establish a complete loss of function and provide therefore valuable information about the earliest essential role of the gene during

development. However, many genes have multiple roles at different stages of development in different tissues and therefore a null allele may cause early embryonic lethality, precluding the study of gene function at later stages of development or in the adult. To bypass these limitations, strategies for conditional mutagenesis based on site-specific recombination have been developed, which allow gene expression to be abrogated in a temporally and spatially controlled manner. The combined use of site-specific recombinase systems, such as the Cre/loxP system and the FLP/FRT system with traditional homologous recombination strategies has become the standard method to generate conditional knockout or knockin alleles [53-55]. The 'knockout-first' strategy represents an elegant and efficient way to create a multipurpose allele [56-57]. This strategy allows, in a single ESC targeting step, to generate both a constitutive and a conditional knockout. This allele is a null allele and a reporter for gene expression in its original configuration. By the combined use of FLP and Cre recombinases the constitutive knockout allele is converted into a conditional allele.

A third possibility to analyse the function of a specific gene is provided by means of RNA-mediated interference (RNAi) [58]. RNAi, first discovered in the nematode worm *Caenorhabditis elegans* [59], is an evolutionary conserved mechanism, whereby double-stranded RNA (dsRNA) acts as sequence-specific inducer of mRNA degradation [60-63]. RNA silencing mechanisms were initially recognized as cellular defense processes that protect organisms from RNA viruses or which prevent the propagation of transposable elements [64-67]. But further studies have revealed the importance of endogenous small noncoding RNAs, among which microRNAs (miRNAs) are the best characterised, that are processed in a pathway that converges on the same components of the RNAi machinery and that play a key role in the posttranscriptional regulation of gene expression. Nowadays, different strategies are used in order to exploit RNAi in mammalian cells. Transfection of short interfering RNAs (siRNAs) results only in a transient knockdown of gene expression

[68], whereas stable silencing is achieved by transcription of short hairpin RNAs (shRNAs) or, more recently, microRNA-adapted short hairpin RNAs (shRNAmir) from stably integrated vectors [69-73]. Despite the power of the RNAi technology, a pitfall is that it almost never fully depletes the target mRNA, which makes the selection and design of highly effective shRNAs for a target gene the crucial steps in RNAi-based functional genomics. Moreover, RNAi-based approaches can result in off-target effects, due to the possibility that the shRNA may cross-react with transcripts of partial sequence similarity, causing the unintentional silencing of nontargeted genes [74]. Therefore some changes in gene expression patterns are specific for the shRNA sequence used for silencing rather than for the suppression of the intended target.

2.2 Recombinogenic DNA engineering in *E. coli*

Engineering versatile targeting constructs for mouse functional genomics, including multipurpose alleles described above, requires the assembly of several functional elements into very large DNA molecules. For this task conventional cloning methods, that rely on the presence of suitable restriction sites, PCR amplification and DNA purification steps, present major limitations. Novel DNA engineering strategies based on homologous recombination *in vivo* in *E. coli* have overcome these constraints and allow complete freedom in DNA design without the size and site limitations imposed by conventional cloning techniques. Homologous recombination occurs through DNA stretches of sequence homology, which are common between the two molecules that recombine. Because, the sequence of the homology regions can be chosen freely, any position on the target molecule can be specifically altered and practically any DNA modification is possible.

Red/ET recombination, a strategy to accomplish recombinogenic engineering, is mediated by phage-derived protein pairs, either RecE/RecT from the Rac prophage or Redα/Redβ from λ phage [75]. The RecE/RecT and Redα/Redβ protein pairs are operationally and

functionally equivalent. RecE and Redα are 5'-3' exonucleases, which digest the 5' ends of double-stranded DNA to leave 3' single-stranded overhangs. RecT and Redβ are DNA annealing proteins that bind to these overhangs and anneal them to complementary single-strand DNA in the cell. The recombination is further assisted by the λ phage-encoded protein Redγ, which inhibits the endogenous *E. coli* exonuclease RecBCD in order to protect introduced linear DNA molecules from digestion by RecBCD. The functional unit comprising all three λ phage proteins can be applied to and induced in any *E. coli* host by transient transformation of an expression plasmid [76]. Using Red/ET recombination, a linear DNA fragment carrying short homology regions flanking a selectable marker gene can be integrated into a circular target DNA (Figure 3a). The length of the homologous regions required for efficient recombination is only 40-60 nucleotides, and thus short enough to be generated by oligonucleotide synthesis. In a very convenient application, the selectable marker is PCR-amplified using oligonucleotides that contain besides the primer sequence the homology regions. In another application, the linear targeting molecule is a PCR-amplified plasmid backbone containing a selectable marker and an origin of replication (Figure 3b). The oligonucleotides used for the PCR reaction contain homology regions that are chosen to define the exact boundaries of the DNA region to be cloned or subcloned. The advantage of this strategy is that the subcloned DNA is not PCR-amplified, thus excluding the risk of PCR-generated mutations and allowing the manipulation of DNA fragments of up to 40 kb. This approach is particularly useful for the assembly of gene targeting constructs as it enables the subcloning of large fragments of genomic DNA, such as those carried on bacterial artificial chromosomes (BACs) [77].

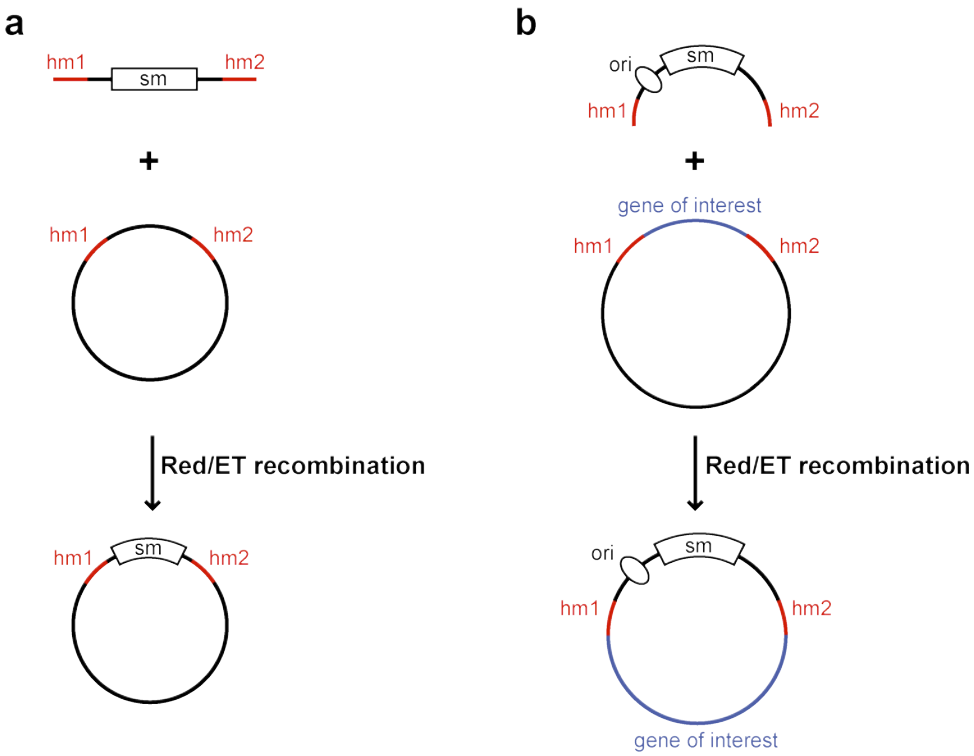

Figure 3. Applications of Red/ET recombination. (a) A linear DNA fragment is generated by PCR reaction, which contains two regions homologous to the regions in the targeting vector (hm1, hm2) and a selectable marker gene (sm). The PCR product and the targeting vector are electroporated into Red/ET competent *E. coli* to allow homologous recombination. The recombined vector contains the selectable marker. **(b)** A genomic DNA sequence is subcloned from a donor molecule (e.g. BAC) into a linear vector backbone using Red/ET recombination. The linear minimal vector is generated by PCR amplification and contains flanking homology arms (hm1, hm2), an origin of replication (ori) and a selectable marker (sm). Importantly, the subcloned DNA fragment is not amplified by PCR, excluding the risk of extraneous changes in the DNA sequence.

3 Aim of the thesis

The work presented in this thesis was initiated in 2006, at a time when several independent lines of evidence were suggesting a new view of chromatin regulation by challenging the dogma of the irreversibility of histone lysine methylation. Two years after the discovery of the first histone lysine demethylase LSD1, the JmjC domain was identified as a signature motif for a new family of histone demethylases. Furthermore, studies at the genome-wide level revealed that in undifferentiated ESCs many developmental regulators are repressed by PcG complexes but poised to be activated by a bivalent chromatin signature, containing both activating H3K4me3 and repressive H3K27me3 modifications. In line with this observation, the comparison of global changes in chromatin between ESCs and NSCs showed that upon differentiation, many of these bivalent domains are resolved differentially leading to transcriptional activation of neural-specific genes and silencing of loci associated with alternative cell lineages. These findings prompted us to explore the relevance of histone lysine demethylation during the early stages of lineage specification using as a model system the monolayer differentiation of ESCs to NSCs. This protocol is a versatile tool that by recapitulating neural specification during development, allowed us to dissect the chromatin dynamics underlying early cell fate transitions. Following our identification of Jmjd3 as a H3K27me3-specific demethylase, we demonstrated its requirement in the commitment of ESCs to the neural lineage. In order to investigate the biological function of Jmjd3 in the context of an animal model and to gain insight into the role of histone lysine methylation during the development of multicellular organisms we used a loss-of-function approach in the mouse.

Materials and Methods

1 Cell culture methods

1.1 Preparation of mouse embryonic fibroblasts (MEFs) for feeder layer

Pregnant mice were sacrificed between embryonic days (E) 11.5 and 13.5 following standard procedures. The intact uterus was carefully extracted and transferred to a 10 cm dish containing sterile phosphate buffered saline (PBS). The uterus was sectioned to release the embryos and each one was placed in a 6 cm dish with PBS. The fetal membranes, umbilical cord, head and organs were removed and the remaining tissues were collectively transferred to a 10 cm dish containing 5 ml trypsin-EDTA (Lonza) and were further dissociated with forceps and scissors and incubated at 37 °C for 5 to 10 min. The cells and tissue pieces were triturated by pipetting up and down and collected in MEF medium which consists of Dulbecco's Modified Eagle's Medium (DMEM with high glucose, with sodium pyruvate and without L-glutamine; Lonza), 10% North American foetal bovine serum (FBS; Gibco), 2 mM L-glutamine (Gibco), 0.1 mM non-essential amino acids (NEAA; Gibco), 50 U/ml penicillin and 50 μg/ml streptomycin (Lonza) and 0.1 mM 2-mercaptoethanol (Gibco). The digested tissue was centrifuged at 280 × *g* for 5 min. The cells were resuspended in MEF medium, plated into several 10 cm culture dishes and incubated in a humidified incubator at 37 °C with 5% CO_2. Cells were passaged every two days at a 1 to 4 ratio. When cells reached confluency, some 10 cm dishes were frozen in 90% FBS with 10% dimethylsulfoxide (DMSO) to prepare stocks of MEFs. For the preparation of feeder layers, MEFs at a maximum of passage three after isolation were used. Confluent MEFs were mitotically inactivated in MEF medium containing 10 μg/ml mitomycin C (Sigma) for 4 h in a humidified incubator at 37 °C with 5% CO_2. Cells were then washed with PBS, trypsinized and seeded at a density of 6×10^4 cells/cm^2 onto

culture dishes. MEF medium was replaced with embryonic stem cell (ESC) medium at least 2 h before using them for ESC culture.

1.2 Culturing mouse embryonic stem cells (ESCs)

1.2.1 Passaging mouse ESCs

The mouse ESCs lines E14Tg2α, 46C [78] and XB814 were routinely propagated in feeder-free conditions. C57BL/6 ESCs, used for the targeting of Jmjd3, were cultured on mitotically inactivated mouse embryonic fibroblast cells. ESCs were incubated at 37 °C, 5% CO_2 in a humidified atmosphere and medium was changed daily. Standard ESC medium consists of Dulbecco's Modified Eagle's Medium (DMEM, with high glucose, with sodium pyruvate, without L-glutamine; Lonza) supplemented with 1000 U/ml leukaemia inhibitory factor (LIF; Chemicon or as 500× prepared by the transgenic facility), 15% foetal bovine serum (FBS, tested for ESC culture; Gibco or PAN), 2 mM L-glutamine (Gibco), 0.1 mM non-essential amino acids (NEAA; Gibco), 25 mM HEPES and 0.1 mM 2-mercaptoethanol (Gibco). Cells were passaged every two days at 70-80% confluency. The cells were rinsed with phosphate buffered saline (PBS, without Ca^{2+} and Mg^{2+}) and were detached in trypsin-EDTA (Lonza) at 37 °C for 5 min. The detached cells were dispersed into single cells by gentle pipetting. Trypsin was inactivated by adding ESC medium and the cells were collected by centrifugation at 280 × *g* for 5 min. The cell pellet was resuspended in fresh ESC medium and cells were plated at the density needed. For the maintenance of ESCs in culture cells were usually splitted at a ratio of 1:10, corresponding to 1-2 × 10^6 cells seeded on a 10 cm dish.

Alternatively to the standard ESC culture conditions, ESCs can also be efficiently maintained in culture under defined culture conditions containing small molecule inhibitors that block extrinsic differentiation inducing signals, the mitogen-activated protein kinase (MAPK/ERK1/2) and glycogen synthase kinase 3 (GSK3), in the presence of LIF [79].

This medium is called 2i/LIF culture medium and comprises N2B27 medium [DMEM/F-12 (with GlutaMax™; Gibco) and Neurobasal™ medium (Gibco) in a 1:1 mixture, with N2 (Gibco), B27 (Gibco), 2 mM L-glutamine (Gibco), 15 mM HEPES and 0.1 mM 2-mercaptoethanol (Gibco)] supplemented with 1 μM of MEK inhibitor PD0325901 (ABCR), 3 μM of GSK3 inhibitor CT99021 (ABCR) and LIF. Under these culture conditions cells were passaged every three days by detaching them with Accutase® (Sigma) and replating on gelatinized plates at a density of 2×10^4 cells/cm^2.

1.2.2 Freezing and thawing of mouse ESCs

For the cryopreservation of ESCs the confluent cells were harvested and collected as written above. Cells grown in standard ESC medium were resuspended in freezing medium consisting of 25% FBS, 10% dimethylsulfoxide (DMSO) in ESC medium. ESCs cultured in 2i/LIF medium were resuspended in 2i/LIF medium with 20% Knockout™ Serum Replacement (KSR; Gibco) and 10% DMSO. Cells were distributed into cryovials at a density of 5×10^6 cells/ml freezing medium and frozen at -80 °C. The next day tubes were transferred to liquid nitrogen for long-term storage.

The frozen cells were quickly thawed in a 37 °C water bath, transferred to a tube containing prewarmed medium and centrifuged at 280 × *g* for 5 min. The cells were resuspended in the respective ESC medium and plated. The next day medium was replaced with fresh culture medium.

1.3 Derivation of ESCs

To derive ESCs homozygous for the Jmjd3 trap allele, timed matings between heterozygous XB814 mice were set up. Plugged females were sacrificed at 3.5 days postcoitus (dpc) and uteri were flushed to collect the embryos at the morula stage. They were cultured *in vitro* in drop cultures of KSOM medium (95 mM NaCl, 2.5 mM KCl, 0.35

mM KH_2PO_4, 0.20 mM $MgSO_4 \cdot 7H_20$, 0.20 mM glucose, 10 mM sodium lactate, 25 mM $NaHCO_3$ phenol red, 0.2 mM sodium pyruvate, 1.71 mM $CaCl_2 \cdot 2H_20$, 0.01 mM EDTA, 1 mM L-glutamine and 1 mg/ml BSA) covered in embryo-tested mineral oil (Sigma) for 24 h in a humidified atmosphere of 5% CO_2 at 37 °C. The blastocysts were transferred individually to a 48-well plate containing mitotically inactivated MEFs. The medium for ESC derivation consists of standard ESC medium supplemented with 50 μM mitogen-activated protein kinase/extracellular signal-regulated kinase (MEK1) inhibitor PD98059 (Cell Signaling) to facilitate the derivation process by suppressing differentiation cues and enhancing the effect of LIF on self-renewal [80-81]. After five to six days, blastocyst outgrowths were disaggregated into small clumps in trypsin-EDTA complemented with 1% chicken serum (Gibco). Cells were replated onto a 24-well plate with inactivated MEFs and allowed to grow for three to five days. After this period, the cells were no longer cultured in the presence of the MEK inhibitor. For the expansion of the ESC population the growing cultures were passaged onto progressively larger areas with feeder. Medium was replaced daily and cultures were monitored for the appearance of distinct ESC colonies. Usually by the 12-well format, emerging ESC-colonies could be seen. When cells reached 80 to 90% confluency, they were trypsinized and transferred into 6-well plates with feeder for three to four days. Each well was then trypsinized and 75% of the cell population was frozen in freezing medium to prepare stocks of the newly established ESC line. The derived ESCs were grown on MEFs for two more passages and then adapted to feeder-free conditions.

1.4 Derivation of neural stem cells (NSCs) from mouse ESCs

Mouse ESCs were differentiated to NSCs in adherent monolayer culture as described [82-83]. In brief, ESCs were trypsinized and plated onto 0.1% gelatine-coated cell culture dishes at a density of 0.7-1 × 10^4 cells/cm^2 in N2B27 medium. Medium was renewed every

day. At day eight of differentiation cultures were dissociated using Accutase® and replated into an uncoated T25-flask in NSC expansion medium, which is composed of Euromed-N medium (Euroclone) supplemented with N2, 2 mM L-glutamine and 20 ng/ml of both murine epidermal growth factor (EGF; Peprotech) and murine fibroblast growth factor 2 (FGF-2; Peprotech). Typically, cells from one 10 cm dish were replated into two T25-flasks. Within 2-3 days cells formed floating aggregates, which were harvested by mild centrifugation and replated onto a new T25-flask. After 3-4 days cell aggregates attached, followed by the outgrowth of bipolar NSCs. Within several passages differentiated cells were eliminated and the culture was enriched for NSCs, which were then routinely splitted every 2-3 days at a ratio of 1:4. For cryopreservation cells were frozen in NSC expansion medium plus 10% DMSO.

1.5 Electroporation of ESCs

The targeting of Jmjd3 was done in C57BL/6 ESCs, growing on feeders. ESCs were trypsinized as described above and 10×10^6 cells were resuspended in 800 µl of ESC medium containing 25 mM NaCl. 30 µg of linearized and purified targeting construct were added and after incubating for 5 min the cell suspension was transferred to an electroporation cuvette (0.4 cm gap; Bio-Rad). Cells were electroporated using a Bio-Rad Gene Pulser electroporation system set to the following parameters: exponential waveform, 250 V, 500 µF, ∞ Ω. After incubating for 5 min, the electroporated cells were transferred into ESC medium and plated onto three 10 cm dishes. 36–48 h after the electroporation the selection with G418 (Geneticin®; Gibco) at a concentration of 150 µg/ml was started. The cells were grown in selection medium for 8-10 days with occasional medium change. Drug-resistant ESC colonies were picked onto a 96-well plate and when grown to 60-80% confluency, clones were splitted at a ratio of 1:3 into three 96-well plates. For each clone

two replica plates were frozen for storage and one plate was expanded onto a gelatinized 48-well plate for DNA extraction and screening by Southern blot analysis.

Blastocyst injections of targeted ESCs were performed by the transgenic facility (IFOM-IEO Campus, Milano).

1.6 Viral infection of ESCs

Viruses for viral-mediated RNA interference (RNAi) were generated essentially as described [72,84]. In brief, the packaging cell lines for virus production, 293T cells for lentiviruses and the retrovirus producer line Phoenix-Eco, respectively, were plated one day before transfection on a 10 cm dish. 20 μg of lentiviral vector pSicoR PGK Puro encoding short hairpin RNAs (shRNAs) [85] and 10 μg of each packaging vector, namely pMDLg/pRRE, RSV-Rev and VSVG [86] were cotransfected in 293T cells by calcium-phosphate precipitation. Phoenix-Eco cells were transfected with 16 μg of retroviral vector LMP expressing microRNA-based shRNA (shRNAmir) [73] and 4 μg of pCL-Eco following the same procedure. Supernatants were collected 36-48 h after transfection, filtered through a 0.45 μm filter and used directly to infect ESCs. ESCs were trypsinized as described. 3-5 × 10^4 ESCs were resuspended in 10 ml viral supernatant, supplemented with 24 mM HEPES, 12 μg/ml Polybrene® (Sigma-Aldrich) and LIF, and were immediately plated onto a 10 cm dish. 6 h after plating infection medium was aspirated and replaced with fresh ESC medium. The following day selection with puromycin (Sigma-Aldrich) at 1 μg/ml was started. After 8-10 days of selection drug-resistant ESC colonies were picked onto a 96-well plate. Clones were gradually expanded by replating into bigger wells in order to freeze for storage and to extract RNA for assessing the knockdown efficiency by real-time RT-PCR.

1.7 Treatment of targeted ESCs with recombinant Cre-recombinase

To induce Cre-mediated recombination in targeted ESCs, the cells were treated with the cell-permeable TAT-Cre fusion protein [87]. ESCs were trypsinized as described above and 2×10^5 cells were plated on a 6-well tissue culture plate in ESC medium. After 6 h cells attached and were washed five times with a 1:1 mixture of PBS and DMEM. For transduction ESCs were incubated with 5 µM of TAT-Cre protein diluted in a 1:1 mixture of PBS and DMEM for 16-18 h. Cells were washed with PBS and cultured in standard ESC medium for further 1-2 days. To confirm that Cre recombination had occurred, genomic DNA was extracted from cells and subjected to PCR reaction.

1.8 Karyotyping

ESCs plated on 0.1% gelatine at 70% of confluency were cultured in the presence of 0.1 µg/ml KaryoMAX® colcemid (Gibco) for 1 h, to block the metaphases. Cells were then trypsinized, collected and centrifuged at 520 × *g* for 10 min. After discarding the supernatant, hypotonic solution (0.075 M KCl in water) was added drop by drop to the pellet while gently flicking the tube and the resulting suspension was incubated at 37 °C for 30 min. For pre-fixation, four to five drops of fixative consisting of three parts methanol and one part acetic acid, were added to the solution, followed by centrifugation at 520 × *g* for 10 min. Afterwards 10 ml of fixative were added dropwise, while gently vortexing to resuspend cells. Following centrifugation at 520 × *g* for 10 min, the pellet was resuspended in 1 ml fixative and 60 µl of the solution were dropped onto each slide pre-warmed at 57 °C from about 30 cm in height. The drop was allowed to spread over the surface and left to dry. Metaphases and nuclei were stained in 1 µg/ml DAPI in saline sodium citrate (SSC) for 5 min and dried upright overnight in the dark. The next day, the slides were mounted in mowiol. For each slide, ten metaphases were randomly picked and

those that were well spread and intact were counted and scored for the number of chromosomes.

2 DNA methods

2.1 DNA extraction

2.1.1 Isolation of genomic DNA from ESCs

Confluent ESCs were lysed in lysis buffer, consisting of 100 mM Tris-HCl pH 8.5, 5 mM EDTA, 0.2% sodium dodecyl sulphate (SDS), 200 mM NaCl and 100 µg/ml proteinase K. Cell lysate was transferred to a 1.5 ml tube and incubated at 55 °C overnight. DNA was precipitated by adding two volumes of cold NaCl/ethanol mix (15 µl of 5 M NaCl per 1 ml of cold 100% ethanol) and incubating at -20 °C for ≥30 min. After centrifugation at 16000 × *g* for 20 min the DNA pellet was washed with 70% ethanol and centrifuged again. Finally, the dried DNA pellet was resuspended in an appropriate volume of water or TE buffer (10 mM Tris-HCl pH 8.0, 1 mM EDTA), repectively.

2.1.2 Isolation of genomic DNA from mouse tails

Tail biopsies were routinely collected by the animal facility. Tail tips were incubated in 500 µl of lysis buffer (100 mM Tris-HCl pH 8.5, 5 mM EDTA, 0.2% SDS, 200 mM NaCl and 100 µg/ml proteinase K) at 55 °C overnight. Proteinase K was heat-inactivated at 94 °C for 5 min and lysate was centrifuged at 16000 × *g* in order to remove non-digested tissue. 5 µl of DNA lysate were diluted in 45 µl of water and 1 µl of DNA dilution was directly used for genotyping by polymerase chain reaction (PCR).

2.2 DNA purification using phenol-chloroform extraction

To remove protein contaminants, DNA samples were purified by means of phenol-chloroform extraction. An equal volume of phenol was added and the phases were mixed by vortexing. Following a centrifugation step at 16000 × *g* for 1 min to separate the phases, the aqueous top layer containing the DNA was transferred to a new tube. The extraction

step was repeated by adding an equal volume of phenol:chloroform (1:1) to the aqueous layer. To remove traces of phenol a final extraction step was performed with one volume of chloroform. The DNA-containing aqueous phase was transferred to a new tube and DNA was precipitated by ethanol precipitation.

2.3 DNA precipitation

DNA was recovered from aqueous solutions using standard ethanol precipitation. In brief, the salt concentration of the solution was adjusted with sodium acetate pH 5.2 at a final concentration of 0.3 M. Then three volumes of cold 100% ethanol were added and DNA was precipitated by incubating at -20 °C for ≥30 min. After centrifugation at 16000 × *g* for 20 min the DNA pellet was washed with 70% ethanol and centrifuged again. Finally, the dried DNA pellet was resuspended in an appropriate volume of water or TE buffer (10 mM Tris-HCl pH 8.0, 1 mM EDTA), repectively.

2.4 Polymerase chain reaction (PCR)

PCR reactions were usually carried out in a total volume of 20 µl with 0.2 mM dNTPs, 0.5 mM primers, DNA template (in various amounts depending on the source), 0.01 U/µl Phusion® DNA polymerase (Finnzymes) and the appropriate buffer provided by the supplier. The reaction conditions varied among different experiments, but generally conformed to the following cycling parameters: 30 s initial denaturation at 98 °C, 35 cycles consisting of 10 s denaturation at 98 °C, 15 s of annealing at the for each primer combination optimized temperature and variable times of extension depending on amplicon length and complexity at 72 °C. The last cycle was followed by a final extension step for 10 min at 72 °C.

PCR reaction was run on an agarose gel in presence of 1× Tris-acetate-EDTA buffer (TAE) and 0.5 µg/ml ethidium bromide. For downstream applications the PCR product

was purified using the QIAquick PCR purification kit or QIAquick Gel Extraction kit (both purchased from Qiagen).

2.5 Plasmid preparation

After 37 °C overnight incubation plasmids were isolated and purified with the Qiagen Plasmid Mini or Maxi kits (Qiagen), respectively. The alkaline lysis based purification procedure was performed according to the manufacturer's protocol.

2.6 Restriction enzyme digestions

DNA digests were carried out with commercially available restriction enzymes following the instructions of the supplier. In general 5-10 units of enzyme were used per 1 µg DNA and the incubation was at least 3 h.

2.7 Ligation

Ligations were set up by mixing vector and insert DNA, at a insert:vector molar ratio of three, in a volume of 15 µl with 1 unit of T4 DNA ligase and the buffer provided by the supplier. The reaction was incubated at 16 °C overnight.

TOPO® Cloning reactions (Invitrogen) of *Taq* polymerase-amplified PCR products were set up according to the manufacturer's protocol.

2.8 Bacterial transformation

2.8.1 Plasmid transformation by heat shock

Chemically competent bacteria were thawed on ice. DNA was added and tubes were left for another 30 min on ice. Tubes were put in 42 °C water bath for 45 s to heat-shock cells. In order to reduce damage of the cells, tubes were put back on ice for 2 min. Then 900 µl

LB-medium without antibiotics were added and bacteria were incubated with shaking for 1 h at 37 °C. About 100 µl of culture were plated on LB plates containing the appropriate antibiotic and incubated at 37 °C overnight (Table 1).

2.8.2 Plasmid transformation by electroporation

To make cells competent for electroporation the following procedure was used. 1.4 ml LB medium were inoculated with 30 µl of fresh overnight culture and incubated with shaking for 2 h at 37 °C. The culture was centrifuged at 11500 × *g* for 30 s at 4 °C and after discarding the supernatant the tube was placed on ice. The cells were resuspended in 1 ml chilled water and centrifuged again. This step was repeated once and the supernatant was discarded, leaving 20-30 µl which were used to resuspend the pellet. For transformation the competent cells were mixed immediately with 1-2 µl DNA and transferred to a precooled 1 mm electroporation cuvette. The cells were electroporated using an Eppendorf Electroporator 2510 at 1350 V. The electroporated cells were resuspended in 1 ml LB medium without antibiotics and transferred to a fresh tube. After incubation with shaking for 1 h at 37 °C, about 100 µl of culture were plated on LB plates containing the appropriate antibiotic and incubated at 37 °C overnight (Table 1).

Table 1. Antibiotic concentrations for *E. coli* selection.

Antibiotic	Working concentration [µg/ml]
Ampicillin	100
Chloramphenicol	15
Kanamycin	30
Tetracycline	3

2.9 Preparation of bacteria for Red/ET cloning

The DNA engineering method Red/ET recombination was used to assemble the targeting vector for the conditional inactivation of Jmjd3 [56-57,76,88]. In a first step, *E. coli* cells were transformed with the Red/ET expression plasmid pSC101-BAD-gbaA-tet by electroporation according to the procedure described above (Figure 4). Since the Red/ET

expression plasmid contains the temperature-sensitive replication origin oriR101, which allows plasmid propagation only at 30 °C, the electroporated cells were incubated in LB medium without antibiotics at 30 °C. After 70 min incubation, 100 µl of culture were plated on LB plates containing 3 µg/ml tetracycline and incubated at 30 °C overnight. Single colonies were picked and grown in LB medium plus tetracycline overnight at 30 °C. The next day, 1.4 ml LB medium containing tetracycline were inoculated with 30 µl of fresh overnight culture and incubated with shaking at 30 °C. When the cells reached an OD_{600} of 0.2 after about 2 h incubation, 10% L-arabinose was added at a final concentration of 0.1-0.2% to induce expression of Red/ET recombination proteins. Following the induction with arabinose, the cells were incubated at 37 °C for a further 1 h until they reached an OD_{600} of 0.3-0.4. The ET-competent cells were harvested, prepared for electroporation and directly used for ET-cloning.

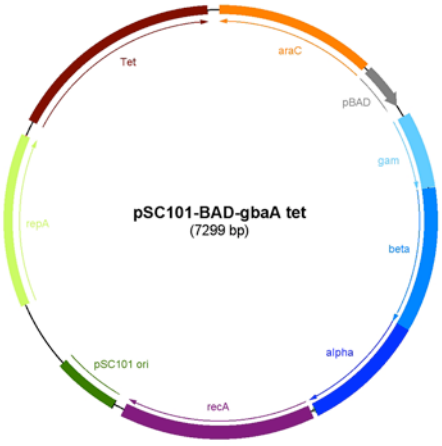

Figure 4. Map of the Red/ET expression plasmid pSC101-BAD-gbaA-tet. The plasmid carries the redα, β, γ genes from the λ phage together with the recA gene in a polycistronic operon under the control of the arabinose-inducible pBAD promoter and confers tetracycline resistance. The origin oriR101 requires expression of the temperature-sensitive RepA protein for plasmid replication.

2.10 Generation of shRNA expression vectors for viral-mediated RNAi

2.10.1 Cloning of shRNA into pSicoR PGK Puro

shRNAs designated for the stable expression in the lentivirus-based vector pSicoR PGK Puro (provided by A. Ventura) were designed using the pSicoOligomaker v1.5 software

(developed by A. Ventura), which is freely available at http://web.mit.edu/jacks-lab/protocols/pSico.html [85]. The synthesised oligonucleotides were 5'-phosphorylated and HPLC-purified. For each shRNA the sense and antisense oligonucleotides were annealed and ligated into HpaI-XhoI digested pSicoR PGK Puro. The insertion of the shRNA was confirmed by PstI/XhoI double restriction digest and positive clones were sequence-verified (Figure 5a).

2.10.2 Cloning of shRNAmir into MSCV/LTRmiR30-PIG (LMP)

shRNAs embedded in the miR-30 context (shRNAmir) were expressed from the microRNA (miRNA)-adapted retroviral vector LMP (Open Biosystems) [73]. Sequences of shRNAs were selected using the shRNA retriever function on the online resource RNAi Central at http://katahdin.cshl.edu/siRNA/RNAi.cgi?type=shRNA. The synthetic single-stranded oligonucleotides were composed of the sense and antisense target sequence, miR-30 miRNA flanking sequences and the miR-30 loop sequence. The miR-30-styled shRNAs were PCR-amplified, digested with EcoRI and XhoI and cloned into the EcoRI and XhoI sites of LMP. All clones that were positive by SacII/XhoI restriction digest analysis were sequence-verified (Figure 5b).

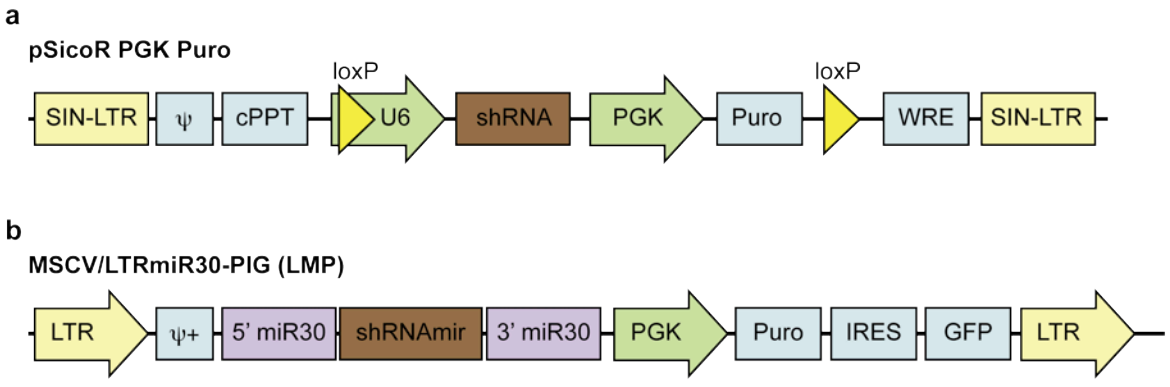

Figure 5. shRNA expression constructs for viral-mediated RNAi. Schematic representations of the shRNA expressing lentiviral vector pSicoR PGK Puro **(a)** and the retroviral-based shRNAmir delivery system LMP **(b)**. Active promoters are shown as arrows. SIN-LTR: self-inactivating long terminal repeats, ψ: packaging signal, cPPT: central polypurine tract, U6: U6 promoter (RNA polymerase III promoter), PGK: phosphoglycerate kinase promoter, Puro: puromycin resistance as mammalian selection marker, WRE: woodchuck hepatitis virus posttranscriptional regulatory element, LTR: LTR promoter (RNA polymerase II

promoter), miR30: 5' and 3'-flanking sequences derived from the endogenous miR-30 primary transcript, IRES: internal ribosomal entry site, GFP: green fluorescent protein.

2.11 Southern blotting

10-20 µg of genomic DNA were digested with the relevant enzyme at 37 °C overnight. The entire digest was run on an 1× TAE agarose gel containing 0.5 µg/ml ethidium bromide. Following electrophoresis DNA gel was incubated with gentle shaking in 0.25 N HCl for 10 min resulting in depurination and thus facilitating the transfer of high molecular weight DNA fragments. The gel was then transferred to denaturing solution (1.5 M NaCl, 0.5 N NaOH) for 30 min to denature the DNA. After rinsing with water, gel was equilibrated in transfer buffer (1.5 M NaCl, 0.25 N NaOH) for 30 min. Blot apparatus for upward capillary transfer was assembled and DNA was transferred onto a Hybond-N+ nylon membrane (GE Healthcare) in alkaline transfer buffer overnight. The Membrane was washed in 6× saline sodium citrate (SSC) for 30 min and baked in an oven at 80 °C for 2 h to crosslink the DNA to the membrane.

Hybridisation was performed in a glass tube in a hybridisation oven equipped with a rotating wheel. Filter was first prehybridised in modified Church and Gilbert buffer (0.5 M sodium phosphate buffer pH 7.2, 7% SDS, 1 mM EDTA) for at least 30 min at 65 °C and then hybridised in the same buffer upon addition of the relevant DNA probe at 65 °C overnight. DNA probes were prepared by random primed labelling with the Ladderman™ Labeling kit (Takara), according to the manufacturer's instructions. After incorporation of [α-^{32}P]-labelled dCTP, unincorporated labelled nucleotides were removed by gel filtration using illustra™ ProbeQuant™ G-50 Micro Columns (GE Healthcare).

After hybridisation the filter was rinsed with washing buffer (40 mM sodium phosphate buffer ph 7.2, 0.1% SDS) at room temperature (RT), followed by one wash of 45 min at 65 °C. Autoradiography was performed by exposing the filter to a storage phosphor screen and subsequent signal detection using a Typhoon™ scanner system (GE Healthcare).

2.12 DNA sequencing

Sequence analysis was carried out by the DNA sequencing facility using the Big Dye™ Terminator Cycle sequencing method (Applied Biosystems) with the relevant primers.

3 RNA methods

3.1 RNA extraction

Total RNA was isolated from confluent cells with TRIZOL® Reagent (Invitrogen) according to the instructions of the manufacturer. Finally, RNA was resuspended in RNAse-free water and quantified with the NanoDrop ND-1000 Spectrophotometer (Thermo Fisher Scientific).

3.2 cDNA synthesis

cDNA synthesis was carried out with the SuperScript™ III First-Strand Synthesis System (Invitrogen) following the instructions of the supplier. In general, 1 µg of total RNA was reverse transcribed using SuperScript III Reverse Transcriptase (Invitrogen) with 250 ng/µl random primers (Invitrogen) and 10 mM dNTPs (Invitrogen) in 20 µL of reaction volume, in the presence of 2 U/µl of RNase inhibitor RNase OUT™ (Invitrogen). Samples were incubated at 25 °C for 5 min, 50 °C for 1 h and 70 °C for 15 min.

3.3 quantitative real-time PCR (qRT-PCR)

qRT-PCR was performed on 7900HT Fast Real-Time PCR system (Applied Biosystems) using Fast SYBR® Green PCR Master Mix or TaqMan® Gene expression assays (Applied Biosystems, Table 2). Correct PCR products were confirmed by melting curve analysis. Each sample was analysed in triplicates and normalised to TATA-Binding Protein (TBP) representing the endogenous control. Normalisation was used to correct sample-to-sample variations in RNA concentration and integrity. Relative mRNA amounts were calculated by the comparative cycle threshold (Ct) method using the formula $2^{-\Delta Ct}$.

Table 2. Primers and assays used for expression analysis with qRT-PCR.

Gene	Primer sequence (5'-3')	Application
Fbxl10	*F:* GAGGTGTGGATGGCAGTCTT *R:* CCAACTGAGGTCAAGGGAGA	SYBR® Green assay
Fbxl11	*F:* CAGGTTGGATTCATGCTGTG *R:* GGATCGGTTGGTTATGCAGT	SYBR® Green assay
Hr	*F:* TGTCAGGCATCCAGAAGACA *R:* GTTCGGTGTAGCAGGAGGAC	SYBR® Green assay
Hspbap1	*F:* GGTGGCATTACGTGGAGTCT *R:* CAGCTGTTGACCTCGTGAGA	SYBR® Green assay
Hif1an	*F:* TCATTGGCATGGAAGGAAAT *R:* GAAATTGGGGAACCTCTCGT	SYBR® Green assay
Jmjd1a	*F:* CACATTTAGGTTCCCAGTCACA *R:* GCCACGATGTTAACACAGGA	SYBR® Green assay
Jmjd1b	*F:* TTCTGCTGGAAGGCTCACTT *R:* GATGCATCCCATTAGCATCC	SYBR® Green assay
Jmjd1c	*F:* AGAAGAGGAAAGGCGAGGTC *R:* TTGGGACCTATCTCACAGCA	SYBR® Green assay
Jmjd2a	*F:* GACCACACTCTGCCCACAC *R:* TCCTGGGGTATTTCCAGACA	SYBR® Green assay
Jmjd2b	*F:* GGCTTTAACTGCGCTGAGTC *R:* GTGTGGTCCAGCACTGTGAG	SYBR® Green assay
Jmjd2c	*F:* CACGGAGGACATGGATCTCT *R:* CGAAGGGAATGCCATACTTC	SYBR® Green assay
Jmjd2d	*F:* GTCTTGGTCGTCGTCCTTGT *R:* AATCCCCCTTCAGAAGCTGT	SYBR® Green assay
Jmjd3	*F:* CCCCCATTTCAGCTGACTAA *R:* CTGGACCAAGGGGTGTGTT	SYBR® Green assay
Jmjd4	*F:* CTCAAGGACTGGCATCTGTG *R:* CTGAAGGAGCGGAAGATGTC	SYBR® Green assay
Jmjd5	*F:* TGTCATGTTAGAGCGGATGG *R:* TGTACCTTGAGCCCACTTCC	SYBR® Green assay
Jarid1a	*F:* CCTCCATTTGCCTGTGAAGT *R:* CCTTTGCTGGCAACAATCTT	SYBR® Green assay
Jarid1c	*F:* GGTGAGCCAAAAACCTGGTA *R:* CAAATTCTCCTGCACACTGG	SYBR® Green assay
Jarid1d	*F:* CCCCAAGGGAGTATGGAGAT *R:* GCCTCCAGAATTCCTTTTCC	SYBR® Green assay
Jarid2	*F:* GGTCTGCTCAGGACTTACGG *R:* TTGGGTTTGGTTTCCTTGAC	SYBR® Green assay
Mina	*F:* GCAAAGGAAGATGTGGCATT *R:* CCTCGAAGAAAGGAGGGAGT	SYBR® Green assay
Nanog	*assay ID:* Mm02384862_g1	TaqMan® assay
Nestin	*assay ID:* Mm00450205_m1	TaqMan® assay
Oct-3/4	*assay ID:* Mm00658129_gH	TaqMan® assay
Pax6	*assay ID:* Mm00443072_m1	TaqMan® assay
Phf2	*F:* GCCAAAGAGATCAGGCTCAG *R:* TGGGCATCTTCACAGTCTTG	SYBR® Green assay
Phf8	*F:* CGCCCAACAAATGCTAATCT *R:* AGAAGTTCCCTCCGAATGCT	SYBR® Green assay
Ptdsr	*F:* AAGGAGGGAACCAACAGGAT *R:* CTGGCAAAGTTCTGGGTGAT	SYBR® Green assay
Sox1	*F:* AGATGCACAACTCGGAGATCAG *R:* GAGTACTTGTCCTTCTTGAGCAGC *assay ID:* Mm01281943_s1	SYBR® Green assay TaqMan® assay
TBP	*F:* CTGGAATTGTACCGCAGCTT *R:* TCCTGTGCACACCATTTTTC *assay ID:* Mm00446973_m1	SYBR® Green assay TaqMan® assay
Utx	*F:* ATCCCAGCTCAGCAGAAGTT *R:* GGAGGAAAGAAAGCATCACG	SYBR® Green assay

3.4 *In situ* hybridisation

3.4.1 Preparation of digoxigenin (DIG)-labelled RNA probe for in situ hybridisation

First, 12 µg of pCDNA3-FLAG-Jmjd3 plasmid, containing the Jmjd3 cDNA sequence as template, were linearized with the restriction enzyme SspI (Figure 6).

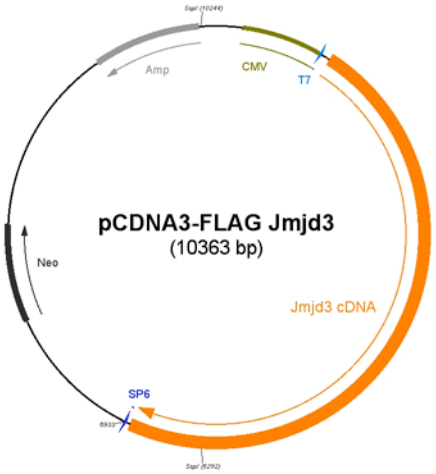

Figure 6. Map of the plasmid containing the Jmjd3 cDNA used as template to synthesize the anti-sense probe for *in situ* hybridisation. The plasmid was linearized with SspI and probe was *in vitro* transcribed by SP6 RNA polymerase.

The digested DNA was cleaned up by phenol-chloroform extraction and standard ethanol precipitation. Next, 1 µg of linearized plasmid DNA were used to set up the *in vitro* transcription reaction, during which the anti-sense probe was synthesized by 20 units of SP6 RNA polymerase (NEB) using the DIG RNA Labeling Mix (Roche). After the reaction, template DNA was removed by DNase treatment. The labelled RNA probe was precipitated with ethanol and resuspended in 50 µl of RNase-free water. To estimate the efficiency of the reaction, 2 µl of probe were run on a 1.6% agarose gel and RNA concentration was measured with the NanoDrop (Thermo Fisher Scientific). The generated RNA probe had a size of 590 bp and hybridised to the 3' end of the Jmjd3 mRNA.

3.4.2 In situ hybridisation

Until the hybridisation step all solutions for washing or incubating the specimens were prepared with diethyl pyrocarbonate (DEPC)-treated water or PBS. DEPC was added to a final concentration of 0.1% and solutions were autoclaved to hydrolyze any remaining DEPC.

Brains were dissected in a physiological solution of 0.9% (w/v) NaCl and 0.6% (w/v) glucose and fixed overnight in 4% (w/v) paraformaldehyde (PFA) at 4 °C. Fixed brains were washed three times with PBS and cryoprotected in 30% (w/v) sucrose overnight at 4 °C. The following day brains were transferred into 5 ml tubes and incubated in a 1:1 mixture of cryostat freezing medium (Bio-Optica) and 30% (w/v) sucrose rotating for 30 min at RT. Brains were frozen in embedding medium on dry-ice and stored at -80°C until further processed. Brains were cut at 10 µm with a Leica cryostat and placed as serial sections onto SuperFrost Ultra Plus® glass slides (Thermo Fisher Scientific). Sections were post-fixed for 10 min in 4% (w/v) PFA, washed three times in PBS and permeabilized with 1 µg/ml proteinase K for 5 min at RT for better probe penetration. Tissue sections were refixed in 4% (w/v) PFA for 5 min, washed thoroughly in PBS and acetylated for 10 min [100 ml acetylation solution were made of 1.3 ml triethanolamine (Sigma-Aldrich), 250 µl 37% HCl and 250 µl acetic anhydride in 98.2 ml water] in order to prevent nonspecific binding of the probe. After three washes in PBS 0.5 ml of warm hybridisation buffer [50% deionized formamide, 5× SSC, 5× Denhardt's Solution (Sigma-Aldrich), 100 µg/ml yeast tRNA, 100 µg/ml denatured salmon sperm DNA] were placed onto slides and incubated for 2 h at RT in a 5× SSC humidified chamber. Prehybridisation solution was removed and replaced with 150 µl of hybridisation buffer containing 500-700 ng/ml of digoxigenin (DIG)-labelled RNA probe (Roche), which has been denatured at 80 °C for 5 min before. Slides were covered with Hybri-slips (Sigma-Aldrich), placed in a chamber humidified with 5× SSC, 50% formamide and incubated at 68 °C overnight. After hybridisation probe

was removed and slides were washed in 0.2× SSC at 68 °C for 1 h, followed by a quick wash in 0.2× SSC for 5 min at RT. Slides were then transferred to B1-buffer (100 mM Tris-HCl pH 7.6, 150 mM NaCl in water) for 15 min at RT. In order to prevent nonspecific antibody binding sections were incubated in B1-buffer supplemented with 5% goat serum (EuroClone) and 2% (w/v) Blocking Reagent (Roche) for 1 h at RT. For the immunological detection of the probe sections were incubated with a sheep polyclonal anti-digoxigenin antibody conjugated to alkaline phosphatase (1:2000, Roche #11093274910) at 4 °C overnight. The following day slides were transferred to B1-buffer for four 30 min washes at RT and then washed twice for 15 min in Alkaline Phosphatase buffer [100 mM Tris-HCl pH 9.5, 100 mM NaCl, 50 mM $MgCl_2$, 0.1% Tween-20, 1 mM Levamisole (Sigma-Aldrich) in water] in order to inhibit endogenous phosphatases. The colorimetric staining was carried out by adding BM Purple (Roche), supplemented with 2 mM Levamisole to each slide and incubation at RT until the desired level of staining developed. Specimens were washed three times in PBS to stop the staining reaction. Slides were briefly rinsed with water, mounted with VectaMount AQ aqueous mounting medium (Vector Laboratories) and staining was examined on an Olympus microscope equipped with a Nikon colour camera.

4 Protein methods

4.1 Immunocytochemistry

Cells, grown on glass coverslips or on μ-Dish 35 mm (Ibidi), were fixed in 4% (w/v) PFA for 15 min at RT, washed in PBS and incubated in permeabilization/blocking buffer: 2% (w/v) BSA, 0.1% Triton X-100 in PBS. Primary antibodies were diluted in PBS containing 2% (w/v) BSA and incubated in a humidified chamber at 4 °C overnight (Table 3). Cells were washed three times in PBS and incubated with species specific secondary antibodies conjugated to FITC and Cy3 (Jackson ImmunoResearch) and Dapi (Sigma-Aldrich). Slides were mounted with Mowiol (Calbiochem). Images were acquired with an Olympus fluorescence microscope equipped with a CoolSNAP *EZ* CCD camera (Photometrics). For clarity, images were adjusted for contrast and brightness using Adobe Photoshop. The automated image acquisition was controlled by the scan^R screening-station (Olympus) and image analysis was performed with ImageJ software.

Table 3. Antibodies used in immunocytochemistry.

Antibody	Working dilution	Supplier
β-III tubulin (TuJ1)	1:2000	Covance #MRB-435P
Cytokeratin 5/8	1:100	BD #550505
GFAP	1:500	Millipore #MAB3402
Nestin	1:500	Millipore #MAB353
Sox2	1:100	Abcam #15830

4.2 Immunohistochemistry

Brains were dissected in a physiological solution of 0.9% (w/v) NaCl and 0.6% (w/v) glucose and fixed overnight in 4% (w/v) PFA at 4 °C. The next day fixed brains were washed three times with PBS and cryoprotected in 30% (w/v) sucrose overnight at 4 °C. Brains were transferred into 5 ml tubes and incubated in a 1:1 mixture of cryostat freezing medium (Bio-Optica) and 30% (w/v) sucrose rotating for 30 min at RT. Brains were frozen in embedding medium on dry-ice and stored at -80 °C until further processed. Brains were

cut at 10 µm with a Leica cryostat and placed as serial sections onto SuperFrost Ultra Plus® glass slides (Thermo Fisher Scientific), as illustrated in Figure 7. Sections were post-fixed for 10 min with 4% (w/v) PFA followed by three washes with PBS. For the detection of nuclear antigens an antigen enhancement step was performed by briefly boiling the slides in 10 mM sodium citrate pH 6.0 using a microwave. Sections were then incubated in permeabilization/blocking solution: 0.2% Triton X-100, 1% (w/v) BSA in PBS for 30 min at RT. Primary antibodies were diluted in PBS plus 2% goat serum (EuroClone), 0.05% Triton X-100 and incubated in a humidified chamber at 4 °C overnight. The antibodies and their dilutions used in this study are listed in Table 4. After three washes in PBS specimens were incubated with species specific secondary antibodies conjugated to FITC (1:50) and Cy3 (1:400; Jackson ImmunoResearch) and Dapi (Sigma-Aldrich).

Specimens were coverslipped with VectaMount AQ aqueous mounting medium (Vector Laboratories).

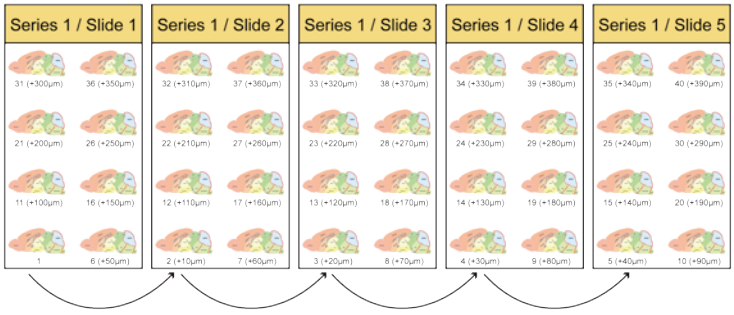

Figure 7. Cutting scheme for serial brain sections. Shown is an example for a series consisting of five slides each with eight brain sections. Brains were cut at 10 µm and consecutive sections were placed in the same position on the following slide.

Table 4. Antibodies used in immunohistochemistry.

Antibody	Working dilution	Supplier
Phox2b	1:500	gift of C. Goridis
Serotonin (5-HT)	1:1000	Sigma-Aldrich #5545
Substance P Receptor (Nk1R)	1:5000	Sigma-Aldrich #S8305
Tyrosine Hydroxylase (TH)	1:500	Inst. Biotech. Jacques Boy #208020234

4.3 FACS sorting

Neural precursors derived from 46C ESCs were trypsinized and sorted in FACS buffer (PBS plus 1% FBS).

4.4 Western blotting

4.4.1 Lysate preparation

Cells were washed in PBS and collected by centrifugation. Cell pellets were flash frozen in liquid nitrogen and stored at -80 °C until use. Cell lysates were prepared on ice in protein extraction buffer (50 mM Tris-HCl pH 7.6, 0.15 M NaCl, 5 mM EDTA, 1% Triton X-100), freshly supplemented with 1× protease inhibitor cocktail (Roche). Samples were sonicated with a Diagenode Bioruptor® sonicator (high power, three cycles of 30 s pulse and 45 s pause each) to lyse cells and to shear genomic DNA. Following centrifugation at maximum speed (16060 × *g*) for 5 min at 4 °C to pellet cell debris, the clear supernatant was collected and transferred to a new tube. Protein concentration was determined by the Bradford assay using BSA (Sigma) as a protein standard. Absorbance was measured at 595 nm with the spectrophotometer.

4.4.2 Gel electrophoresis

Proteins were separated by sodium dodecyl sulfate polyacrylamide gel electrophoresis (SDS-PAGE). To denature proteins, 5× loading buffer [250 mM Tris-HCl pH 6.8, 10% SDS, 30% glycerol, 100 mM DTT, 0.01% (w/v) bromophenol blue] was added to protein lysates and samples were boiled for 5 min at 95 °C. For the detection of Jmjd3, 100 µg of total protein were loaded on a 5% polyacrylamide gel and run at 110 V for 2 h.

4.4.3 Immunoblotting

Proteins were transferred onto a PVDF (polyvinylidene fluoride) Immobilon™-P membrane (Millipore) in semi-dry conditions using a Trans-Blot SD Semi-Dry Transfer Cell (BioRad) at 90 mA for 2 h. The efficiency of protein transfer and even loading between the samples were checked by incubating the membrane for 5 min in Ponceau Red. Membranes were blocked in 5% (w/v) skimmed milk powder in Tris-buffered saline with 0.1% Tween 20 (TBST) for 1 h at RT. Primary antibodies were diluted in blocking solution and membranes were incubated at 4°C overnight with rocking. The homemade polyclonal anti-Jmjd3 antibody was used at a dilution of 1:500 and the monoclonal anti-vinculin was diluted 1:10000. The next day, blots were washed in TBST for 5 min at least three times and then incubated with secondary antibodies goat-anti-mouse IgG or goat anti-rabbit IgG conjugated with horseradish peroxidase (Bio-Rad) diluted at 1:15000 in blocking solution for 30 min at RT. Membranes were washed three times for 10 min each in TSBT and bands were detected using Amersham ECL Western Blotting Detection Reagents (GE Healthcare) following the manufacturer's instructions.

4.5 Chromatin immunoprecipitation (ChIP)

Adherent cells were cross-linked by adding formaldehyde to the culture medium at a final concentration of 1%. After 5 min fixation the reaction was quenched by adding Tris-HCl pH 7.6 to a final concentration of 125 mM, cells were thoroughly washed in PBS and harvested by scraping. Cell membranes were disrupted in L1 swelling buffer [50 mM Tris-HCl pH 8.0, 2 mM EDTA, 0,1% NP-40, 10% Glycerol, 1× protease inhibitor cocktail (Roche)], 900 µl for a 10 cm dish. Nuclei precipitated and resuspended in 600 µl of nuclear lysis buffer (50 mM Tris-HCl pH 8.0, 5 mM EDTA, 1% SDS, 1× protease inhibitor cocktail). Shearing of genomic chromatin was performed with a Diagenode Bioruptor® sonicator (high power, four cycles of 30 s pulse and 30 s pause each) yielding DNA with

an average fragment size from 200 to 1000 bp. DNA concentration was measured with NanoDrop (Thermo Fisher Scientific) and DNA of different samples was employed in equal quantities for the immunoprecipitation. Salt and detergent concentrations in the immunoprecipitation were adjusted for an optimal antibody performance by diluting the sonicated lysate with nine volumes of dilution buffer (50 mM Tris-HCl pH 8.0, 5 mM EDTA, 200 mM NaCl, 0.5% NP-40) for ChIP assays on Jmjd3 and total histone H3 or by adding 1/10 volume of 10% Triton X-100 for the immunoprecipitation of histone H3 trimethyl-lysine 27 (H3K24me3). Lysate was precleared with 50 µl slurry of salmon sperm DNA saturated protein A sepharose beads (GE Healthcare), rotating for 1 h at 4 °C. Beads were pelleted by centrifugation and antibody was added to precleared extract (Table 5). Immunoprecipitation was carried out a 4 °C overnight. ChIP complexes were collected by incubating with 20 µl of salmon sperm DNA/protein A sepharose beads for 30 min at 4°C. ChIP-beads complexes were washed four times in washing buffer (20 mM Tris-HCl pH 8.0, 2 mM EDTA, 0.1% SDS, 1% NP-40, 500 mM NaCl) and three times in 1× TE. ChIP complexes were eluted in 120 µl of 1× TE containing 2% SDS at 65 °C for 15 min and the crosslink of proteins to DNA was reversed at 65 °C overnight. DNA was purified with the QIAquick PCR Purification Kit (Qiagen), following the manufacturer's instructions and eluted in 100 µl of provided buffer EB. 5 µl of DNA were used in a 25 µl qRT-PCR reaction using the primers listed in Table 6. The abundance of target genome DNA was normalised relative to that of input.

Table 5. Antibodies used in ChIP assays.

Antibody	Amount per ChIP reaction	Supplier
Jmjd3	3 µg	homemade
H3K27me3	2 µg	Upstate #07-449
Histone H3	1 µg	Abcam #ab1791

Table 6. Primers used for qRT-PCR after ChIP.

Gene	Primer name	Primer sequence (5'-3')
Pax6	Px6TS1	*F:* GGAGGACAATACCAGCCAGA *R:* GGTTCAGCTCGGCAGATTAG
Pax6	Px6TS2	*F:* AAGCGAACCGTGGCTCGG *R:* ATTAGCGAAGCCTGACCTCTG
Pax6	Px6B1	*F:* AGGCAGAGGGGTCTAGCTTC *R:* CAAGCAAGTGGGAAGGTGAT
Nestin	Nes	*F:* TTCTTCGGGCAGTGTTTCTT *R:* GACGGTGCAGTGTTTTGTGT
Sox1	Sox	*F:* CACAGTTCAGCCCTGAGTGA *R:* CACAAACCACTTGCCAAAGA
Prolactin	Prl	*F:* CCTTCATTTCTGGCCAATGT *R:* GCCTGAGAGAACCACAGCTT

4.6 *In vivo* demethylation assay

HEK 293 cells were transfected with pcDNA3-FLAG expressing FLAG-tagged Jmjd3 or the FLAG-tagged mutated version carrying an amino acid substitution in the catalytic site, along with the empty pcDNA3-FLAG vector as control. Proteins were extracted with Laemmli sample buffer [62.5 mM Tris-HCl pH 6.8, 2% SDS, 10% glycerol, 100 mM DTT, 0.01% (w/v) bromophenol blue]. Subsequently protein extracts were immunoblotted and assessed with antibodies specific for the various methylated lysine residues (Table 7).

4.7 *In vitro* demethylation assay

The C-terminus of murine Jmjd3, comprising residues 1141 through 1641 was cloned into the pETM14 expression vector in frame with a 6× His-tag, expressed in bacteria and purified from the soluble fraction. The demethylation assay was carried out by incubating 10 μg of recombinant Jmjd3 and 5 μg of calf thymus histone H3 for 4 h in a reaction buffer containing 50 mM Tris pH 8.0, 10% glycerol, 1 mM α-ketoglutarate, 80 μM $FeSO_4$ and 2 mM ascorbic acid. The reaction mixtures were analysed by western blotting using specific antibodies (Table 7).

Table 7. Antibodies used for *in vivo* and *in vitro* demethylation assays.

Antibody	Supplier
H3K4me1	Abcam #ab8895
H3K4me2	Abcam #ab7766
H3K4me3	Abcam #ab8580
H3K9me1	Upstate #07-450
H3K9me2	Upstate #07-441
H3K9me3	Upstate #07-442
H3K27me1	Upstate #07-448
H3K27me2	Upstate #07-452
H3K27me3	Upstate #07-449
H3K36me3	Abcam #ab9050

5 Physiological and electrophysiological analyses

All experiments were carried out in accordance with European guidelines for the care and use of laboratory animals (86/609/EEC). All efforts were made to minimise the number of animals used and their suffering.

5.1 Measuring blood glucose level of newborn mice

The neonates were decapitated and 5 µl of blood were analysed using the test strip-based Accu-Chek Active® blood glucose testing system (Roche).

5.2 *In vivo* breathing studies

Breathing movements of surgically delivered E18.5 embryos were recorded for 3-5 min by the whole-body plethysmography technique in a thermostated chamber equipped with a differential pressure transducer (EMKA Technologies). The technical set-up is illustrated in Figure 8.

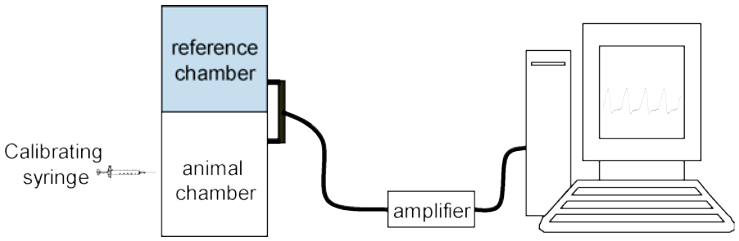

Figure 8. Experimental set-up for in vivo breathing studies. A differential pressure transducer was placed between the animal chamber (20 ml) and the reference chamber. The pressure difference between the two chambers was measured to obtain an index of the respiratory activity. Calibrations (10 µl) were made at the beginning and at the end of each recording session by injecting air in the animal chamber with a Hamilton syringe.

For *in utero* recordings, pregnant females were deeply anaesthetised with isoflurane (3% at the beginning and later 2.2%). A median incision was made along the white line to access the uterine horns and a given embryo was isolated with preserved umbilical irrigation.

Chest muscle electromyograms and cardiac pulses were recorded with thin copper wires inserted in the chest muscle. Signals were filtered, amplified (Neurolog System; Digitimer) and visualised on memory scope or stored on PC.

5.3 *In vitro* preparations

Pregnant mice were sacrificed by cervical dislocation at the desired developmental stage (E16.5 or E18.5). Embryos were removed form the uterine horns and placed in oxygenated artificial cerebrospinal fluid (aCSF), composed of 129 mM NaCl, 3 mM KCl, 1.26 mM $CaCl_2$, 1.15 mM $MgCl_2$, 21 mM $NaHCO_3$, 0.58 mM NaH_2PO_4, 30 mM glucose, pH 7.4 and saturated with carbogene (95% O_2, 5% CO_2). Embryos were kept in aCSF at RT until used in electrophysiological recording sessions. En bloc brainstem preparations were isolated by an anterior section performed at the level of the isthmus and a posterior section performed caudal to the fourth cervical root (C4). Isolated brainstem preparations were then transferred into the recording chamber ventral side up. C4 phrenic root activity was recorded with suction electrodes, filtered, amplified and integrated (Figure 9).

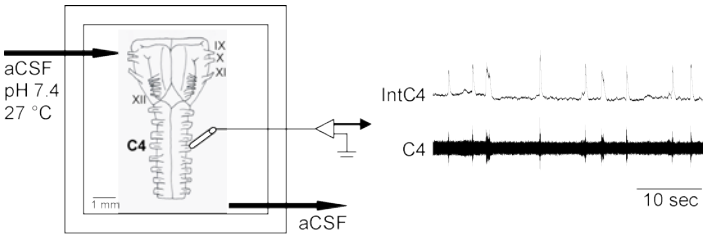

Figure 9. Schematic representation of the en bloc brainstem preparation. The *in vitro* activity of the isolated respiratory rhythm generator (RRG) is recorded at the C4 ventral root. Shown is an example of raw and integrated phrenic bursts (bottom and top traces, respectively).

At E16.5, the brainstem and spinal cord were isolated with the ribcage remaining attached and rhythmic diaphragmatic electromyogram discharges were recorded *in vitro*.

Results

The objective of this thesis was to study the role of histone lysine demethylation in the establishment and maintenance of cell identity. To this end I focused on one of the best described in vitro differentiation systems, the neural induction of mouse embryonic stem cells (ESCs) in adherent monolayer conditions [82]. This protocol accurately mirrors cellular events and signalling pathways involved in neural specification during development, therefore providing a tool for dissecting molecular mechanisms of neural commitment [89]. The expression analysis of 24 JmjC genes during the derivation of neural stem cells (NSCs) from ESCs in adherent monolayer culture revealed that Jmjd3 was highly upregulated during the initial stages of neurulation and was then downregulated once the NSC state had been achieved. This expression pattern suggested a potential function of Jmjd3 during the early stages of neural commitment. The functional relevance of Jmjd3 during neural differentiation *in vitro* was assessed by RNA interference (RNAi)-mediated gene silencing. To study the role of Jmjd3 *in vivo* we pursued two complementary approaches: i) the constitutive inactivation based on a random gene trap integration and ii) the conditional inactivation by gene targeting through homologous recombination.

1 Functional characterisation of Jmjd3 *in vitro*

1.1 Jmjd3 is specifically upregulated at the outset of neural commitment

In order to explore the relevance of histone demethylation to lineage commitment the differentiation of ESCs into neural stem cells (NSCs) in adherent monolayer culture was used as experimental system [82-83]. This protocol enables the derivation of a homogenous population of NSC capable of continuous self-renewal and multipotent

differentiation into the three main cell types of the central nervous system (CNS) – neurons, astrocytes and oligodendrocytes [90]. By avoiding the heterogeneity associated with standard procedures of ESC differentiation, this experimental system allowed to specifically trace the importance of putative histone demethylases for the commitment to the neural lineage. Thus, homogeneous cultures of NSCs were generated and characterised by immunocytochemistry. NSCs expressed uniformly neural precursor markers like the intermediate filament protein Nestin and SRY-related transcription factor Sox2 and lacked the expression of terminal differentiation markers such as the astrocytic marker glial fibrillary acidic protein (GFAP) and neuronal marker β III-tubulin (Figure 10).

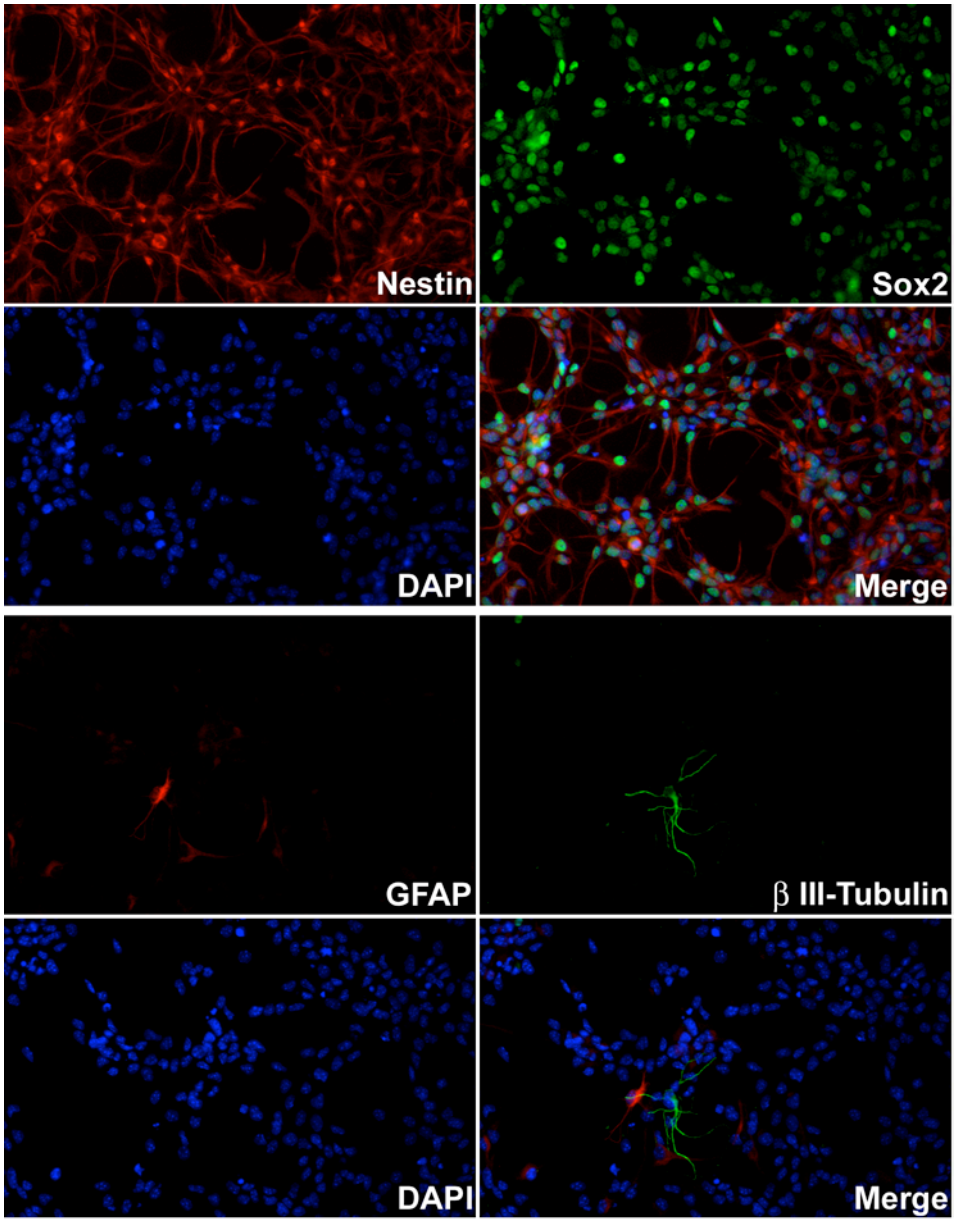

Figure 10. Generation of NSCs from ESCs. ESC-derived NSCs constitute a homogeneous population of neural precursors. They show uniform expression of neural precursor markers Nestin and Sox2 and virtually no immunoreactivity for neuronal (β III-tubulin) or astrocyte (GFAP) antigens.

With the *in vitro* differentiation system in place the role of JmjC domain-containing proteins during neural differentiation was investigated. The expression of 24 JmjC genes was analysed at the mRNA level by quantitative real-time PCR (qRT-PCR) at day 8 and day 26 of NSC derivation (Figure 11). By day 8 of differentiation, cells have irreversibly committed to neural fate and about 70% of the population consists of neural precursors [78]. Neural precursors were replated in the presence of epidermal growth factor (EGF) and fibroblast growth factor 2 (FGF-2). These conditions progressively enriched the culture for bipolar cells that were passaged regularly until a homogenous culture of NSCs was obtained (corresponding to the day 26 sample). The results revealed distinct patterns of expression for individual JmjC genes. Several genes were expressed at stable levels, such as Jmjd1b, Jmjd5 and Utx, whereas others increased or decreased steadily during the course of differentiation. On the contrary, five JmjC genes (Jmjd2b, Jmjd3, Jarid1a, Jarid1c and Phf8) were first upregulated at day eight (early neural precursors) and then downregulated at day 26 (established and self-renewing NSCs) suggesting, that they could be involved in the epigenetic transition underlying the outset of neural commitment. Among these genes, Jmjd3 showed the greatest upregulation at day eight (sixfold increase) with a decrease to near ESC-level at day 26. This data suggested a role for certain JmjC domain-containing proteins, in particular Jmjd3, in the earliest phase of the commitment of ESCs to the neural lineage. Hence, the focus of the present study became the elucidation of the functional relevance of Jmjd3 during the early stages of neural commitment.

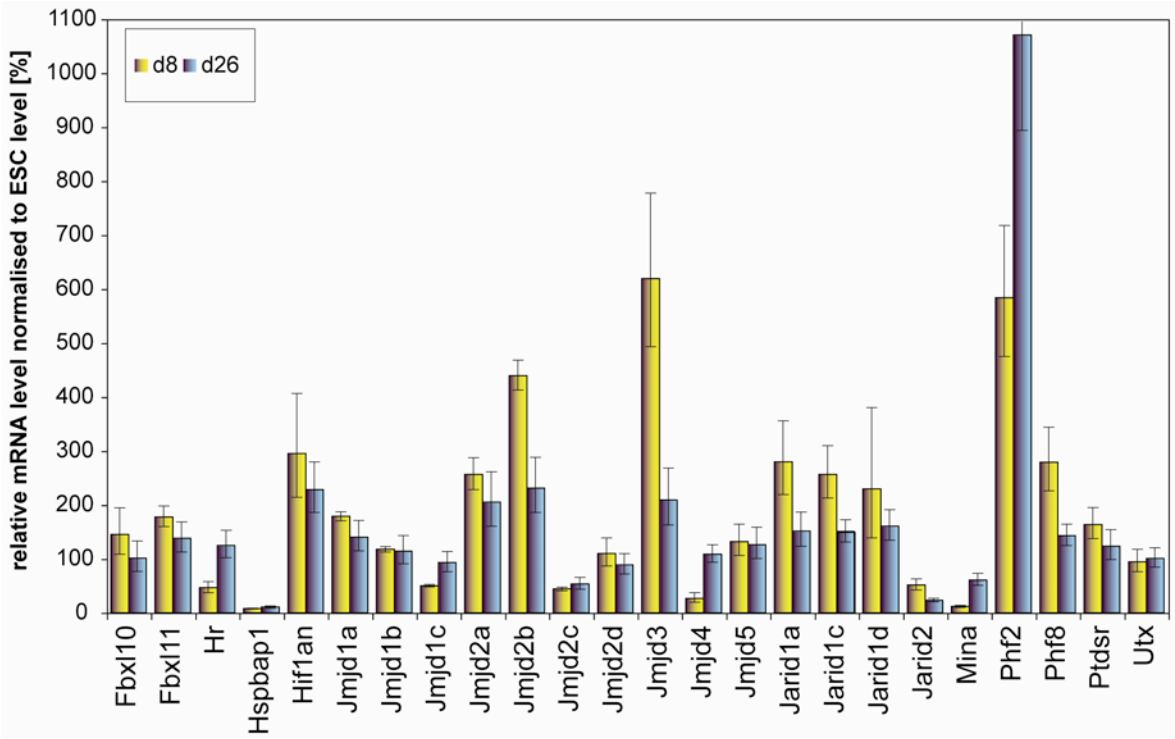

Figure 11. Expression profiling of JmjC genes during NSC derivation. mRNA levels were quantified by qRT-PCR at day eight and day 26 of differentiation. The bars represent the means ± S.D. of qRT-PCR triplicates normalised to TBP and undifferentiated ESC. For each gene the transcript level in wild-type ESCs was set as 100%.

To analyse the expression of Jmjd3 on the protein level a polyclonal antibody was raised in collaboration with Abgent (Figure 12). The antibody recognized the C-terminus of Jmjd3, encompassing the JmjC domain (amino acids 1141 – 1641).

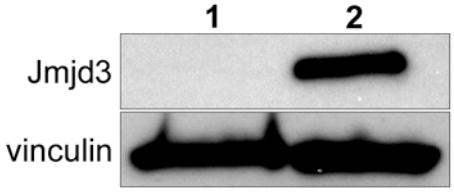

Figure 12. Specificity of the anti-Jmjd3 polyclonal antibody. Upper panel: western blot with anti-Jmjd3 antibody on untransfected 293 cells (lane 1) and 293 cells overexpressing the full-length Jmjd3 protein (lane 2). Lower panel: the same samples probed with anti-vinculin as loading control.

Western blot analysis during the derivation of NSCs from ESCs in adherent monoculture revealed that Jmjd3 protein expression peaks already at day four of neural differentiation and is downregulated in established self-renewing NSC cultures (Figure 13). In contrast to

the mRNA level, the protein level in NSCs is even lower compared to ESCs, suggesting the possibility of posttranscriptional regulatory mechanisms.

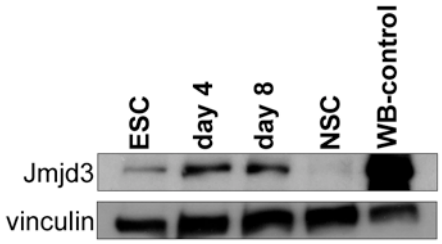

Figure 13. Protein expression levels of Jmjd3 during the ESC to NSC transition. Levels of Jmjd3 peak at day four to eight and are greatly reduced in established NSC cultures. Protein extract from cells overexpressing Jmjd3 was used to localise the Jmjd3 band (WB-control). Vinculin served as loading control.

1.2 Jmjd3 is a demethylase specific for histone H3 trimethyl-lysine 27 (H3K27me3)

For the biochemical characterisation of Jmjd3 a collaboration was started with Gioacchino Natoli, from the European Institute of Oncology (IEO, Milano, Italy), whose group had just begun to study the function of Jmjd3 during the differentiation of macrophages. They had observed that Jmjd3 is rapidly induced in macrophages upon activation by inflammatory stimuli. This result together with our observation showed that Jmjd3 is highly upregulated in two different cell systems that both entail processes of cell fate specification, the differentiation of macrophages and the differentiation of ESCs to NSCs. In order to assess the ability of Jmjd3 to catalyse histone demethylation, full-length Jmjd3 and a mutant version, carrying a H1388A mutation in the iron-binding centre of the catalytic site of the JmjC domain, were overexpressed in HEK 293 cells as FLAG-tagged fusion proteins. Protein extracts were subjected to western blot analysis and the methylation state of various histone lysine residues was evaluated with specific antibodies (Figure 14a). Ectopic expression of wild-type Jmjd3 resulted in a decrease of H3K27me3 level, whereas no reduction was observed for any other of the tested methylated lysine marks. H3K27me3 level in cells overexpressing the mutant form was unaffected, demonstrating that loss of H3K27me3 in Jmjd3-overexpressing cells is due to the

enzymatic activity of Jmjd3 and that the demethylating activity of Jmjd3 is dependent on a catalytically active JmjC domain.

Next, it was tested whether Jmjd3 could demethylate H3K27me3 *in vitro* (Figure 14b). The C-terminal part of Jmjd3 (amino acids 1141 – 1641) was fused to a polyhistidine tag and overexpressed in bacteria. In an *in vitro* demethylation reaction using histone H3 as substrate purified recombinant Jmjd3 demethylated efficiently H3K27me3 and with lower activity H3K27me2, whereas no reactivity was observed for H3K27me1. Furthermore it was demonstrated that this demethylase activity depends on the presence of iron Fe(II), confirming that Jmjd3 uses an oxidative demethylation mechanism, which had been shown to require Fe(II) and α-ketoglutarate as cofactors [28].

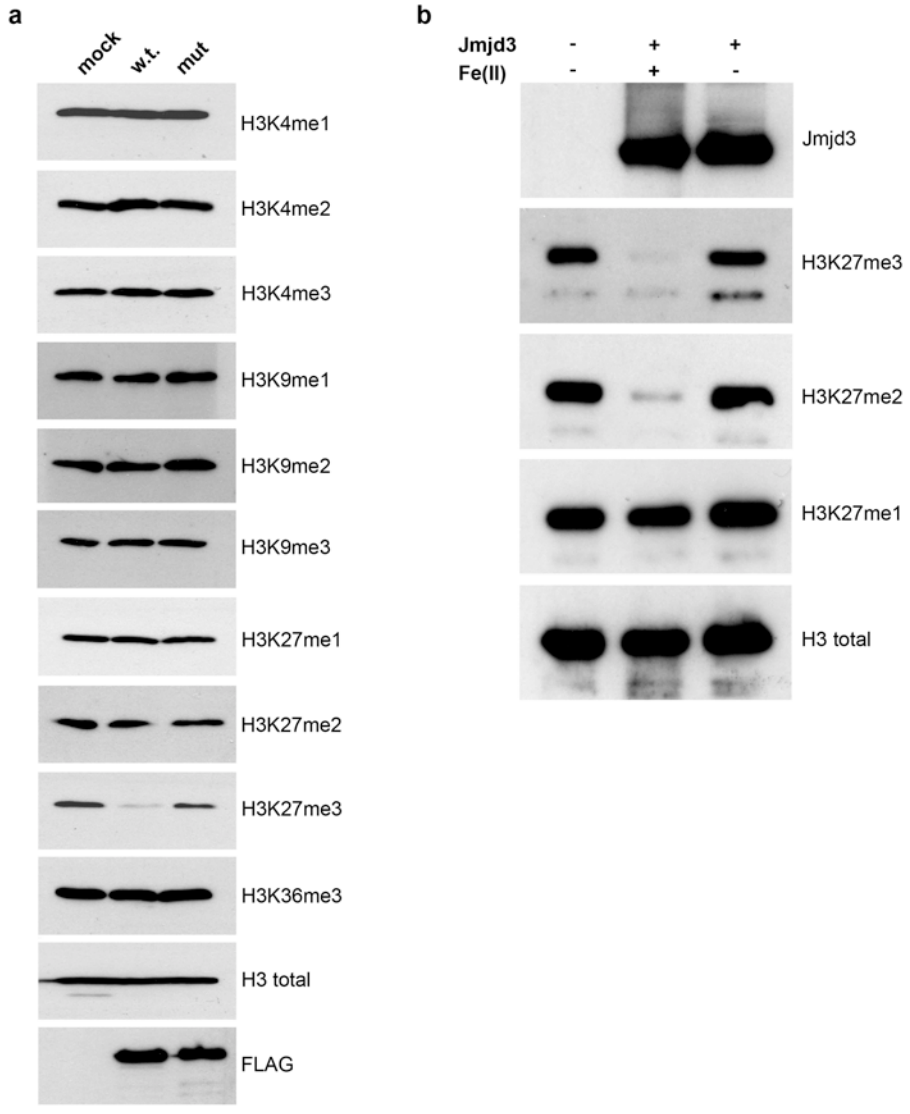

Figure 14. Jmjd3 is a H3K27me3-specific demethylase. (a) Effect of Jmjd3 overexpression in 293 cells on histone lysine methylation. FLAG-tagged wild-type Jmjd3 (w.t.) and an iron-binding deficient mutant version were overexpressed in 293 cells. Lysate from cells transfected with the empty expression vector is shown in the first lane (mock). Histone methylation was assessed by western blot using the indicated antibodies. **(b)** Recombinant Jmjd3 demethylates H3K27me3 *in vitro* in an iron-dependent manner. The C-terminus of Jmjd3, encompassing the JmjC domain and fused to a 6× His-tag was expressed in bacteria. The *in vitro* demethylation activity of recombinant Jmjd3 using histone H3 as substrate was analysed by immunoblotting with antibodies specific for mono-, di- and trimethyl H3K27. The effect of Fe(II) removal from the reaction is shown.

In summary, the above results indicated that Jmjd3 selectively demethylates H3K27 with a strong preference for the trimethylated form. The observation that a histone H3K27 demethylase is specifically upregulated at the initial phase of ESC differentiation suggested that its activity may be functionally involved in the dynamic regulation of the H3K27me3 mark which accompanies differentiation.

1.3 Jmjd3 is required for neural commitment

The functional relevance of Jmjd3 during neural commitment was assessed by RNA interference (RNAi)-mediated gene knockdown. To enable sustained gene silencing, we employed two different short hairpin RNAs (shRNAs), stably expressed from two different viral-based systems, lentiviruses and retroviruses. The lentiviral vector pSicoR PGK Puro expresses RNAi-inducing shRNAs under the control of the U6 RNA polymerase III promoter [85]. For this system, one shRNA targeting Jmjd3 was designed (shJd3-1) and one non-silencing control shRNA against firefly luciferase (shLuc), lacking sequence homology to the mouse genome. A second Jmjd3-specific shRNA design (shJd3-2) targeting a different region of Jmjd3 mRNA was cloned into the mircoRNA (miRNA)-adapted retroviral expression system LMP. The constitutive expression of this shRNAmir is driven by a RNA polymerase II promoter [73]. The target sequences of the shRNAs are

listed in Table 8 and the positions of the shRNAs targeting Jmjd3 are depicted in Figure 15.

Table 8. Target sequences of shRNAs used for RNAi.

shRNA name	Target sequence (5'-3')	Position on mRNA	Expression vector
shJd3-1	ACACCACCATCGCTAAATA	4225	pSicoR PGK Puro
shJd3-2	GCACTCGATGCCTCATTCATA	1334	LMP
shLuc	GAGCTGTTTCTGAGGAGCC		pSicoR PGK Puro

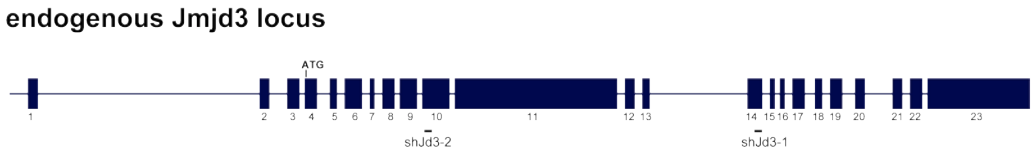

Figure 15. Localisation of shRNAs targeting Jmjd3. Scheme of the mouse Jmjd3 locus showing exons and the target sites of the shRNAs (shJd3-1 and shJd3-2) relative to the genomic sequence.

ESCs were infected with shRNA-expressing viruses and selected in puromycin to isolate and establish several ESC clones that stably expressed the shRNA constructs. ESC clones were analysed for Jmjd3 expression levels by qRT-PCR. For further characterisation the clone with the highest knockdown efficiency was selected for each Jmjd3 hairpin design, clone Jmjd3-kd1 for shJd3-1 and Jmjd3-kd2 for shJd3-2, as well as one control clone expressing shRNA against luciferase (Luc). The choice of two clones expressing two independent shRNAs against Jmjd3 aimed at minimising potential off-target effects. qRT-PCR analysis revealed for Jmjd3-kd1 more than 90% reduction in Jmjd3 mRNA level and slightly higher Jmjd3 residual levels for Jmjd-kd2. The specificity of Jmjd3 knockdown was confirmed by immunoblotting (Figure 16).

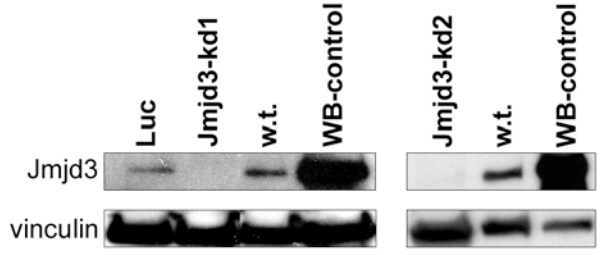

Figure 16. Protein levels of Jmjd3 in RNAi knockdown ESC clones. Western blot analysis for Jmjd3 expression confirmed efficient knockdown of Jmjd3 in ESC clones Jmjd3-kd1 and Jmjd3-kd2. No reduction

of Jmjd3 was observed in cells expressing the control Luc shRNA (Luc). Protein extract from cells overexpressing Jmjd3 was used to localise the Jmjd3 band (WB-control). Vinculin served as loading control.

Both Jmjd3-kd clones had markedly reduced Jmjd3 protein levels, whereas levels of Jmjd3 in the Luc control clone were not affected, thus indicating that Jmjd3 is not required for the maintenance of ESC. Expression analysis by qRT-PCR showed that the pluripotency markers Oct4 and Nanog were overall unaffected by Jmjd3 depletion (Figure 17). The slight increase of Oct4 expression in Jmjd3-kd2 ESCs could be explained by the fact that a population of ESCs, cultured under standard conditions with leukaemia inhibitory factor (LIF) and serum, represents a dynamic distribution of states with varying degrees of pluripotency that are accompanied, and most likely caused, by fluctuations in the expression of pluripotency-associated transcription factors [91-92]. Moreover, unlike what has been described for ESCs having elevated Oct4 levels [93], Jmjd3-kd2 ESCs did not show an increased spontaneous differentiation into primitive endoderm-like cells.

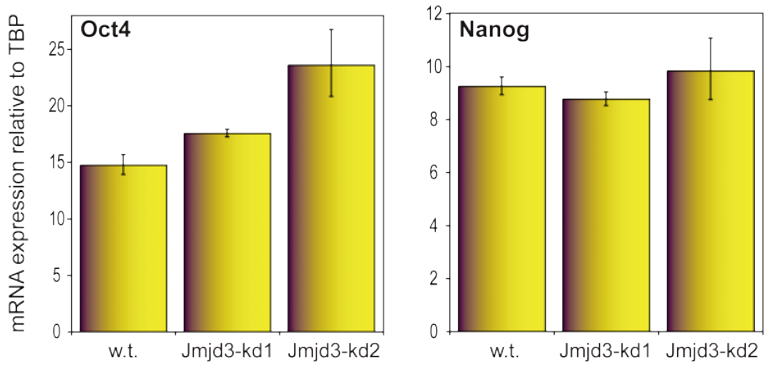

Figure 17. Expression of Oct4 and Nanog in undifferentiated Jmjd3-kd ESC clones. qRT-PCR analysis of Oct4 and Nanog mRNA levels in wild-type (w.t.) and Jmjd3-kd ESC clones. Bars represent the means ± S.D. of qRT-PCR triplicates normalised to TBP.

To examine whether the loss of Jmjd3 influences the ability of ESCs to differentiate into NSCs, the Jmjd3-kd ESCs were subjected to the adherent monolayer differentiation protocol described above. Whereas wild-type cells and cells expressing the control Luc shRNA formed neurulating rosettes which developed into dense clusters with intricate outgrowth of elongated bi- or tripolar neural precursors, Jmjd3-kd cells formed these

structures at much lower frequency, with the majority of cells flattening out and acquiring a polygonal shape. Cultures of differentiating wild-type and Luc-control cells showed by day seven of the differentiation protocol the typical pattern of neurulating clusters from which tightly juxtaposed neural precursors protrude. These outgrowing cells with characteristic palisade-like shape stained intensely positive for Nestin (Figure 18a, b upper panels). Both Jmjd3-kd clones had a markedly different morphology, with much fewer Nestin expressing clusters, in which the signal intensity was anyway lower than in the control cells. Moreover, the signal pattern of these Nestin-immunopositive clusters appeared diffuse and less structured, with only sporadic cases of radial growth of tightly packed precursors. Instead these abnormal clusters were surrounded by extensive sheets of flat cells, which stained positive for the epithelial cell marker Cytokeratin and comprised the majority of cells in Jmjd3-kd cultures (Figure 18a, b lower panels). In the control cultures the immunostaining for Cytokeratin was observed only in sporadic patches, as expected under these differentiation conditions.

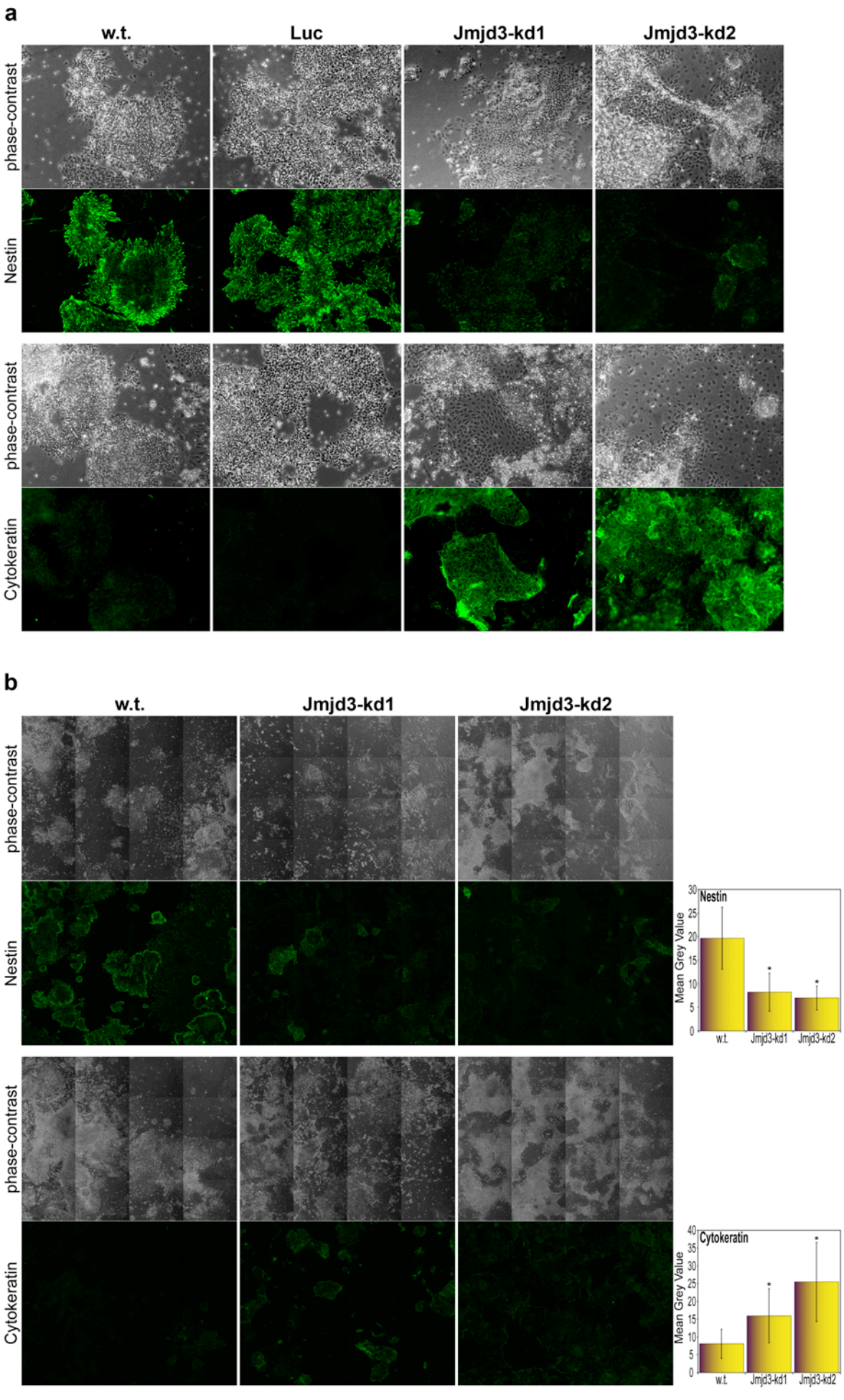
a
w.t.
Luc
Jmjd3-kd1
Jmjd3-kd2
phase-contrast
Nestin
phase-contrast
Cytokeratin
b
w.t.
Jmjd3-kd1
Jmjd3-kd2
phase-contrast
Nestin
Nestin
Mean Grey Value
30
25
20
15
10
5
0
w.t.
Jmjd3-kd1
Jmjd3-kd2
phase-contrast
Cytokeratin
Cytokeratin
Mean Grey Value
40
35
30
25
20
15
10
5
0
w.t.
Jmjd3-kd1
Jmjd3-kd2

Figure 18. Jmjd3 is required for neural commitment. (a) Immunostainings for Nestin (upper panel, second row) and Cytokeratin (lower panel, second row) and phase-contrast images (first rows of both panels) of wild-type cells (w.t.), control cells expressing Luc shRNA and Jmjd3-kd cells, acquired at day seven of monolayer differentiation protocol. **(b)** Immunostainings for Nestin (upper panel, second row) and Cytokeratin (lower panel, second row) and phase-contrast images (first rows of both panels) of wild-type (w.t.) and Jmjd3-kd cells, at day seven of differentiation in adherent monolayer. Sixteen contiguous images, providing a representative coverage of the culture dish, were automatically acquired. After background correction mean grey values were calculated using ImageJ software. Bars represent the means ± S.D. of the single images. Asterisks indicate statistically significant differences as compared to wild-type cells, $p<0.01$ (Student's *t*-test).

Based on these observations we next asked, whether the few Nestin-positive cells in the Jmjd3-kd cultures eventually managed to form NSCs. To this end, the Jmjd3-kd cells were replated in the presence of EGF and FGF-2 at day eight and further processed according to the monolayer differentiation protocol. Eventually after several passages the Jmjd3-kd cells managed to generate a homogeneous population of self-renewing NSCs, which were morphologically indistinguishable from NSCs derived from control cells. Yet, for Jmjd3-depleted cells it required more time until a stable NSC culture was established compared to control cells. As the process of NSC derivation entails a strong selection, progressively enriching the culture for neural precursors the hypothesis was that the few Jmjd3-kd cells that eventually managed to neurulate may have been those with residual levels of Jmjd3, which would enable them to undertake differentiation. Consistently with this prediction, at day seven of neural differentiation both Jmjd3-kd clones showed a significant upregulation of Jmjd3 on the mRNA level, with higher levels in Jmjd3-kd2 as expected on the basis of the lower knockdown efficiency already observed for this hairpin in the undifferentiated state (Figure 19a).

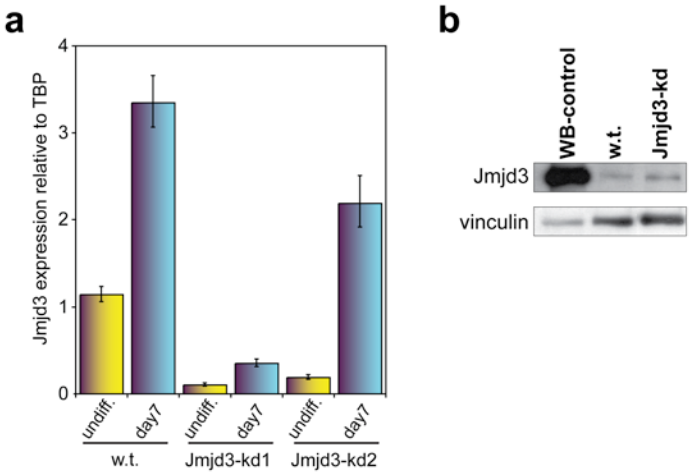

Figure 19. Jmjd3 expression in Jmjd3 knockdown cells during differentiation. (a) qRT-PCR analysis of Jmjd3 mRNA levels in wild-type (w.t.) and Jmjd3-kd clones at day seven of differentiation. Bars represent the means ± S.D. of qRT-PCR triplicates normalised to TBP. **(b)** Levels of Jmjd3 protein in NSCs derived from wild-type (w.t.) and Jmjd3-kd cells were assessed by western blot. Protein extract from cells overexpressing Jmjd3 was used to localise the Jmjd3 band (WB-control). Vinculin served as loading control.

As the RNAi machinery is active during differentiation, the upregulation of Jmjd3 in Jmjd3-kd cells reflects most likely the selection pressure that enriches the culture for those cells with less efficient knockdown and therefore higher levels of Jmjd3. In agreement with this assumption, the NSCs derived from the few Jmjd3-kd cells that started neurulation had indeed reacquired normal Jmjd3 protein levels (Figure 19b), suggesting that the ESC to NSC transition depends on the presence of Jmjd3.

1.4 Jmjd3 regulates neural markers

To investigate the molecular mechanism through which Jmjd3 is involved in ESC neural commitment, the expression of key developmental regulators and marker, such as Sox1, Pax6 and Nestin was analysed by qRT-PCR. Pax6, a homeodomain transcription factor, controls in the developing brain the differentiation of the radial glia, the source of neural progenitors for both neuronal and glial lineage and its expression profile is recapitulated in ESC-derived NSCs [94]. Nestin is a neurofilament protein specifically upregulated during neural differentiation and widely used as NSC marker [95]. The transcription factor Sox1

is one of the earliest known markers of neuroectodermal precursors in the mouse embryo with a key role in early neural specification [96]. During adherent monolayer differentiation Sox1 expression starts to be transiently upregulated at day three, peaks between days six to eight and is completely lost in NSCs [78].

As shown in (Figure 20) Jmjd3-kd ESCs started off with lower levels of Pax6, Nestin and Sox1 and failed to appropriately upregulate all the three markers by day seven when neural commitment peaked. The reductions of the mRNA levels were less severe in Jmjd3-kd2, likely due to the lower knockdown efficiency and the greater residual upregulation of Jmjd3.

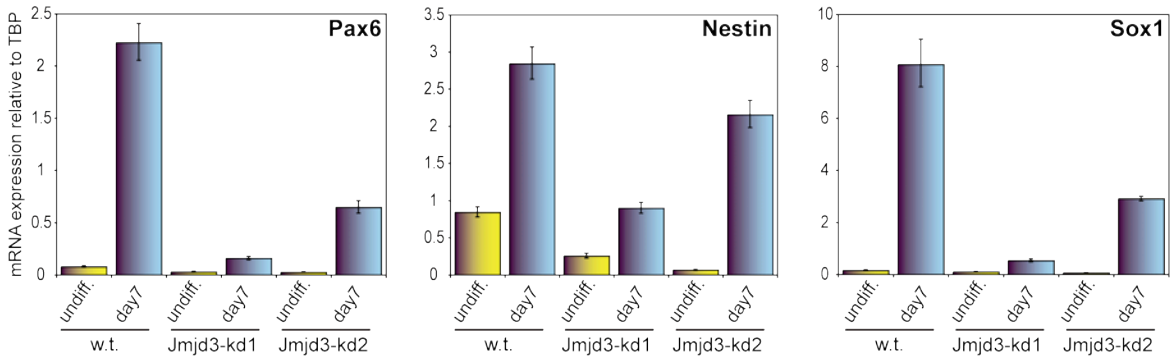

Figure 20. Loss of Jmjd3 impairs upregulation of the neural markers Pax6, Nestin and Sox1 during differentiation. mRNA levels of Pax6, Nestin and Sox1 in wild-type (w.t.) and Jmjd3 knockdown (Jmjd3-kd) cells were quantified by qRT-PCR at the undifferentiated ESC state and at day seven of monolayer differentiation. Bars represent the means ± S.D. of qRT-PCR triplicates normalised to TBP.

The reduced upregulation of Pax6, Nestin and Sox1 correlated with the partial upregulation of Jmjd3 in Jmjd3-kd clones at day seven of differentiation, suggesting that these genes could be direct targets of Jmjd3 and exquisitely sensitive to the dynamics of its protein levels.

In order to investigate whether Jmjd3 physically binds to the promoters of these genes chromatin immunoprecipitation (ChIP) experiments were performed. For Pax6 both annotated transcription start sites (TS1 and TS2) were probed with three PCR primer sets, one located 200 bp upstream of TS1 and two located 900 bp upstream and 1.4 kb downstream, respectively of TS2 (Figure 21). The primers for Nestin and Sox1 annealed in

regions 450 bp and 300 bp, respectively upstream of their transcription start sites. All the corresponding amplicons were located within the previously defined bivalent domains.

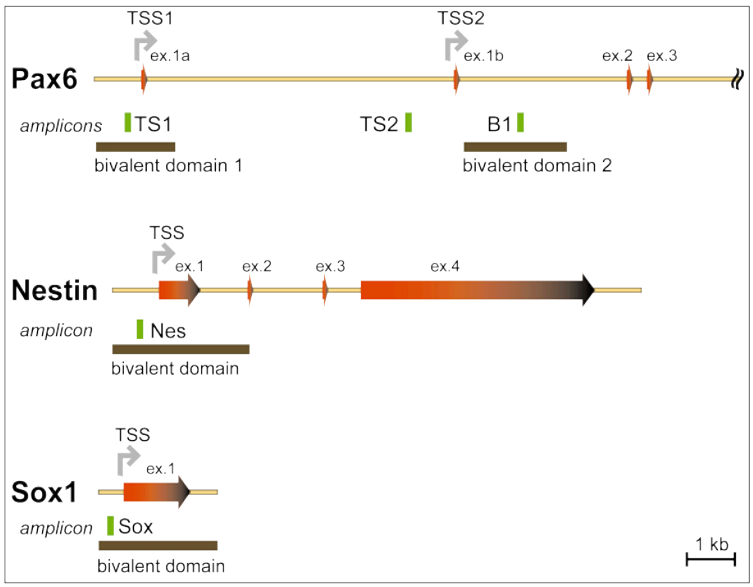

Figure 21. Scheme of the genomic regions analysed with ChIP assay. The Pax6 (upper panel), Nestin (middle panel) and Sox1 (lower panel) *loci* are drawn to scale, showing exon - intron structure, the transcription start sites (TSS), the regions covered by the so-called bivalent domains and the location of the amplicons analysed by qRT-PCR after immunoprecipitation.

Jmjd3 binding was assessed in undifferentiated wild-type ESCs and at day four and eight of neural differentiation. Jmdj3 was found to be recruited to the regulatory regions of both Pax6 and Sox1 already at day four with a substantial increase at day eight (Figure 22a). On the Nestin promoter region binding of Jmjd3 was only detected at day eight.

Together with the differentiation impairment of Jmjd3-kd cells, these findings are consistent with the role of Jmjd3 as an activator of the neural specification program in ESCs. Thereby Jmjd3 acts directly both on genes that orchestrate this program, like for instance Pax6 and Sox1 and on genes encoding for structural components of neural precursors, like Nestin.

Although on day seven of differentiation the majority of the cells has acquired neural identity the culture is still heterogeneous with persisting undifferentiated ESCs and differentiated non-neural cell types [78]. In order to confirm the specificity of Jmjd3

involvement in the induction of neural differentiation a systems that allows to purify neural precursors to homogeneity, the Sox1-GFP knockin ESC line (46C), was used [78]. In 46C ESCs the coding sequence for green fluorescent protein (GFP) is targeted to the endogenous Sox1 locus, which drives expression of the GFP reporter only upon neural induction and permits the isolation of GFP-positive neural precursors by FACS sorting. Using this reporter system, about 56% of GFP-positive neural precursors were recovered at day seven of monolayer differentiation (Figure 22b). ChIP assay on this highly homogeneous cell population confirmed the specific recruitment of Jmjd3 to the transcription start sites of Pax6, Nestin and Sox1, whereas no binding was detected to the promoter of the negative control Prolactin (Figure 22c).

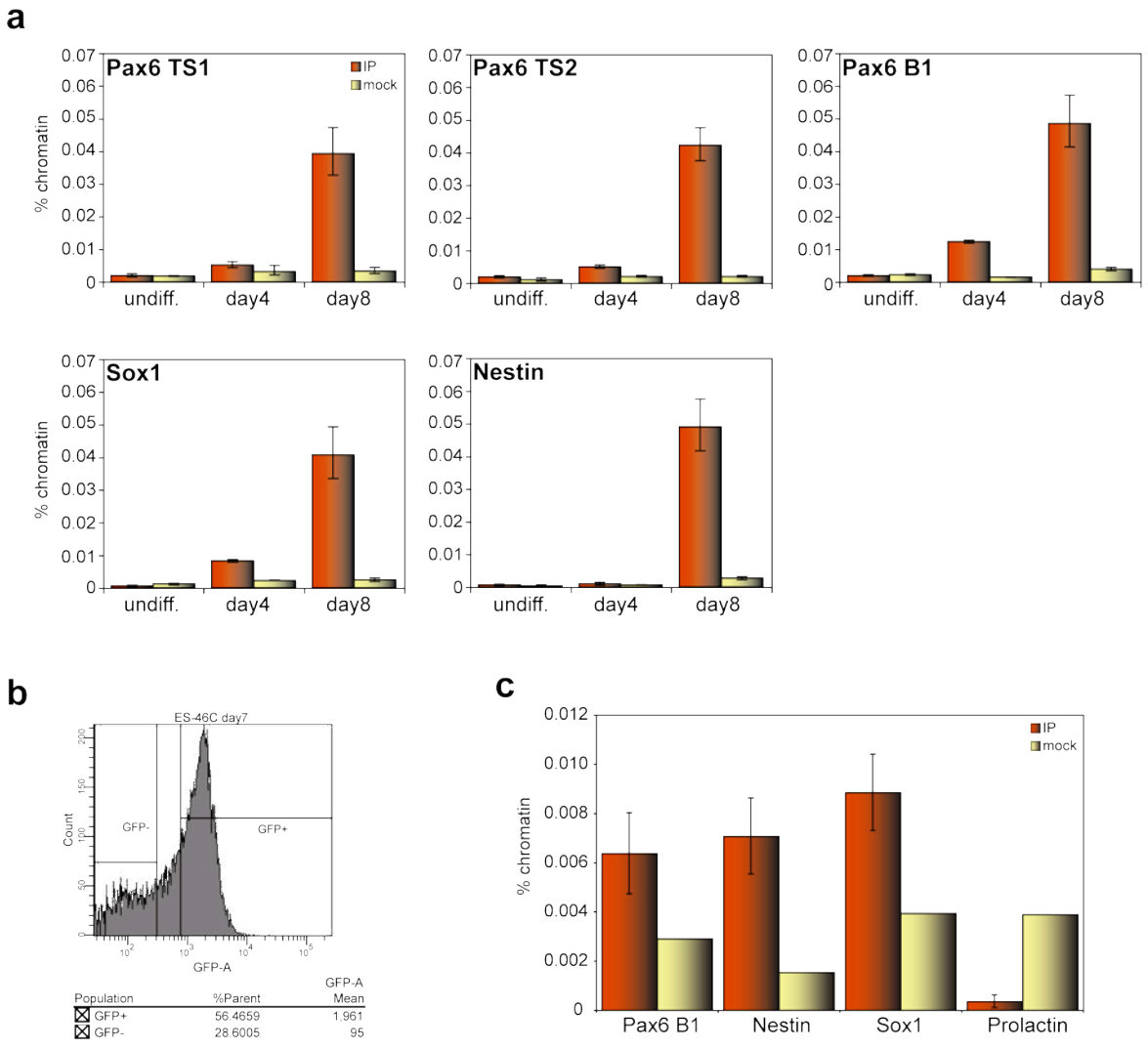

Figure 22. Jmjd3 is recruited to the promoter regions of Pax6, Nestin and Sox1 during neural differentiation. (a) ChIP analysis showing levels of Jmjd3 occupancy at the genomic regions of Pax6, Nestin

and Sox1 outlined in Figure 21 in differentiating wild-type ESCs. Levels of enrichment are shown as percentage of input chromatin. Error bars represent standard deviation of qRT-PCR triplicates. undiff.: undifferentiated ESCs, day 4 and day8: time points of differentiation protocol **(b)** FACS scan of Sox1-GFP ESCs at day 7 of monolayer differentiation. The background threshold was set with undifferentiated Sox1-GFP ESCs. **(c)** ChIP assay showing Jmjd3 recruitment to Pax6, Nestin and Sox1 in sorted GFP-positive neural precursors. The Prolactin gene promoter does not show any enrichment for Jmjd3. Levels of enrichment are shown as percentage of input chromatin. Bars represent the mean ± S.E.M. of three independent immunoprecipitations.

1.5 Jmjd3 targets show distinct patterns of H3K27 methylation and expression

In ESCs Pax6, Nestin and Sox1 are marked by H3K4me3/H3K27me3 bivalent domains [30,48], a chromatin signature that is dynamically regulated during differentiation. Hence, the observation that Jmjd3 is recruited to their promoters led to the prediction that Jmjd3 controls the H3K27 methylation state of these genes during differentiation. To this end, H3K27me3 levels at the transcription start sites (TSS) of Pax6, Nestin and Sox1 were assessed by ChIP analysis in undifferentiated ESCs, at day eight of monolayer differentiation and in NSCs. This detailed analysis confirmed the finding [30,48] that in NSCs the bivalent domains of Pax6 and Nestin are resolved by loss of H3K27me3, whereas Sox1 retained the H3K27me3 mark (Figure 23).

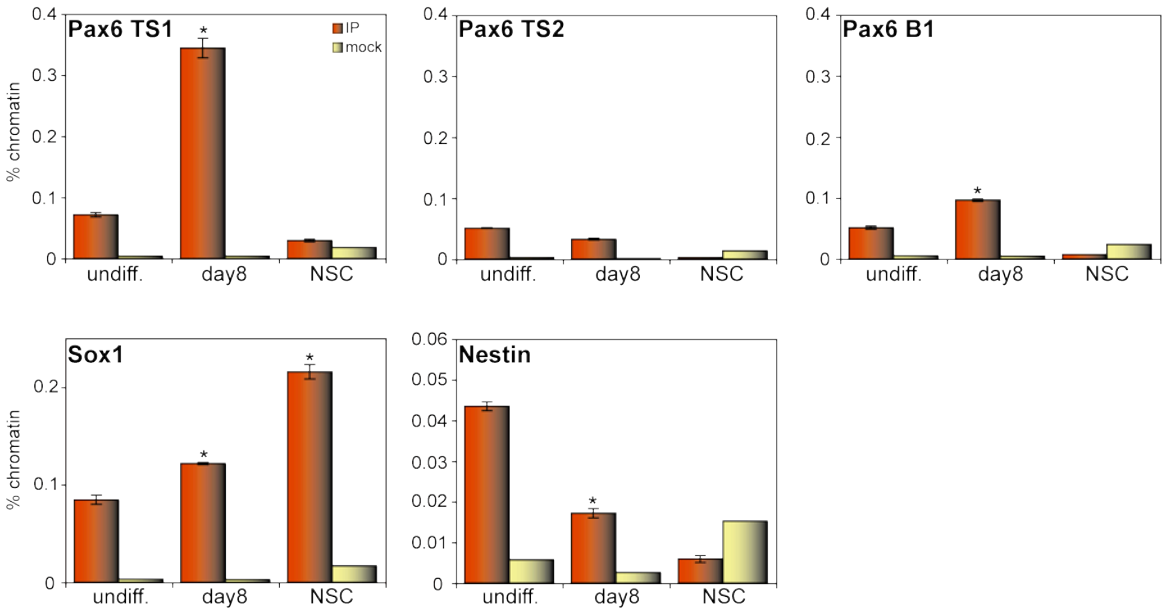

Figure 23. Analysis of H3K27me3 at the Pax6, Nestin and Sox1 genes during neural differentiation. ChIP analysis showing levels of H3K27me3 enrichment at the genomic regions of Pax6, Nestin and Sox1

outlined in Figure 21 in differentiating wild-type ESCs. Levels of enrichment are shown as percentage of input chromatin. Bars represent the mean ± S.E.M. of three independent immunoprecipitations. Asterisks indicate statistically significant differences as compared to undifferentiated cells, $p<0.01$ (ANOVA). undiff.: undifferentiated ESCs, day8: eight days after the beginning of the differentiation protocol, NSC: neural stem cells.

For Pax6 H3K27me3 levels showed a significant increase both upstream of the first transcription start site (TS1) and downstream of the second transcription start site (B1), whereas the basal levels of H3K27me3 upstream of the second transcription start site (TS2) did not change during the first eight days of differentiation. It is noteworthy that all three regions showed a bivalent domain dynamics with selective loss of H3K27me3 in NSCs and progressive recruitment of Jmjd3. Apparently in the case of Pax6 initial Jmjd3 binding is without consequences on H3K27me3 levels and complete demethylation is observed only in NSCs, possibly to stabilise and sustain its expression. This suggests either the existence of mechanisms responsible for a late activation of the demethylation activity of Jmjd3, for instance the binding of additional transcription factors and cofactors or the involvement of another H3K27me3 demethylase, a possibility which cannot formally be ruled out at this stage.

In the case of Sox1, whose expression is highest at days six to eight and is absent in NSCs, the ChIP results showed a small but significant increase in H3K27me3 levels already at day eight and a much greater increase in NSCs. These data suggest that high levels of H3K27me3 may lock Sox1 expression in the repressed state in NSCs, while lower levels may still allow its upregulation at day eight, indicating that H3K27me3 by itself might not correlate directly with the transcriptional state. This finding provides support for the assumption that the H3K27me3 status contributes to transcriptional output in combination with other histone modifications and regulatory signals. Moreover, the observation that the progressive upregulation of Pax6 and Sox1 expression coincides with an increase in H3K27me3 levels at their regulatory regions reveals that the presence of H3K27me3 is

compatible not simply with basal transcription but also with increases in transcriptional activity, suggesting that the H3K27 methylation status may fulfil different regulatory functions at different genes and in different cellular contexts.

Finally, at the Nestin transcription start site the progressive reduction of H3K27me3 during differentiation coincides with Jmjd3 occupancy suggesting a direct and causal link between Jmjd3 recruitment and H3K27me3 demethylation. In order to prove this hypothesis, the H3K27me3 status at the Nestin transcription start site was probed in Jmjd3-depleted cells. As shown in Figure 24, whereas in wild-type cells H3K27me3 decreased by about 60% at day seven of differentiation, in Jmjd3-kd clones it remained at the same level observed in undifferentiated ESCs. Normalisation of H3K27me3 levels to total histone H3 confirmed the higher levels of H3K27me3 on the Nestin promoter at day seven of differentiation in the absence of Jmjd3 compared to wild-type cells (Figure 24b), thus excluding that the differences in the H3K27me3 level are caused by variations in the nucleosome density.

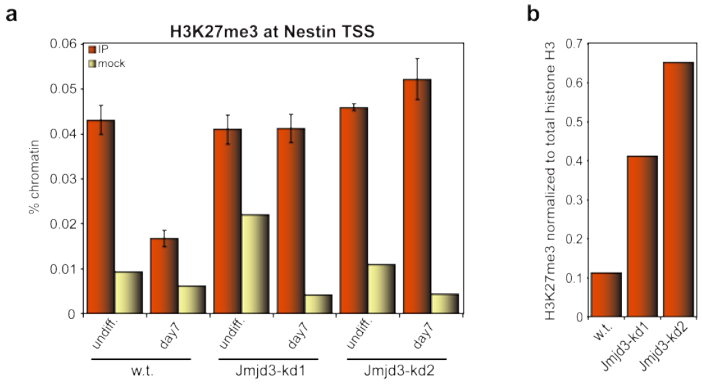

Figure 24. Jmjd3-kd cells fail to demethylate H3K27me3 on the Nestin promoter during neural differentiation. (a) ChIP analysis showing levels of H3K27me3 on the Nestin promoter in wild-type (w.t.) and Jmjd3 knockdown cells in the undifferentiated state (undiff.) and at day seven of monolayer differentiation. Levels of enrichment are shown as percentage of input chromatin. Bars represent the mean ± S.E.M. of three independent immunoprecipitations. **(b)** Levels of H3K27me3 enrichment at the Nestin promoter on day seven of differentiation (shown in Figure 24a) normalised to total histone H3.

This result provides a functional demonstration that Jmjd3 demethylates H3K27me3 at the Nestin promoter during the neural specification process in ESCs.

In conclusion, these studies establish Jmjd3 as H3K27me3 demethylase required for neural commitment. The dynamics of H3K27 demethylation and its correlation to transcriptional activity appear to follow distinct gene-specific patterns and prompt further investigations into the changes of this chromatin mark at the onset of differentiation.

2 Functional characterisation of Jmjd3 *in vivo*

2.1 Constitutive inactivation of Jmjd3 *in vivo* based on a gene trap approach

To investigate the role of Jmjd3 *in vivo* we inactivated it in the mouse through a constitutive knockout allele generated by gene trap mutagenesis. This technique generates randomly loss-of-function mutations and can often report at the same time the expression pattern of the mutated gene. Gene trap ESC lines are freely available through the International Gene Trap Consortium (IGTC, http://www.genetrap.org/). We identified in the public database an ESC line in which according to the posted sequence tag the gene trap insertion had occurred in the first intron of Jmjd3. The line with the name XB814 had been generated by introducing the pGT0pfs gene trap vector into E14Tg2α ESCs derived from the 129/Ola strain. The pGT0pfs vector contains a splice acceptor site from mouse *engrailed-2* (sA) and a promoterless lacZ-neomycin phosphotransferase fusion (βgeo) followed downstream by a simian virus-40 polyadenylation signal [97-99]. Since Jmjd3 is expressed in ESCs, integration of this cassette into the first intron is expected to produce a fusion transcript between the first exon of Jmjd3 and the βgeo cassette, resulting in truncation of the nascent transcript and hence in a loss of the functional allele (Figure 25).

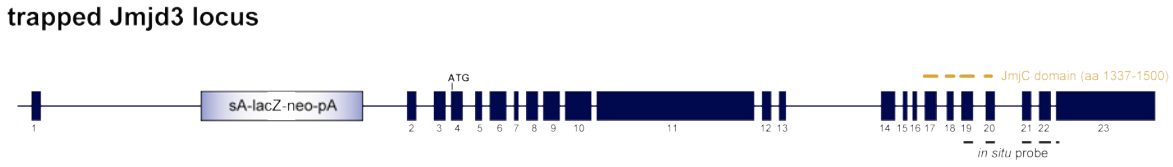

Figure 25. Scheme of the trapped Jmjd3 locus. Shown are exons and the trap cassette, which comprises a splice acceptor (sA), a lacZ-neo fusion and a polyadenylation signal (pA). Jmjd3 expression was assessed by RNA *in situ* hybridisation. The probe hybridised to the mRNA sequence corresponding to exons 19 to 23. Exons 17 to 20 encode for the JmjC protein domain.

2.1.1 Mapping the integration site of the gene trap vector

The feeder-independent XB814 ESCs were grown in standard ESC culture conditions in the presence of LIF and serum. To confirm Jmjd3 as the trapped gene and to identify the exact insertion point of the gene trap vector a PCR strategy was set up. The PCR was based on a reverse primer located in the trap cassette and four forward primers annealing at different sites within intron one of Jmjd3 (Table 9).

Table 9. PCR primers used to map the gene trap insertion site.

Name	Sequence (5'-3')
J3GTi-1	TCTGCTGTAACCCACTGCTG
J3GTi-2	GGAATGTCATGCTTCACTGCCAAG
J3GTi-3	GTCTGGTGTCTTTGGTCGTCCAG
J3GTi-4	GCACTTGACCACAGTTTAGCGT
GTbgeo	AGTATCGGCCTCAGGAAGATCG

All four primer pair combinations yielded a PCR product, which was progressively shorter the closer the forward primer was located with respect to the trap cassette, thus confirming that the insertion had indeed occurred in Jmjd3 and indicating that the insertion point is in the 3' region of intron one (Figure 26). The shortest amplicon was cloned into a TOPO® vector and subsequent sequence analysis identified the insertion point of the gene trap vector at bp position 4187 of intron one.

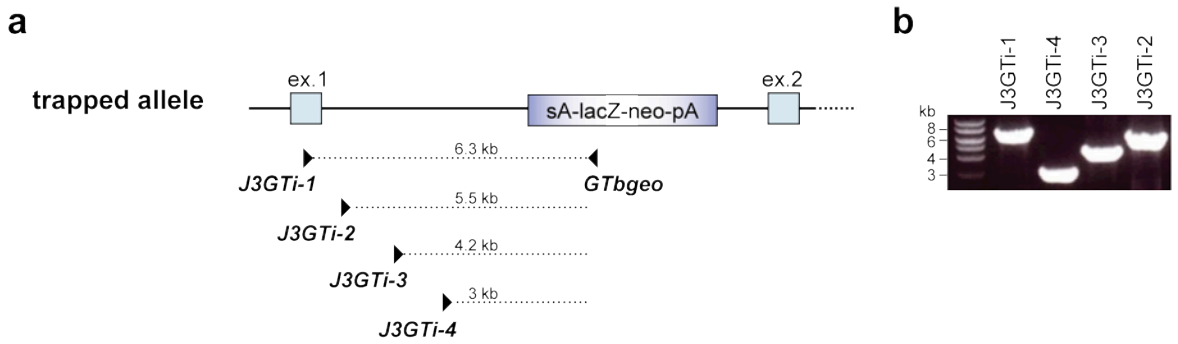

Figure 26. Identification of the insertion site of the gene trap vector by PCR. Four forward primers, annealing to different regions in exon one and intron one, respectively, were used in combination with a reverse primer located in the trap cassette. All PCR reactions yielded a product, which was progressively

shorter the further downstream the forward primer annealed in intron one, demonstrating that the insertion of the trap cassette had occurred in the 3' region of intron one.

2.1.2 Setting up the genotyping strategy for the trapped Jmjd3 allele

Having identified the insertion point of the trap cassette in intron one of Jmjd3, a triplex PCR-based strategy was designed to distinguish the trapped from the wild-type allele using the primers listed in Table 10.

Table 10. Primers for genotyping the Jmjd3 trap allele by PCR.

Name	Sequence (5'-3')
JBaygd	AGGATACAGGAGCCACGCG
JBaygr	TGACTCTCCACTCGATCACCC
GTrev	TCCGGAGCGGATCTCAAAC

The forward and the first reverse primer, both located in intron one flanking the insertion site, amplify a PCR product of 282 bp for the wild-type allele. Under the PCR conditions we set up, these primers do not yield the amplification of the 11.7 kb product from the trapped allele (Figure 27). The second reverse primer in the PCR reaction is located in the trap cassette and therefore only the trapped allele yields a PCR product, which is 259 bp and can be easily distinguished from the wild-type amplicon on a 3% agarose gel.

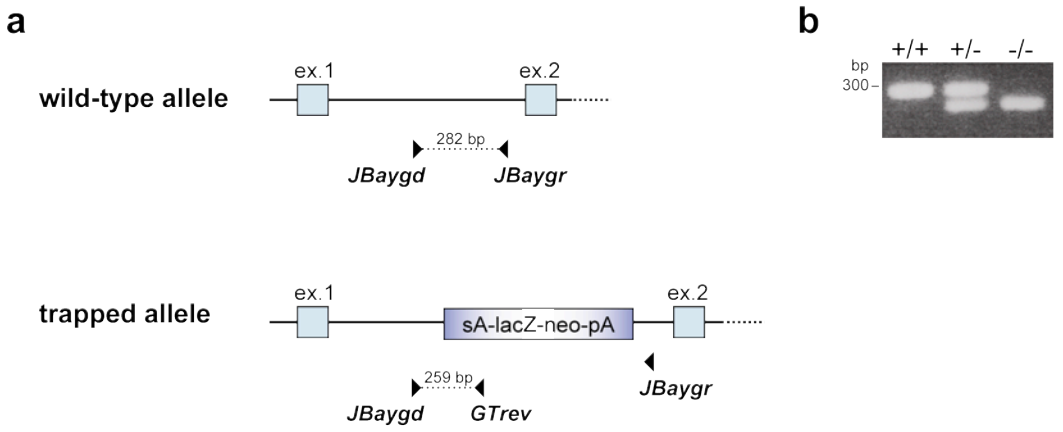

Figure 27. Genotyping of the Jmjd3 gene trap allele. (a) A triplex PCR-based strategy was used to identify the Jmjd3 gene trap allele. The scheme shows the position of the three primers. **(b)** The primer pair JBaygd/JBaygr amplified from the wild-type allele a 282 bp product, whereas the theoretical product of 11.7

kb from the trapped allele was not amplified. The primer pair JBaygd/GTrev yielded only from the trapped allele a product, which was 259 bp.

2.1.3 Generation of the XB814 mouse line

The XB814 mouse line was generated by injecting XB814 gene trap ESCs into C57BL/6 blastocycts. One male coat colour chimera was obtained and crossed to wild-type C57BL/6 females to transmit the trapped Jmjd3 allele through the germline. Germline transmission was confirmed by PCR analysis on genomic DNA extracted from tail biopsies.

2.1.4 Jmjd3$^{-/-}$ ESCs as tool to validate the Jmjd3 trap allele

We then sought to derive Jmjd3 ESCs homozygous for the trap allele as a valuable system that would allow us to dissect the function of Jmjd3 during neural commitment in greater detail. Furthermore, it would enable us to avoid the intrinsic limitations of RNAi, such as the incomplete knockdown of expression which resulted in the selection of cells with residual levels of Jmjd3 during the derivation of NSCs in monolayer conditions. XB814 mice, heterozygous for the trap allele, were intercrossed to obtain blastocysts which were used to derive stable ESC lines. From 16 blastocycts five ESC lines were established, of which two were wild-type, two were heterozygous and one was homozygous for the trap allele (Figure 28).

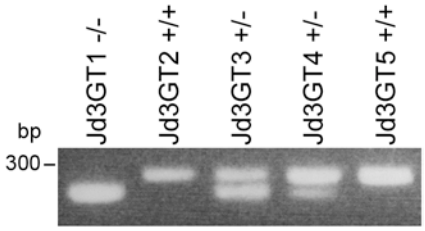

Figure 28. Genotyping of derived ESC lines. Five ESC lines were established from intercrosses of heterozygous XB814 mice. Genotyping analysis revealed that out of these five lines two were wild-type, two were heterozygous and one was homozygous for the trap allele.

Surprisingly, western blot analysis on ESC lysates revealed only a slight reduction in Jmjd3 protein level for the homozygous line compared to wild-type cells (Figure 29).

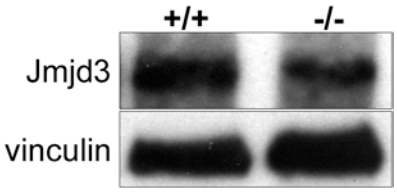

Figure 29. Protein level of Jmjd3 in ESC homozygous for the Jmjd3 gene trap allele. Western blot analysis for Jmjd3 expression shows only a mild decrease in homozygous Jmjd3 mutant ESCs (-/-) compared to the wild-type ESC clone (+/+). Vinculin served as loading control.

This result could be explained either by a non-functioning gene trap vector, by the existence of an additional transcription start site downstream of the inserted trap cassette or by skipping of the cassette through alternative splicing. The original XB814 gene trap ESCs proved to be, as expected, G418 resistant, and the resistance was further confirmed by the growth of the homozygous ESCs we established in ESC medium containing G418 (175 μg/ml). This observation allowed us to exclude the possibility that the trap cassette was non-functional, leading us to examine the potential existence of an alternative transcription start site within the 5'-untranslated region. Since the translation initiation codon (ATG) is mapped to exon four, the transcriptional status of the first five exons was analysed at the mRNA level using reverse transcription polymerase chain reaction (RT-PCR). For each of the four primer pairs the forward and reverse primer annealed in neighbouring exons, thus yielding a product only if the exons have been spliced together. A fifth primer pair located in the 3' region of the Jmjd3 mRNA spanning exons 14 to 16 served as internal control for the protein coding transcript (Table 11).

Table 11. RT-PCR primers to identify Jmjd3 transcript variants.

Localisation	Sequence (5'-3')
exons 1-2	*F:* AGGTTCCCCCAGGCACCATG *R:* GACTTCTCTATCCACAGAAA
exons 2-3	*F:* TTACTGAGGCGGAGACAAGG *R:* TGACAGTCTCTGGCCTTCTG
exons 3-4	*F:* AGAAGGCCAGAGACTGTCAC *R:* AAAGGCTTCCCGTGCAGAG
exons 4-5	*F:* TCTGCACGGGAAGCCTTTG *R:* TTAGGGTGCCCGGAGCTAC
exons 14-16	*F:* ACCACCATCGCTAAATACGC *R:* ACCTCTTGGCATCAGACAGG

The primer pair annealing to the transcript in which exon one is spliced to exon two yielded a product for wild-type cells, whereas no amplification was detected for homozygous ESCs (Figure 30). This result indicated that the transcription starting from exon one was efficiently disrupted by the trap cassette. The RT-PCR for the downstream exon combinations yielded products in the wild-type as well as in the homozygous ESCs, confirming the presence of an additional transcription starting site downstream of the trap cassette in intron one. In general the Jmjd3 mRNA level was slightly lower in homozygous cells compared to wild-type cells, which was in accordance with the reduced Jmjd3 protein level observed for the homozygous cells.

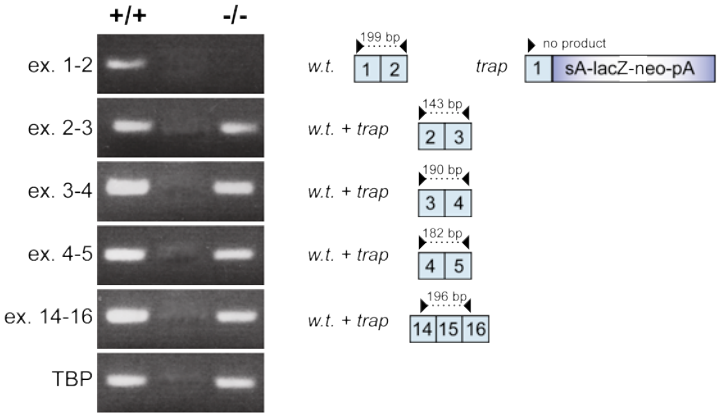

Figure 30. Identification of Jmjd3 transcript variants by RT-PCR. In Jmjd3$^{-/-}$ ESC no product was detected for the primer pair spanning exons one and two, thus indicating that the trap cassette efficiently traps the Jmjd3 transcript after exon one. All other primer combinations yielded a product in Jmjd3 mutant ESCs, demonstrating the presence of a second transcription start site downstream of the trap cassette in intron one. TBP served as housekeeping control.

Since overall the Jmjd3 protein level was similar between wild-type and homozygous ESCs we could not use the homozygous Jmjd3 gene trap ESCs as an experimental system to study the role of Jmjd3 in the context of differentiation.

Taken together, these findings show that this insertion of the gene trap vector in the Jmdj3 locus, at least at the onset of embryogenesis, did not generate a null mutation, but more likely resulted in a hypomorphic allele.

2.1.5 Jmjd3 mutants die at birth

When we intercrossed XB814 mice heterozygous for the trap allele we failed to obtain Jmjd3$^{-/-}$ pups at weaning age, i.e. three weeks after birth. We therefore hypothesised that homozygous mutants die either during embryonic development or sometime between birth and weaning. In order to assess whether this Jmjd3 allele was embryonic lethal, embryos from heterozygous intercrosses were dissected at different developmental stages between embryonic day (E) 10.5 and 18.5. Embryos homozygous for the trap allele were recovered at a normal Mendelian ratio for all time points up to E18.5, just before birth, suggesting that the lethality occurs at birth or during the first three weeks postnatally (Table 12).

Table 12. Distribution of genotypes between E10.5 and P0. Table showing the number of wild-type, heterozygous and homozygous genotypes of embryos at the indicated stage of development (E10.5-E18.5) and of neonates at P0. Out of 37 homozygous mutants genotyped at P0, 25 were born dead or died immediately after birth and 12 were initially alive but died within 24 h.

Embryonic day	Genotype +/+	+/-	-/-
E10.5	4 (15%)	16 (62%)	6 (23%)
E11.5	3 (33%)	5 (56%)	1 (11%)
E12.5	11 (38%)	11 (38%)	7 (24%)
E14.5	2 (13%)	9 (56%)	5 (31%)
E15.5	4 (44%)	2 (22%)	3 (33%)
E16.5	17 (19%)	45 (51%)	27 (30%)
E18.5	87 (27%)	157 (49%)	79 (24%)
P0	32 (25%)	58 (46%)	37 (29%) † 25 dead at birth * 12 died ≤24h

To determine the exact time point at which homozygous mice were dying, timed matings between heterozygotes were set up and neonates were thoroughly monitored from the moment they were born. Thereby special care was taken to disturb the delivery process as little as possible and to avoid any additional stress for the mother. Immediately after the female had given birth, neonates were briefly separated from the mother to take a small tail biopsy for genotyping and to mark them by injecting subcutaneously a drop of India ink. This strategy enabled us to genotype each newborn pup and to monitor it starting at birth.

The analysis revealed that about 70% of all homozygous mutants genotyped at P0 were born dead or died within minutes of delivery and only 30% of the mutants survived the first few hours (Table 12). Out of 12 mutants being followed, two were alive for about 24 h which was the longest survival time ever observed. The perinatal lethality was limited to the homozygous mutant genotype, as the dead pups were all homozygous mutants with the exception of one heterozygote found among the dead. Homozygous mutants started to appear paler in their skin colour immediately after birth and were less reactive upon light stimulation than their wild-type and heterozygous littermates. They were hunched and displayed sudden bouts of cramped movements, including gasping behaviour like efforts to breathe. The heart beat was irregular and none of the mutant pups showed an apparent milk spot, indicating the lack of feeding (Figure 31). Importantly, the mother showed normal nursing behaviour, including grooming and breastfeeding the pups, demonstrating that the monitoring procedure did not cause any distress to the mother and the neonates.

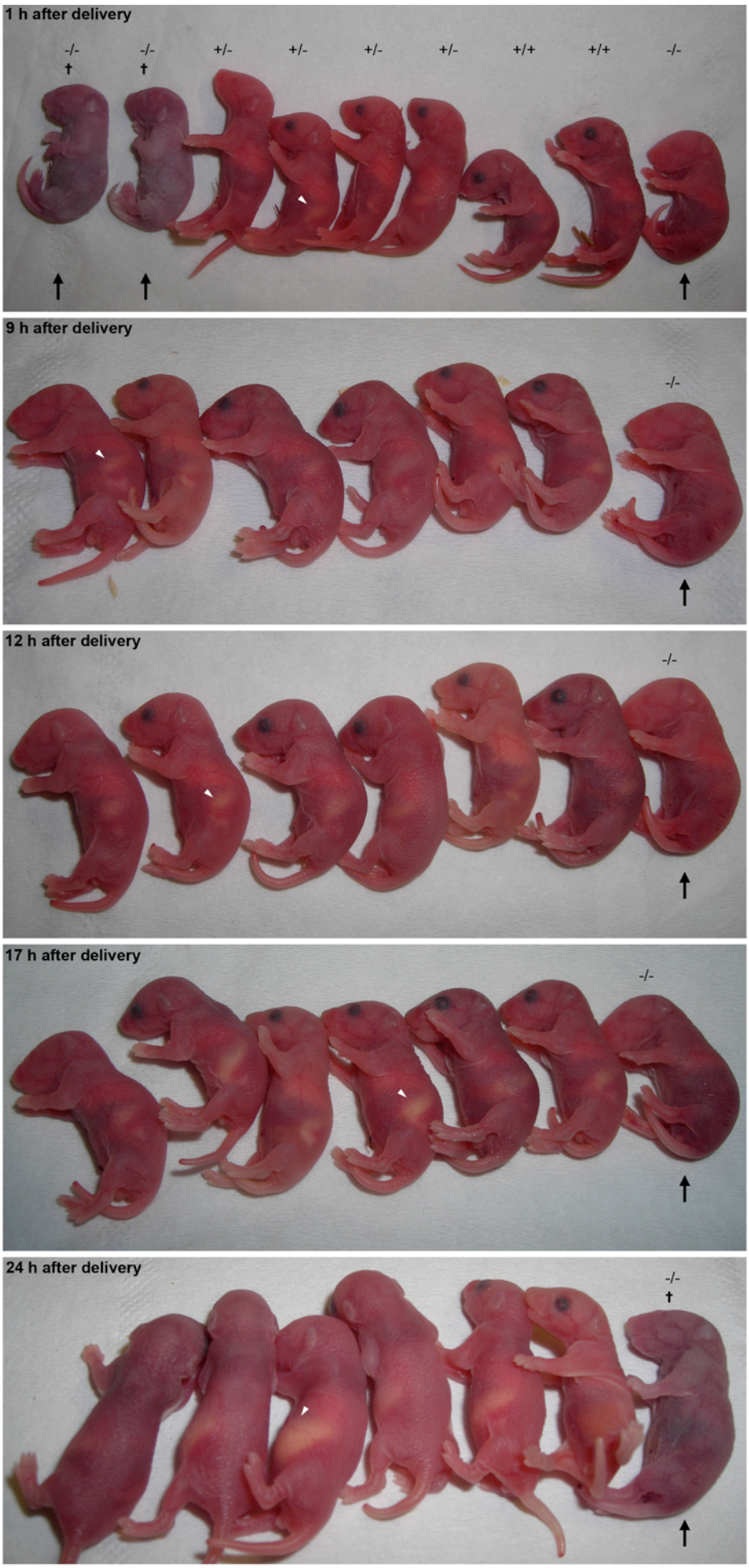
1 h after delivery
-/-
†
-/-
†
+/-
+/-
+/-
+/-
+/+
+/+
-/-
9 h after delivery
-/-
12 h after delivery
-/-
17 h after delivery
-/-
24 h after delivery
-/-
†

Figure 31. Jmjd3$^{-/-}$ mutants have a perinatal lethal phenotype. A litter of nine newborn pups was closely observed for one day starting at birth. Two homozygous mutants were found dead one hour after delivery, a third mutant survived for about 20 h (black arrows). Wild-type and heterozygous littermates had milk in the stomach (white arrow heads), a clear sign of nursing, whereas the mutant has not fed. The mutant neonate suffered of gasping behaviour and became cyanotic with time as evident in the fourth panel (17 h after delivery).

Together, these results demonstrate that mice homozygous for the Jmjd3 gene trap allele die perinatally.

2.1.6 Jmjd3 is expressed in the developing brain during embryogenesis

To identify the cause of the perinatal lethality of Jmjd3 mutant mice we first analysed the expression pattern of Jmjd3 during late foetal stages. Since none of the available antibodies against Jmjd3 worked convincingly in immunohistochemistry the expression of Jmd3 was assessed at the transcript level using radioactive *in situ* hybridisation (in collaboration with Antonio Simeone, CEINGE, Napoli, Italy). *In situ* hybridisation was performed on sagittal and coronal embryo sections of developmental stages between E9.75 and E16 (Figure 32). Jmjd3 transcripts were detected by an anti-sense probe which hybridised to the 3' region of the Jmjd3 locus spanning exons 19-23. At E9.75 Jmjd3 expression was evident in all three primary brain vesicles of the neural tube, namely the hindbrain (Hb), the midbrain (Mb) and the forebrain (Fb). Signal was also detected in the spinal cord (Sc), the dorsal root ganglia (drg) and the ear vesicle (ev). One day later, the expression pattern remained unaltered with notable expression in the developing central nervous system (CNS) in particular the mesencephalon (Mes), the diencephalon (Di) and the telencephalon (Te). Furthermore, Jmjd3 transcripts were observed in the developing olfactory system comprising the olfactory epithelium (oe) and the nasal pit (np). From E12.5 to E16, the time of cortical neurogenesis, Jmjd3 expression was maintained in the CNS with the highest levels in the cerebral cortex (cx), basal ganglia (Bag), dorsal midbrain and

cerebellum (cb). At E16 Jmjd3 was present also throughout other organs such as kidney (ki), lung (lu) and stomach (st).

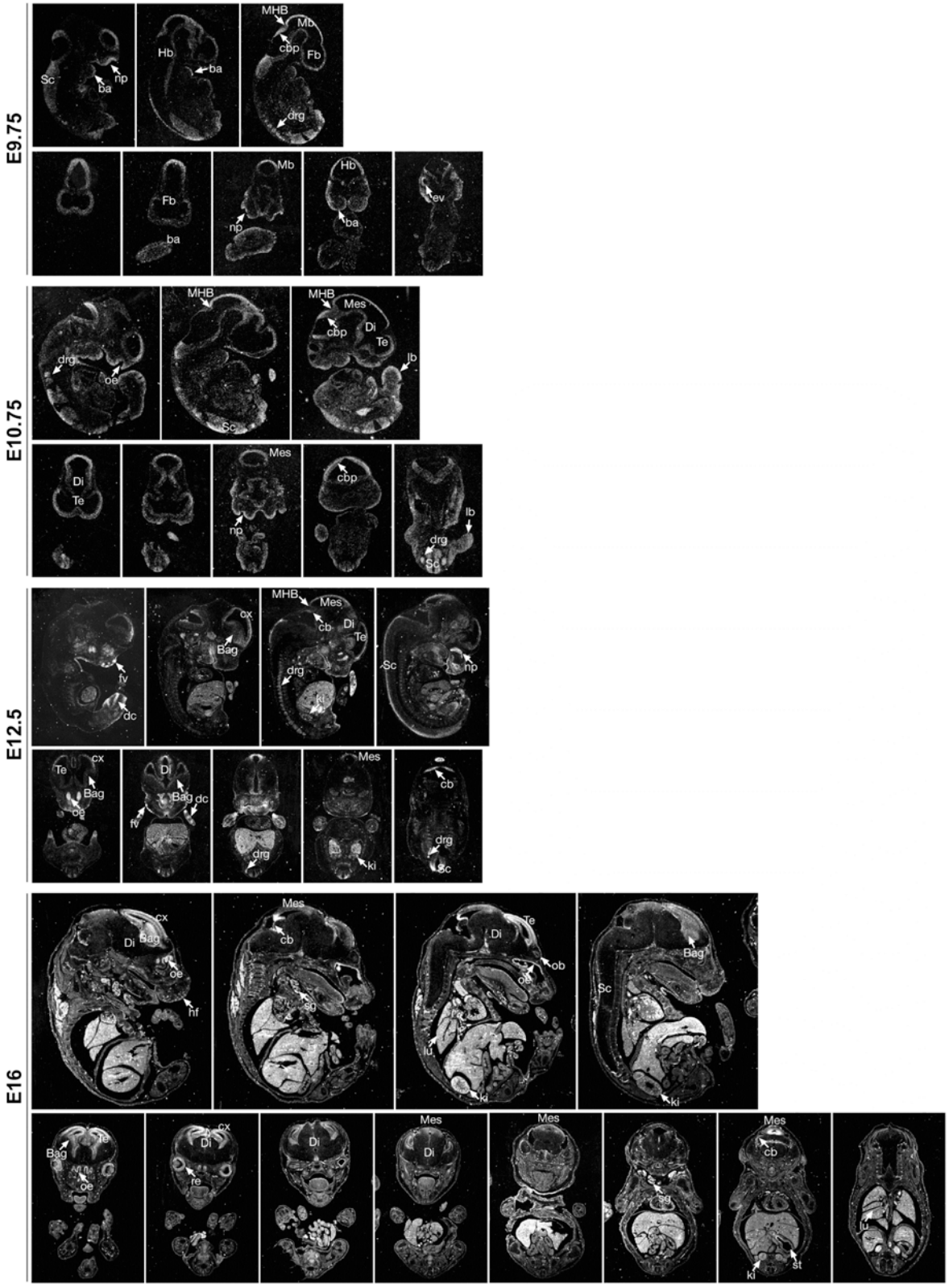

Figure 32. Radioactive *in situ* hybridisation for Jmjd3 in mouse embryos at different developmental stages. For each embryonic stage, the panel consists of two rows representing sagittal and coronal sections, respectively. In summary, Jmjd3 expression was predominantly detected in structures of the developing CNS.

Regions of specific signal are indicated by the following abbreviations: *ba:* branchial arch, *Bag:* basal ganglia, *cb:* cerebellum, *cbp:* cerebellar primordium, *cx:* cortex, *dc:* digit cartilage, *Di:* diencephalon, *drg:* dorsal root ganglia, *ev:* ear vesicle, *Fb:* forebrain, *fv:* follicle of vibrissa, *Hb:* hindbrain, *hf:* hair follicle, *ki:* kidney, *lb:* limb bud, *lu:* lung, *Mb:* midbrain, *MHB:* midbrain-hindbrain border, *Mes:* mesencephalon, *np:* nasal pit (olfactory placode), *ob:* olfactory bulb, *oe:* olfactory epithelium, *re:* neural retina, *Sc:* spinal cord, *sg:* salivary gland, *st:* stomach, *Te:* telencephalon.

In summary, this analysis showed that Jmjd3 was predominantly expressed in the developing CNS of late-stage embryos. Specifically, Jmjd3 expression was substantially upregulated between E10.5 and E16.5 and displayed at E16.5, at the peak of neurogenesis, a specific pattern in the cortex and the dorsal midbrain.

2.1.7 Jmjd3 expression is absent in homozygous mutant embryos at E16.5

To assess Jmjd3 expression in mutant animals we dissected embryos at E16.5 and performed *in situ* hybridisation on wild-type and homozygous mutant littermates. Wild-type embryos displayed the expression pattern described above, with the strongest signal in the cortex, basal ganglia, midbrain and cerebellum and organs such as liver, lung and kidney, whereas on sections of Jmjd3$^{-/-}$ foetuses the overall signal was drastically reduced and almost undetectable, evidencing the absence of the Jmjd3 transcript, in particular the sequence region encoding for the JmjC domain (Figure 25Figure 33). This observation was the formal proof that the trap cassette was functional *in vivo* by efficiently trapping and truncating the endogenous Jmjd3 transcript, suggesting that the Jmjd3 trap allele is a strong hypomorphic allele *in vivo*.

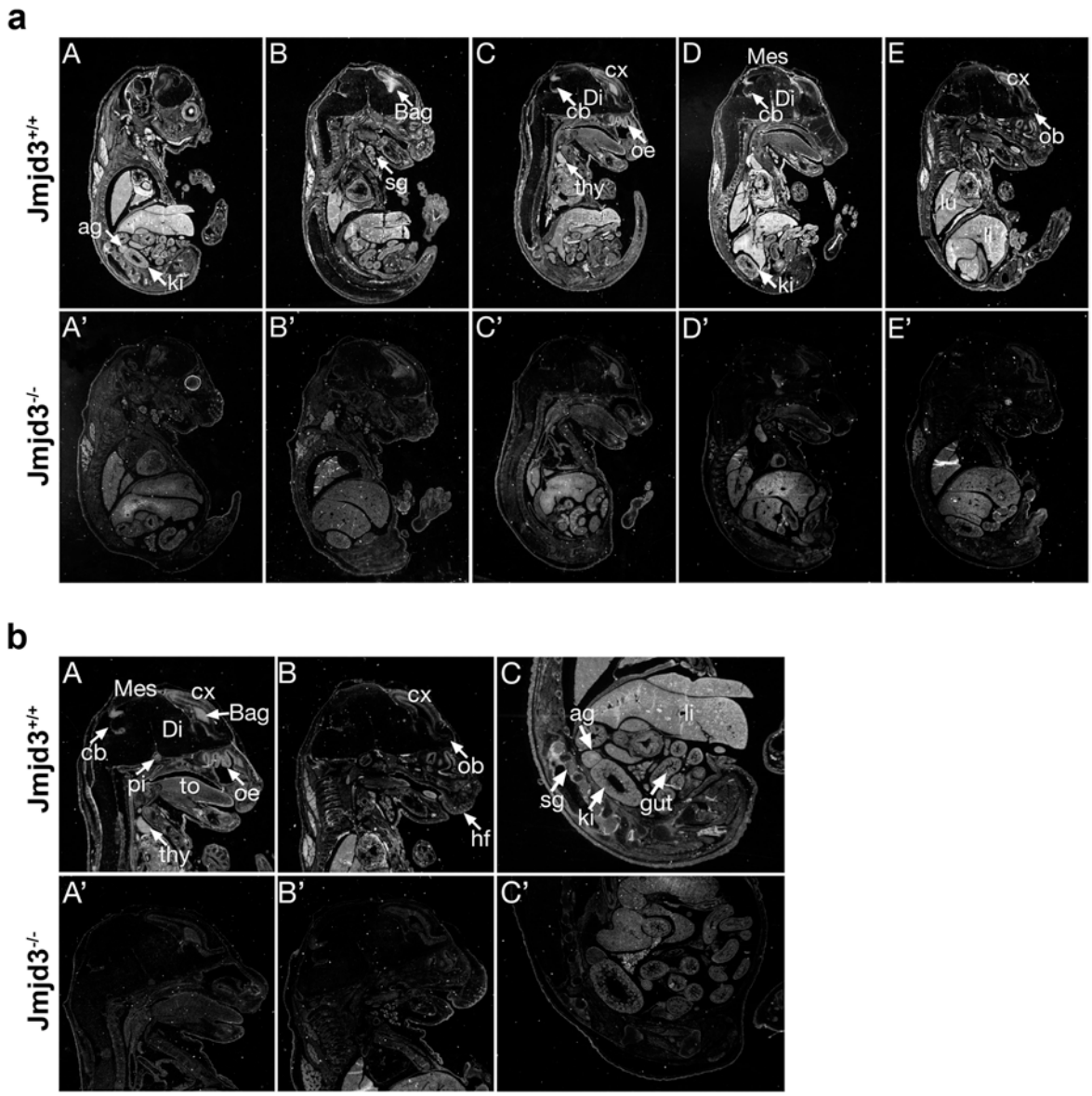

Figure 33. Jmjd3 transcript is absent in homozygous mutant foetuses at E16.5. RNA *in situ* hybridisation showing Jmjd3 expression on serial sagittal sections of wild-type ($Jmjd3^{+/+}$) and homozygous mutant ($Jmjd3^{-/-}$) embryos at E16.5 of embryogenesis. **(a)** $Jmjd3^{+/+}$ embryos (upper row) showed Jmjd3 expression in regions of the brain, like for instance cortex, cerebellum, midbrain and the olfactory system and in organs such as liver, lung and kidney. In $Jmjd3^{-/-}$ mutants (lower row) almost no signal was detected, indicating the absence of the Jmjd3 transcript. **(b)** Close-ups of (a) showing the head (A, B, A', B') and the organs of the abdominal cavity (C, C'). Regions of specific signal are indicated by the following abbreviations: ag: adrenal glands, *Bag:* basal ganglia, *cb:* cerebellum, *cx:* cortex, *Di:* diencephalon, *gut:* gut, *hf:* hair follicle, *ki:* kidney, *li:* liver, *lu:* lung, *Mes:* mesencephalon, *ob:* olfactory bulb, *oe:* olfactory epithelium, *pi:* pineal gland, *sg:* salivary gland, spinal ganglia, *thy:* thymus, *to:* tongue.

2.1.8 Histological analysis of Jmjd3 mutants

To investigate the cause of the perinatal lethality of homozygous mutants we carried out a thorough histological examination of the main vital organ systems. Wild-type and

homozygous mutant neonates were fixed in 4% formaldehyde immediately after birth and further processed for hematoxylin and eosin (H&E) staining on serial sections. The skin was well developed and displayed normal keratinocyte differentiation. We therefore excluded that defects in skin barrier function could cause perinatal lethality through transepidermal water loss. Further, there were no malformations or abnormalities in the entire gastrointestinal tract that could lead to feeding, digestion or absorption difficulties. The musculoskeletal system and the peripheral respiratory apparatus, including lungs, ribcage and diaphragm were also free from alterations in morphology or architecture. Liver and the hematopoietic organs bone marrow, spleen and thymus appeared also to be normally developed.

Histological analysis of the brain revealed instead that the cerebellar cortex of Jmjd3$^{-/-}$ newborn mice had a moderate decrease in foliation in comparison to wild-type littermates (Figure 34). This mutant phenotype was exhibited with a variable penetrance and could however not explain the neonatal lethality of the homozygous mutant mice, as the cellular organization and neural circuit of the mouse cerebellum develop mostly postnatally.

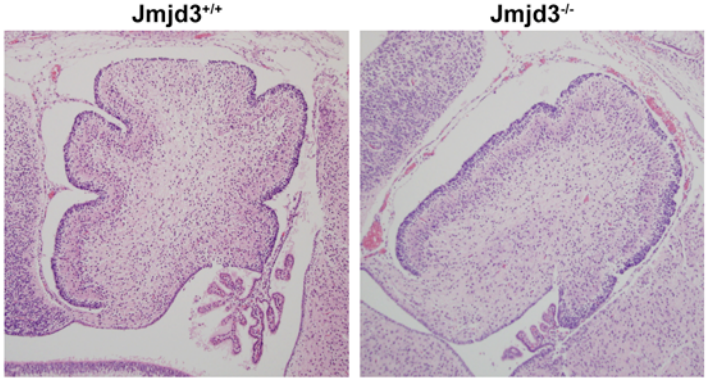

Figure 34. Jmjd3$^{-/-}$ mutants exhibit a moderate cerebellar afolia. H&E staining of a section of the cerebellum of newborn mice with wild-type (Jmjd3$^{+/+}$) and homozygous mutant (Jmjd3$^{-/-}$) genotype, respectively.

Taken together, this analysis showed that in Jmjd3$^{-/-}$ mice the vital organs were histologically normal with no gross abnormalities in structure and morphology.

We therefore undertook a systematic analysis of other possible causes of perinatal lethality. After birth, newborns must adapt quickly to new metabolic requirements and regulate their own energy homeostasis. Studies have shown that defects in glucose homeostasis can cause symptoms such as severe hypoglycemia that are associated with low survival of newborn mice [100-101]. In order to examine whether Jmjd3$^{-/-}$ mice die of hypoglycaemia, we measured the blood glucose level of neonates immediately after birth. To make sure that for all mice the blood glucose was measured under nonfeeding conditions, the newborns were separated from the mother as soon as she completed delivery. The animals were then decapitated and the blood glucose level was measured for each pup with no knowledge of the genotype, using a standard strip-based glucometer assay. The average blood glucose level of Jmjd3 mutants (43 mg/dl, n = 6) was similar to that of wild-type littermates (50 mg/dl, n = 12) and to values published in the literature, thus excluding hypoglycaemia as the cause of the perinatal lethality.

2.1.9 Jmjd3$^{-/-}$ mutants fail to breathe during the perinatal period

Respiratory failure is another common cause of perinatal lethality and could explain our observations that at birth Jmjd3 mutants showed few and irregular breathing movements, turned cyanotic and died within minutes after delivery. Moreover, the only two neonates that survived long enough to be followed also showed evident defects in breathing behaviour.

Breathing is a vital and complex motor behaviour in mammals that regulates gas exchange in the lungs to maintain metabolic processes and control pH. Shaped through evolution by the constrain to be fully functional at birth, development of the respiratory network is completed during embryogenesis with the first signs of organised activity detected at late prenatal stages [102-106]. From the moment of birth, the correct function of the neural network generating rhythmic respiratory movements is crucial to ensure neonatal survival

by regulating airflow into and out of the lungs and maintaining constant blood oxygenation. Physiological and anatomical studies revealed that respiratory rhythmogenesis relies on the activity of a brainstem respiratory rhythm generator (RRG) Figure 35). In fetal and neonatal rodents, the RRG is composed of two distinct, but functionally coupled oscillators located in the ventrolateral part of the rostral medulla: the preBötzinger complex (preBötC) [107] and the retrotrapezoid nucleus/parafacial respiratory group (RTN/pFRG) [108-110]. The RTN/pFRG is a small region near the medullary surface ventral to the facial motor nucleus (nVII) and contains chemosensitive neurons that respond to CO_2 through the detection of changes in pH [111-112]. Recent studies in mice showed that the embryonic parafacial (e-pF) oscillator (the embryonic forerunner of the RTN/pFRG) displays spontaneous rhythmic activity starting from embryonic day (E) 14.5 [113]. The preBötC is anatomically characterised as a heterogeneous population of glutamatergic interneurons in the ventral respiratory column, located beneath the nucleus ambiguus (Amb) [107,114-115]. The current view is that neurokinin-1 receptor (NK1R)-expressing rhythmic pacemaker neurons within the preBötC network form the cellular kernel for generating the respiratory rhythm required for driving inspiratory muscle activity [116-121]. The preBötC emerges independently of the e-pF and becomes active at E15.5, with the e-pF coupling to it [113,122]. A variety of additional neuronal groups in the hindbrain, including serotonergic and catecholaminergic brainstem neurons, neurons in the nucleus of the solitary tract (NTS) and the dorsal respiratory group and neurons of the pontine respiratory group, have been described to coordinate respiratory activity by processing information from peripheral and central sensory afferents and modulating neuronal input [123-126].

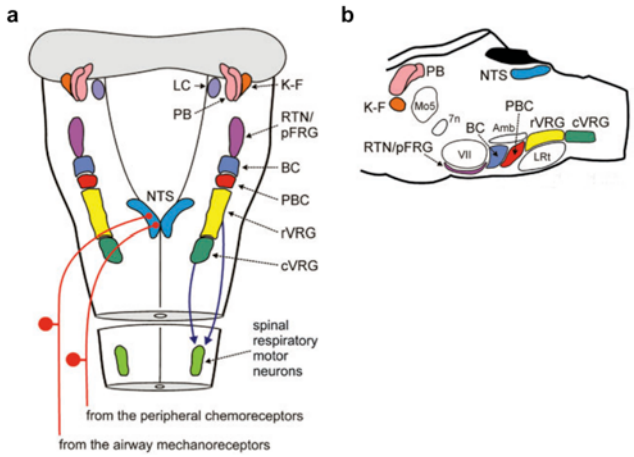

Figure 35. Neuroanatomy of the respiratory network in the rodent brainstem. Schematic drawings of the main groups of respiratory neurons in horizontal **(a)** and sagittal **(b)** views of the brainstem. *7n*: facial nerve, *Amb*: nucleus ambiguus, *BC*: Bötzinger complex, *cVRG*: caudal ventral respiratory group, *K-F*: Kölliker-Fuse nucleus, *LC*: locus coeruleus, *LRt*: lateral reticular nucleus, *Mo5*: motor nucleus of the trigeminal nerv, *NTS*: nucleus of the solitary tract, *PB*: parabrachial nucleus, *PBC*: preBötzinger complex, *RTN/pFRG*: retrotrapezoid nucleus and parafacial respiratory group, *rVRG*: rostral ventral respiratory group, *VII*: facial motor nucleus. From [127].

To investigate whether the perinatal phenotype of Jmjd3$^{-/-}$ mutants is due to breathing anomalies we performed physiological and histological analyses in collaboration with Gérard Hilaire (CRN2M, Marseille, France).

Embryos were exteriorised from uterine horns at E18.5 and assessed for their respiratory activity by recording *in vivo* breathing-associated pressure changes (plethysmography). Wild-type and heterozygous mice initiated, immediately upon exteriorization, breathing that consisted in a gasping-like behaviour for 2-5 min and was characterised by deep respiratory movements at a low frequency (about 2-5 c·min^{-1}) involving the entire body muscles and including wide mouth opening. Thereafter, they produced normal robust respiratory cycles at a faster rhythm (Jmjd3$^{+/+}$: 46 ± 7 c·min^{-1}, n = 10; Jmjd3$^{+/-}$: 45 ± 30 c·min^{-1}, n = 2). In contrast, all mutant neonates (n = 8) failed to show any signs of ventilation or respiratory efforts (Figure 36), like gasping, and died shortly after exteriorization.

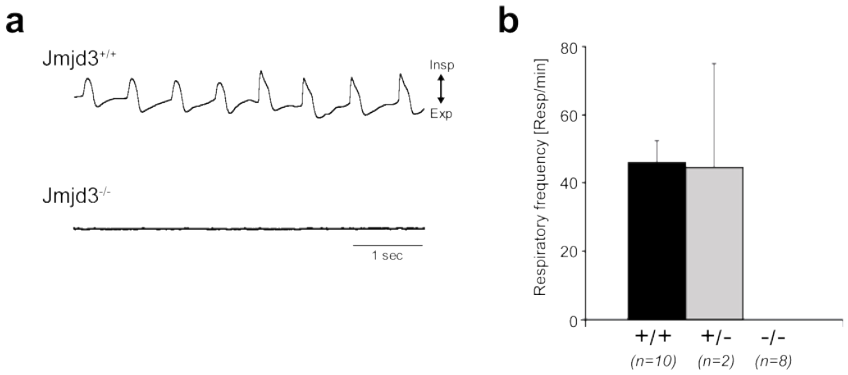

Figure 36. Jmjd3 mutants do not breathe *in vivo*. (a) Plethysmographic recordings of breathing activity *in vivo* from surgically delivered wild-type ($Jmjd3^{+/+}$) and mutant ($Jmjd3^{-/-}$) E18.5 embryos after caesarean section. All wild-type mice initiated respiratory cycles of inspirations (upward deflections) and expirations (downward deflections), whereas none of the $Jmjd3^{-/-}$ mice showed any sign of ventilation. **(b)** Quantification of breathing frequency in breaths per minute. Bars represent the mean ± S.E.M.of n mice.

To exclude that the primary cause for perinatal death could have been a heart failure which in turn could have determined respiratory fatigue, we then recorded electrocardiograms of embryos *in utero*. As shown in Figure 37, at E18.5, the heart was beating in both $Jmjd3^{+/+}$ (61 ± 9 $c \cdot min^{-1}$, n = 6) and $Jmjd3^{-/-}$ (102 ± 17 $c \cdot min^{-1}$, n = 5) embryos, thus excluding heart failure as a determinant of the perinatal phenotype of our mutants.

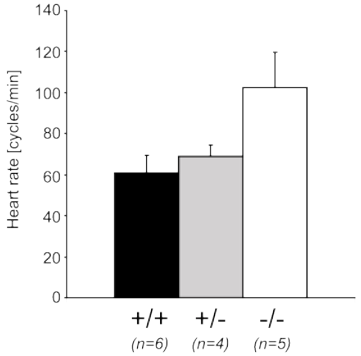

Figure 37. Jmjd3 mutants have normal cardiac activity. Heart rate of E18.5 embryos was monitored *in utero* by electrocardiography. Bars represent the mean ± S.E.M.of n mice.

Next, we assessed whether muscular or neuromuscular dysfunctions could cause the lack of ventilation in Jmjd3 mutants. Single electrical shocks were applied to the diaphragm or the phrenic nerve of either exteriorised or in *utero* embryos at E18.5. Electrical stimulations of the diaphragm or the phrenic nerve induced diaphragmatic contractions in

both wild-type and mutant embryos (data not shown), demonstrating that the contractile properties of the respiratory muscles were preserved in the mutants.

2.1.10 The respiratory rhythm generator is not functioning in Jmjd3$^{-/-}$ mice at E18.5

The absence of functional anomalies in the peripheral respiratory and cardiac systems in Jmjd3 mutants, pointed to a central respiratory defect. We therefore examined the respiratory rhythmic activity generated *in vitro* by the central respiratory network isolated in en bloc brainstem preparations at E18.5 [128]. Experiments were done in medullary-spinal cord preparations which produce rhythmic bursts of potentials in the fourth cervical root (C4), where the phrenic nerve exits to innervate the diaphragm. In preparations of wild-type (n = 6) and heterozygous (n = 14) embryos, rhythmic bursts of potentials were detected from the cervical phrenic roots at a phrenic burst frequency of 12 ± 4 c·min^{-1} and 8 ± 1 c·min^{-1}, respectively. Recordings performed on Jmjd3 mutant preparations (n = 8) revealed the absence of any rhythmic or tonic phrenic nerve activity (Figure 38).

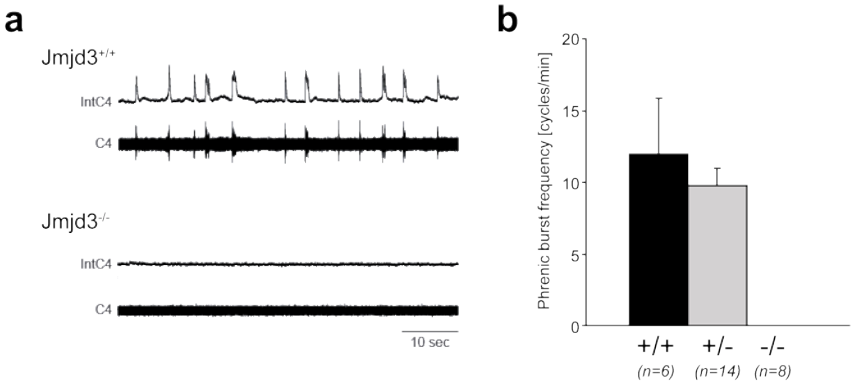

Figure 38. Jmjd3$^{-/-}$ brainstem preparations lack respiratory rhythmic activity *in vitro*. (a) Electrophysiological recordings of the phrenic burst activity *in vitro* in medullary-spinal cord preparations isolated from wild-type (Jmjd3$^{+/+}$) and mutant (Jmjd3$^{-/-}$) E18.5 embryos. Wild-type preparations showed a respiratory rhythmic activity, whereas mutant preparations failed to produce any phrenic nerve activity. Shown are the integrated (top traces) and raw (bottom traces) phrenic burst discharges. **(b)** Quantification of phrenic burst frequency. Bars represent the mean ± S.E.M.of n mice.

The lack of rhythmic phrenic bursts in Jmjd3$^{-/-}$ embryonic preparations could be the consequence of a defect either in respiratory rhythmogenesis or in synaptic transmission of

the medullary respiratory drive to the cervical phrenic motoneurons or of a combination of both defects. Therefore, we first analysed whether the phrenic motoneurons were able to respond to spinal synaptic inputs *in vitro*. The respiratory output pathways running from the medulla towards the phrenic motoneurons were activated by applying single electrical shocks to the spinal cord within the ventromedial and the ventrolateral spinal columns at the level of the second cervical segment. Each electrical shock induced a short latency response of the C4 phrenic motoneurons in both wild-type and mutant preparations. This analysis demonstrated that the C2-C4 pathway was functional and phrenic motoneurons were able to respond to spinal synaptic excitation in Jmjd3$^{-/-}$ mutants.

Second, to assess whether the phrenic motoneurons were responsive to synaptic inputs from the medulla, we applied single electrical shocks to the medulla at the level of the ventral respiratory column (VRC). In brainstem preparations, the synchronous activation of rhythmogenic neurons by single-shock electrical stimulation applied in the VRC during expiration shortens the expiratory period, triggers a phrenic inspiratory burst and resets the phase of bursts [129]. A response to electrical stimulation in the controlateral medulla was consistently observed in wild-type preparations (Figure 39a). By contrast, in mutant preparations single-shock electrical stimulation of the VRC did not induce a phrenic burst (Figure 39a). However, single-shock electrical stimulations in the contro- and ipsilateral medulla induced brief responses of phrenic motoneurons in mutant samples (Figure 39b, c). Repetitive stimulation (100 Hz for 3 s) of the VRC induced a long-lasting non-rhythmic discharge on the otherwise silent phrenic roots, which persisted for about 20 s (Figure 39d). Similarly, long-lasting phrenic discharges were induced by applying repetitive stimulation to the median raphe area of wild-type and mutant preparations.

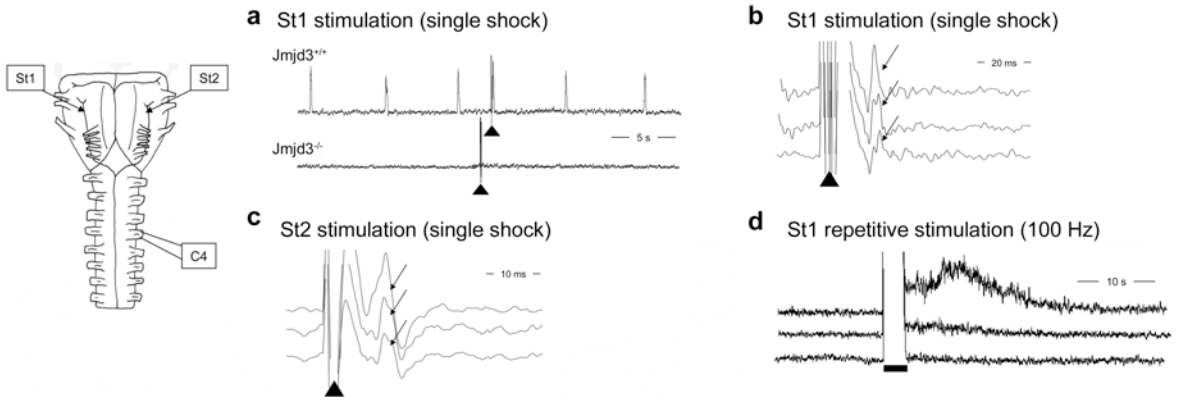

Figure 39. Phrenic motoneurons of Jmjd3$^{-/-}$ embryonic preparations were silent but could be activated by electrical stimulation of the medulla. Schematic drawing of the en bloc preparation showing controlateral (St1) and ipsilateral (St2) stimulation sites of the medulla and the C4 phrenic nerve recording. **(a)** Upper and lower traces show the presence and absence of rhythmic phrenic bursts (integrated discharges) in en bloc preparations from wild-type and Jmjd3$^{-/-}$ embryos, respectively, at E18.5. Applying a single-shock electrical stimulation (1 ms, 2 V; black triangle) in the controlateral medulla during expiration (silent phrenic interval) triggered a premature phrenic burst in wild-type but did not induce a phrenic burst in Jmjd3$^{-/-}$ preparations. **(b,c)** In Jmjd3$^{-/-}$ preparations, brief responses of phrenic motoneurons could be induced by single-shock of stimulation applied to the controlateral **(b)** and ipsilateral **(c)** medulla. Note that the amplitude of the phrenic responses was dependent on the stimulus strength (from top to bottom: 3, 1.5 and 1 V; pulse duration 1 ms) and the latency was longer for controlateral than ipsilateral sites (about 18 ms and 10 ms, respectively). **(d)** In Jmjd3$^{-/-}$ preparations, applying repetitive stimulation (100 Hz for 3 s; black bar) to the same site of the controlateral medulla induced long-lasting discharges (20 s) of the otherwise silent phrenic motoneurons, but no rhythmic phrenic bursts. The amplitude and the duration of the induced discharges was dependent on the stimulus strength (from top to bottom: 3, 1.5 and 1 V; pulse duration 1 ms).

Together these results showed that the VRC, when activated, could induce sustained discharges of the phrenic motoneurons, indicating that the synapses and the pathway between the medullary respiratory centres and the phrenic motoneurons were functional in Jmjd3$^{-/-}$ preparations. Given the ability of phrenic motoneurons to be activated by spinal as well as medullary synaptic inputs, the lack of C4 rhythmic bursting activity in Jmjd3 mutant mice was an indication for a silent or defective respiratory rhythm generator (RRG). The fact that no rhythmic respiratory phrenic bursts were detected during and after the long-lasting discharge induced by repetitive electrical shocks applied to the rostral ventrolateral medulla or the raphe area, suggested a defective rather than quiescent RRG in Jmjd3$^{-/-}$ neonates.

2.1.11 Jmjd3 is expressed in the respiratory network of the ventrolateral medulla

We next investigated whether Jmjd3 was expressed in the regions of the brainstem presiding over breathing regulation. To this end we performed *in-situ* hybridisation on sagittal wild-type E18.5 brain sections using a non-radioactive DIG-labelled probe. Jmjd3 expression was evident throughout the brainstem with the highest levels in the ventrolateral medulla. In order to localise the two main neuronal groups involved in respiratory rhythmogenesis, the preBötzinger complex (preBötC) and the retrotrapezoid nucleus/parafacial respiratory group (RTN/pFRG) we used immunohistochemical staining for neurokinin-1 receptor (NK1R). The comparison of the *in situ* hybridisation pattern of Jmjd3 with that of the NK1R staining by overlapping aligned images of adjacent sections identified Jmjd3-positive cells predominantly in the pontine nuclei, superior olive, facial motor nucleus (nVII) and the area of the preBötC (Figure 40).

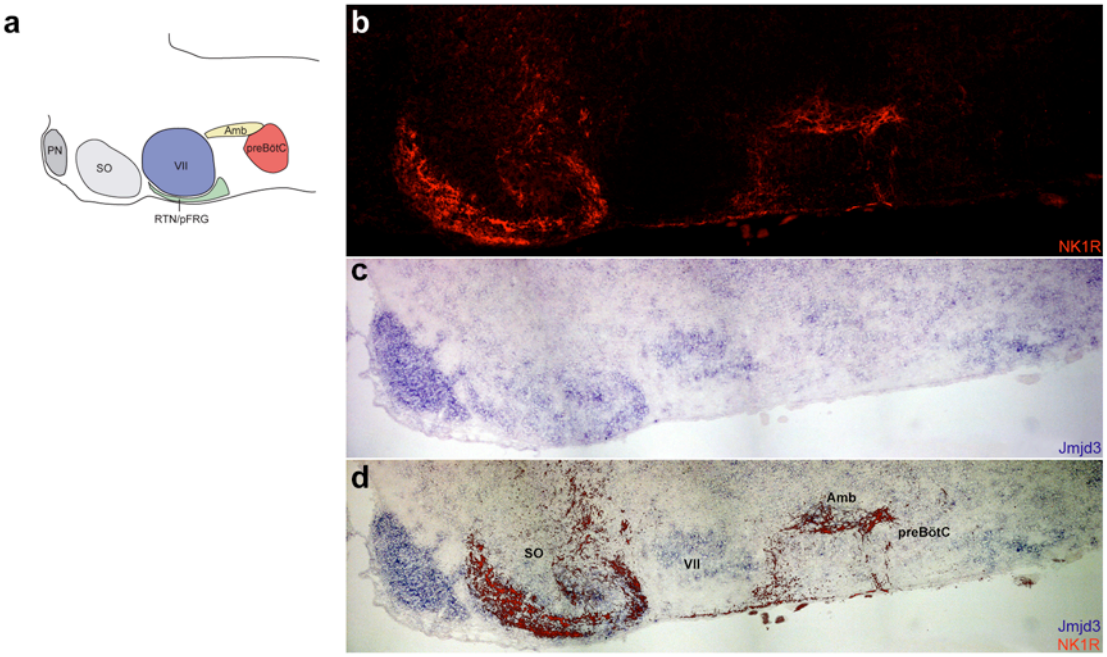

Figure 40. Jmjd3 is expressed in the preBötC. (a) Schematic drawing of the anatomic organization of the murine E18.5 brainstem in a sagittal view. *Amb*: nucleus ambiguus, *preBötC*: preBötzinger complex, *PN*: basilar pontine nuclei, *RTN/pFRG*: retrotrapezoid nucleus and parafacial respiratory group, *SO*: superior olive, *VII*: facial motor nucleus. **(b)** Immunohistochemistry for NK1R on 10 µm sagittal frozen section from wild-type E18.5 brainstem. **(c)** Jmjd3 *in situ* hybridisation on 10 µm sagittal frozen section from wild-type E18.5 brainstem, adjacent to the section used for NK1R staining in **b** and showing the same area. **(d)** Overlap

of **b** and **c** to reveal areas of Jmjd3 expression. Images were aligned with respect to the ventral limit of the medulla.

We then analysed Jmjd3 expression in brainstem sections of mutant E18.5 embryos by *in situ* hybridisation. Wild-type embryos (n = 2) displayed the expression pattern described above with notable expression in the ventral respiratory column, including the neural network of the preBötC, whereas in brainstems of mutant littermates (n = 3) the overall signal was almost undetectable (Figure 41). The lack of the Jmdj3 transcript in mutant brains, also in regions with high levels of Jmjd3 expression, such as the cerebral cortex, was in agreement with the observations described above on sections of E16.5 embryos which demonstrated the overall absence of Jmjd3 expression in mutant embryos.

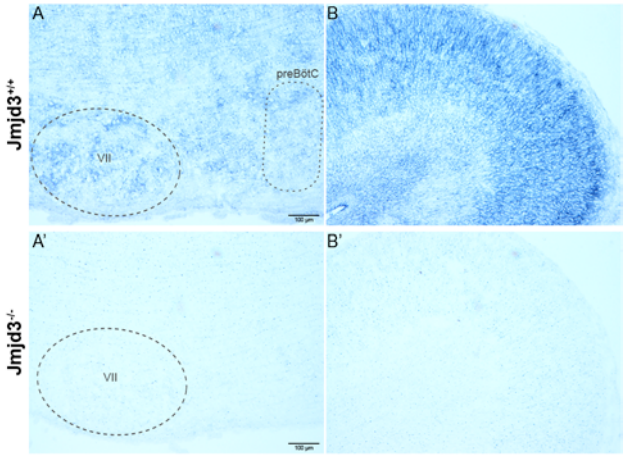

Figure 41. Jmjd3 transcript is absent in the brain of Jmjd3$^{-/-}$ embryos at E18.5. Jmjd3 *in situ* hybridisation on 10 µm sagittal frozen brain sections from wild-type (upper row) and mutant (lower row) E18.5 embryos. Jmjd3$^{+/+}$ embryos displayed Jmjd3 expression in the ventral respiratory column, including the VII motor nucleus and the preBötC (A). In comparison, the strongest signal was detected in the cerebral cortex (B). In Jmjd3$^{-/-}$ mutants the signal was almost undetectable in both, the rostral ventrolateral medulla (A') and the cerebral cortex (B'), indicating the absence of the Jmjd3 transcript.

In summary, these results showed that cells of the RRG, in particular the preBötC express Jmjd3 and that in Jmjd3$^{-/-}$ embryos the respiratory network is deprived of a Jmjd3 transcript encoding the catalytic JmjC domain.

2.1.12 The preBötC of Jmjd3$^{-/-}$ embryos shows neuro-anatomical anomalies at E18.5

Given the expression of Jmjd3 in the preBötC and the finding that Jmjd3$^{-/-}$ embryos lack respiratory rhythmogenesis at E18.5 we examined whether changes in neuronal architecture of the preBötC could explain the functional defect of the RRG in mutants. To this end, we performed immunohistochemical analysis of E18.5 embryos for the two markers that are commonly used and widely recognized to define the neural networks that are crucial for respiratory rhythm generation. The retrotrapezoid nucleus/parafacial respiratory group (RTN/pFRG) lays ventrally to the VII motor nucleus and is immunoreactive for the transcription factor Phox2b [113,130]. As shown in Figure 42 immunohistological staining for Phox2b on sagittal sections revealed a clearly identifiable group of Phox2b expressing neurons below the VII motor nucleus, corresponding to the RTN/pFRG area, in both wild-type and mutant E18.5 embryos.

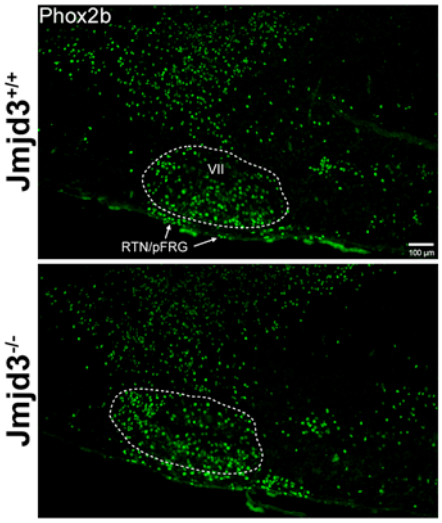

Figure 42. Jmjd3$^{-/-}$ mutants show normal Phox2b expression in the RTN/pFRG at E18.5. Immunohistochemical stainings for Phox2b on 10 µm sagittal frozen sections from wild-type and mutant E18.5 brainstems. Jmjd3$^{+/+}$ and Jmjd3$^{-/-}$embryos displayed immunoreactivity for Phox2b in the RTN/pFRG and the VII motor nucleus (dashed line).

The observation that Phox2b expression was not affected by the absence of Jmjd3 suggested that Jmjd3 was not required for normal development of Phox2b-expressing neurons in the RTN/pFRG group. The embryonic preBötC has been previously defined as

a diffuse group of NK1R expressing neurons extending below the nucleus ambiguus towards the ventral surface of the medulla, at the level of the inferior olive [116,122]. Immunostaining for NK1R on coronal sections confirmed this distribution of NK1R-expressing neurons in the preBötC of wild-type embryos (n = 7), whereas the corresponding area in Jmjd3$^{-/-}$ brainstems (n = 10) did not display the normal structure. As shown in Figure 43, a NK1R signal was detected below the nucleus ambiguus in mutant samples, but the intensity of the signal was weaker and the network was smaller with a distribution of NK1R-expressing neurons more diffuse and less structured than in wild-type samples.

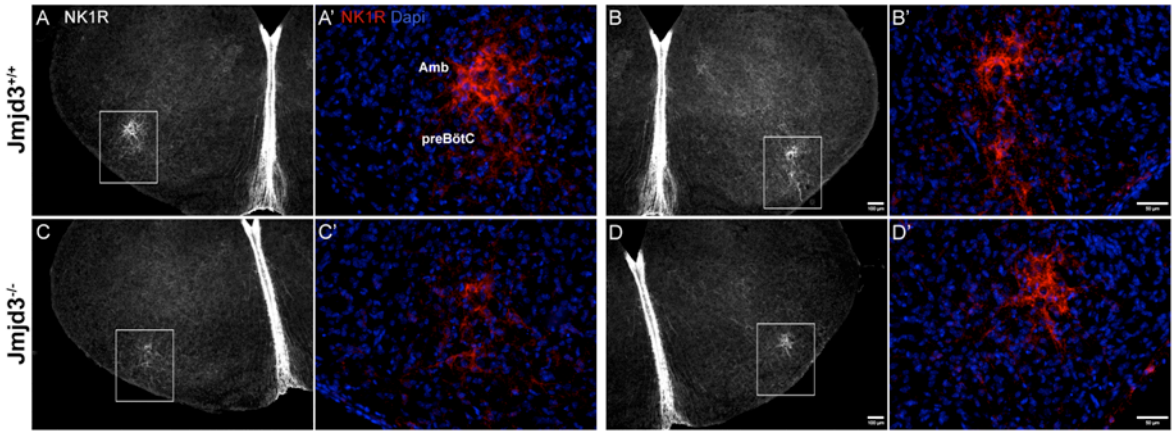

Figure 43. Abnormal preBötC structure in Jmjd3$^{-/-}$ mutants at E18.5. Immunohistochemical stainings for NK1R on 10 µm coronal frozen sections from wild-type (upper row) and mutant (lower row) E18.5 brainstems. A, B, C and D are representative images with A', B', C' and D' showing at higher magnification the area highlighted with the white rectangle. In sections from Jmjd3$^{+/+}$ embryos, strong immunoreactivity for NK1R was detected in the nucleus ambiguus (Amb) and the preBötC, extending towards the ventral surface of the medulla. Jmjd3$^{-/-}$ brainstems displayed fewer, more dispersed NK1R-positive neurons in the preBötC region.

We next examined whether the major hindbrain neuromodulatory groups involved in respiratory control have anatomical defects in Jmjd3 mutant embryos. Using immunohistochemistry for the neurotransmitter serotonin, we did not detect any differences between Jmjd3$^{+/+}$ and Jmjd3$^{-/-}$ samples in the presence of serotonergic neurons in the nucleus raphe (Figure 44). Furthermore, staining for tyrosine hydroxylase did not show apparent abnormalities in the catecholaminergic neurons of the locus coeruleus in the

pons (Figure 44). These results showed that the main neuronal groups of both monoaminergic systems were present, thus indicating that the neuromodulatory groups were not affected in Jmjd3$^{-/-}$ mice.

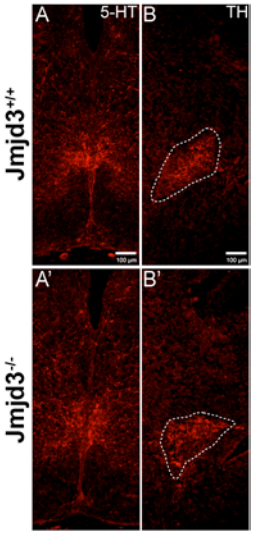

Figure 44. Normal anatomy of neuromodulatory groups in Jmjd3$^{-/-}$ brainstems. The main neuronal groups of the monoaminergic systems did not have apparent defects in Jmjd3 mutants. Analysis of the nucleus raphe in Jmjd3$^{+/+}$ (A) and Jmjd3$^{-/-}$ (A') brainstems by immunostaining for serotonin (5-HT) on coronal sections. Analysis of the catecholaminergic neurons of the locus coeruleus (dashed line) in sagittal Jmjd3$^{+/+}$ (B) and Jmjd3$^{-/-}$ (B') brainstem sections by immunostaining for tyrosine hydroxylase (TH).

In conclusion, this detailed histological analysis, together with the electrophysiological data presented above, demonstrated that Jmjd3 contributes to the embryonic formation of the preBötC and that loss of Jmjd3 leads to a non-functional RRG at E18.5.

2.1.13 The RRG of Jmjd3$^{-/-}$ embryos is functional at E16.5

The maturation of the mouse respiratory network has been shown to occur sequentially, with the RTN/pFRG group being functionally mature first, as early as E14.5 and the preBötC maturing one day later at E15.5. As our immunohistological data showed altered preBötC but normal RTN/pFRG areas in the absence of Jmjd3 at E18.5, we next investigated whether Jmjd3 is involved in the initial phase of preBötC formation or rather in the functional maturation, which is crucial for the preBötC to be active at birth. To this end, we analysed embryos at E16.5 at the electrophysiological level. Foetuses were

exteriorised and immediately placed in artificial cerebrospinal fluid (aCSF) containing KCl and bubbled with carbogene. In general, most embryos survive under these conditions and produce breathing movements *in vivo* at a low frequency with wide mouth opening. Rhythmic chest respiratory movements were observed in most wild-type (around 90%) and about half of the mutant embryos (Figure 45a). The visual observation of these chest respiratory movements was confirmed by recording of rhythmic chest electromyograms using a suction electrode that touched the ribcage muscles. In addition, the brainstem was isolated with the ribcage remaining attached to the spinal cord and rhythmic diaphragmatic electromyogram discharges were recorded *in vitro* (Figure 45b). Rhythmic contractions occurred in seven out of eight wild-type samples and in half of the Jmjd3 mutants (Figure 45b).

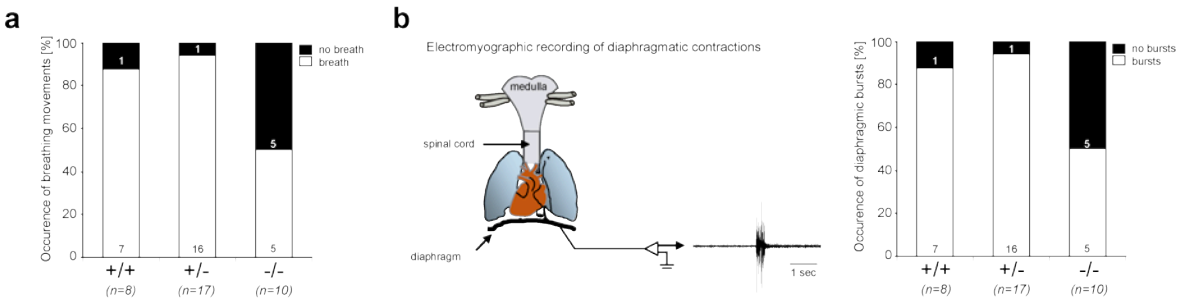

Figure 45. The RRG is functioning in some Jmjd3$^{-/-}$ mutants at E16.5. (a) E16.5 foetuses were exteriorised and monitored for the occurrence of breathing movements *in vivo*. Half of the mutant embryos produced breathing movements *in vivo*. **(b)** Schematic drawing of the experimental set-up to record electromyograms of diaphragmatic contractions *in vitro*. After dissection of the brainstem with the ribcage remaining attached to the spinal cord, the diaphragm rhythmically contracts *in vitro*. Rhythmic diaphragmatic bursts were detected in five out of ten mutant preparations.

These results showed that at E16.5 the RRG of at least some Jmjd3 mutant embryos was functioning and able to produce a central rhythmic respiratory drive *in vitro* and breathing movements *in vivo*.

In summary, we have shown that Jmjd3 is expressed in the preBötC, the principal site of respiratory rhythmogenesis. Our findings show that Jmjd3$^{-/-}$ embryos, when exteriorised at E18.5, fail to produce breathing movements *in vivo* and to generate *in vitro* respiratory

activity. However, the silent respiratory motoneurons can be activated by spinal cord and brainstem stimulations, demonstrating that the output pathways from the medullary respiratory centres are functional in mutants and therefore suggesting that the rhythmogenic mechanisms in the RRG are defective. Furthermore, our results provide evidence that the preBötC respiratory oscillator is developed and is active at E16.5 despite the absence of Jmjd3. This implies that the loss of Jmjd3 impairs the late maturation of the preBötC and prevents its functionality at E18.5, leading to perinatal death of all Jmjd3$^{-/-}$ mutants.

2.2 Generation of a conditional knockout mouse model for Jmjd3 by gene targeting

In order to circumvent the developmental lethal phenotype caused by constitutive ablation of Jmjd3, the generation of a conditional knockout allele for Jmjd3 was pursued in parallel. To this end, a Jmjd3 multipurpose allele based on the 'knockout-first' approach was created [57]. This strategy allows in a single ESC targeting step to generate both a constitutive and a conditional knockout. In its original configuration the resulting allele creates a null mutation at the RNA processing level and a reporter for Jmjd3 expression through the lacZ marker (Figure 46). The endogenous RNA transcript is captured and truncated by a splice acceptor (sA) and a polyadenylation signal (pA), respectively, so that the exons downstream of the cassette are not transcribed into mRNA, hence producing a knockout based on RNA processing. By the combined use of FLP and Cre recombinases the constitutive knockout allele is converted into a conditional allele, which permits studying the loss-of-function phenotype in a spatially and temporally controlled manner.

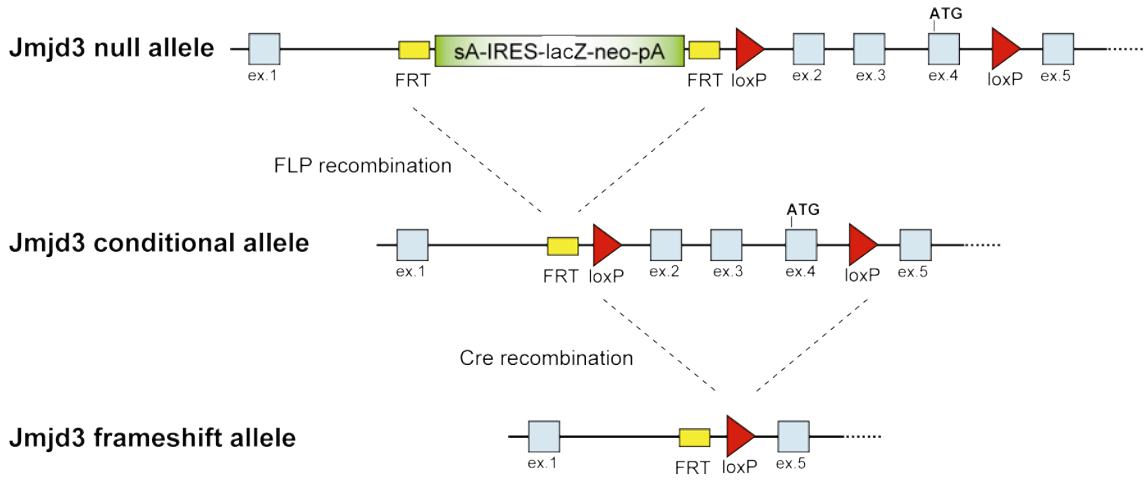

Figure 46. The Jmjd3 multipurpose allele. The Jmjd3 multipurpose allele is created by insertion of a FRT flanked reporter cassette, comprising a splice acceptor (sA), an internal ribosomal entry site (IRES), a lacZ-neo fusion and a polyadenylation signal into the first intron of Jmjd3 and the additional insertion of two loxP sites to flank exons two to four. After homologous recombination in ESCs the targeted allele constitutes both, a null allele based on trapping and truncation of the endogenous mRNA and a reporter for Jmjd3 expression. FLP-mediated recombination is used to restore gene function and to establish the conditional allele. Subsequent Cre recombination deletes exons two to four, resulting in the loss of the translation initiation codon ATG. Only the first five exons of the Jmjd3 gene are shown.

2.2.1 Cloning of the Jmjd3 targeting construct

The annotated mouse Jmjd3 gene spans approximately 15.2 kb of genomic sequence on chromosome 11 and is comprised of 23 exons, of which the first three are noncoding exons and exon four contains the translation initiation codon (ATG). Transcription analysis has demonstrated that in ESCs the first exon constitutes a functional transcription start site, which is in accordance with ChIP studies showing that the 5'-untranslated region preceding exon one is associated with a broad peak of histone H3 trimethyl-lysine 4 (H3K4me3), a mark selectively enriched at active promoters. Since the targeting cassette is promoterless it had to be inserted downstream of a transcribed exon in order to be functional in ESCs. Given the genomic structure of Jmjd3 with most of the intronic regions being very small, we therefore decided to target the first intron of Jmjd3. In this configuration the cassette prevents transcription of the protein-coding exons, thus generating a null allele. The strategy for the conditional allele was based on the insertion of two loxP sites flanking exons two to four, such that upon Cre recombination, the translation initiation site is lost.

The targeting vector for the conditional inactivation of Jmjd3 was assembled using Red/ET recombination [76,88], as schematically summarised in Figure 47. This DNA engineering method is based on homologous recombination in *E. coli* mediated by phage proteins and allows to efficiently modify large fragments of chromosomal and plasmid DNA without using restriction endonucleases and DNA ligase.

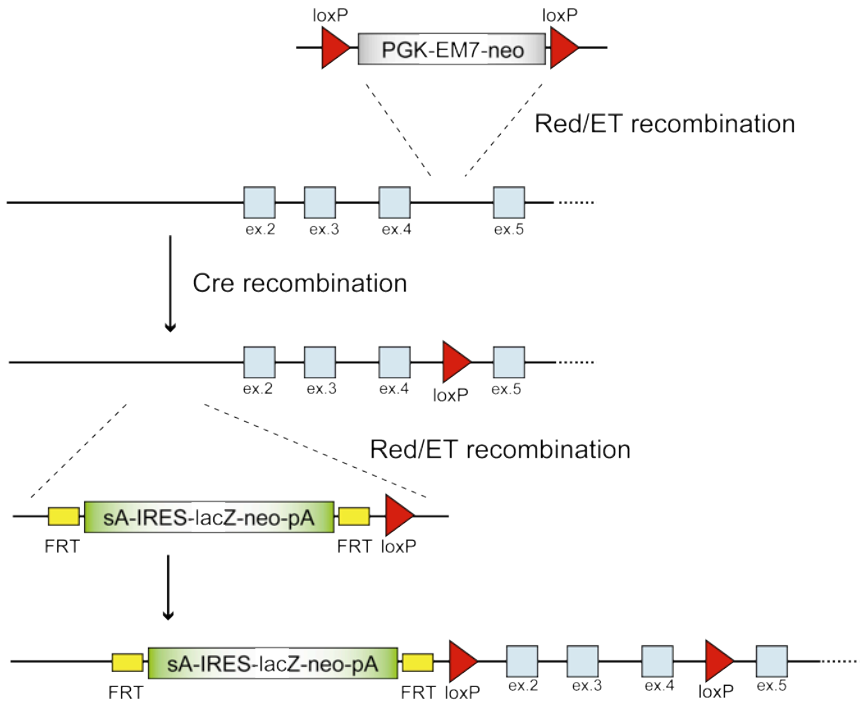

Figure 47. Strategy to engineer the multipurpose targeting construct for Jmjd3. Step one involves cloning of a loxP flanked selectable marker cassette into intron four of the Jmjd3 gene, using Red/ET recombination. Next, the selectable marker is excised by transient expression of Cre recombinase, leaving behind a single loxP site in intron four. In the final step, the βgeok cassette including two flanking FRT sites and a single loxP site is placed into intron one by Red/ET recombination. All steps are performed in *E. coli.*. The backbone of the targeting vector is not shown. ex.: exon, EM7: prokaryotic promoter, FRT: target site for FLP recombinase, IRES: internal ribosomal entry site, lacZ: reporter gene encoding β-galactosidase, loxP: target site for Cre recombinase, neo: selection marker neomycin phosphotransferase, PGK: eukaryotic promoter, pA: SV40 polyadenylation signal, sA: splice acceptor element from *engrailed-2*.

To engineer the backbone for the targeting construct, a 10.5 kb fragment of the mouse Jmjd3 locus comprising the genomic region between intron one and intron 13 was subcloned from a BAC into the pACYC177 plasmid by Red/ET recombination. This step allows to subclone the genomic fragment based on the Southern strategy designed beforehand. First the pACYC177 plasmid was PCR amplified with the oligonucleotides listed in Table 13, generating a linear minimal vector flanked by stretches homologous to the BAC sequence immediately flanking the region to be subcloned (Figure 48a).

Table 13. Oligonucleotides used generate a linear minimal vector with flanking homology arms by PCR reaction. The homology regions to Jmjd3 are indicated in bold. The inserted I-SceI recognition sites are indicated in italics and the PCR primer sequences which anneal to the template pACYC177 are shown in regular font.

Name	Sequence (5'-3')
SubJmjd3-5'	**TGAGAGGTTTTCAGGTGGTAGAGAGGCAAGTGAAGTACAGGGATAAACCAT** *TAGGGATAACAGGGTAAT*TCACGAGGCAGACCTCAGCGCTAGCGG
SubJmjd3-3'	**TAGGGCTGGCACACACCATTAATCCCAGCAGTGAGGCAGAGGCAGGTAGAT** *TAGGGATAACAGGGTAAT*TGAAGACGAAAGGGCCTCGTGATACGCC

Each oligonucleotide contained 51 nucleotides of homology to the Jmjd3 BAC at its 5' end, the restriction site for the homing endonuclease I-SceI and the PCR primer sequence annealing to the pACYC177 template in the 3' region. The rare I-SceI sites were included to linearize the targeting construct before ESC electroporation. After transformation of the *E. coli* BAC host with the Red/ET expression plasmid pSC101-BAD-gbaA-tet, the linear vector fragment with homology arms (PCR product) was electroporated into the cells and recombination took place. Recombinant colonies harbouring the subcloned fragment (pACYC177-Jmjd3) were identified by selection for ampicillin (Figure 48b).

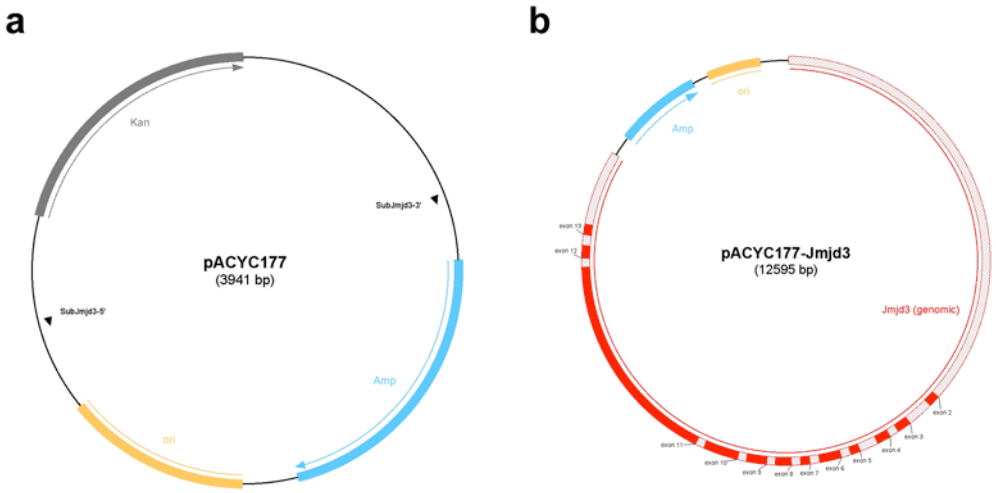

Figure 48. Plasmids used to subclone Jmjd3 from a BAC by Red/ET recombination. (a) A linear minimal vector with flanking regions homologous to the genomic sequence of Jmjd3 was constructed by PCR amplification of plasmid pACYC177 using the oligonucleotides SubJmjd3-5' and SubJmjd3-3'. **(b)** In the next step, the PCR product was used to subclone a 10.5 kb fragment of the mouse Jmjd3 locus by Red/ET recombination. Recombinant clones were identified by selection for ampicillin resistance.

In the next step, the first loxP site was inserted into intron four of Jmjd3 by Red/ET recombination. To this end, a loxP flanked PGK-neo cassette was amplified from the pR6K-PGK-EM7-neo plasmid by PCR using the oligonucleotides listed in Table 14.

Table 14. Oligonucleotides used to amplify the loxP flanked selectable marker cassette by PCR. The homology arms to the fourth intron of Jmjd3 are indicated in bold. The loxP sites are shown in blue and the inserted EcoRI recognition site is indicated in italics. The residues which anneal in the PCR reaction to the template pR6K-PGK-EM7-neo are shown in regular font.

Name	Sequence (5'-3')
2loxP-F	**GCATTTCTCTCCCAGTCTTCTCTGTCCATTGCTGTCATTTTCCACGAGTT**ATAACTTCGTATAATGTATGCTATACGAAGTTATCCGCATTCTACCGGGTAGGGG
2loxP-R	**TCAGAGGGAAGAGCAGATGAGACTGGCATCTGGACCCACAACAGAACAGA***GAATTC*ATAACTTCGTATAGCATACATTATACGAAGTTATACGGCGCGCCGCACACAAAAAC

Each oligonucleotide consisted of 50 bp of homology to intron four of Jmjd3, followed on the 3' by the loxP site and the sequence which anneals to the PCR template pR6K-PGK-EM7-neo (Figure 49). Thus, the resulting PCR product was flanked by the homology arms to intron four plus the loxP sites and contained the selectable marker neomycin phosphotransferase (*neo*) under the control of the prokaryotic promoter EM7, thus conferring kanamycin resistance to recombinant *E. coli* cells.

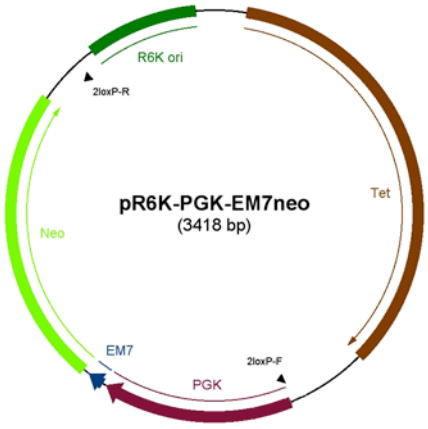

Figure 49. PCR template for the floxed PGK-EM7-neo cassette. The plasmid pR6K-PGK-EM7-neo served as template to generate the loxP flanked PGK-EM7-neo cassette with homology arms using the oligonucleotides 2loxP-F and 2loxP-R.

A key advantage of the pR6K-PGK-EM7-neo plasmid is its R6K origin, which requires for replication the initiator protein π, encoded by the *pir* gene. Since this Red/ET cloning step was performed in *E. coli* lacking the *pir* gene the plasmid, used as template during the PCR reaction, could not be propagated and therefore one possible source of background was drastically reduced. The purified and concentrated PCR product was directly electroporated into *E. coli* carrying the targeting plasmid pACYC177-Jmjd3 and the Red/ET expression plasmid pSC101-BAD-gbaA-tet. After transformation cells were incubated on LB plates containing ampicillin and kanamycin. Six colonies were picked, of which all showed the correct KpnI digestion pattern for the recombined plasmid (pACYC177-Jmjd3flox-neo), consisting of two bands of 10253 bp and 3940 bp, respectively (Figure 50).

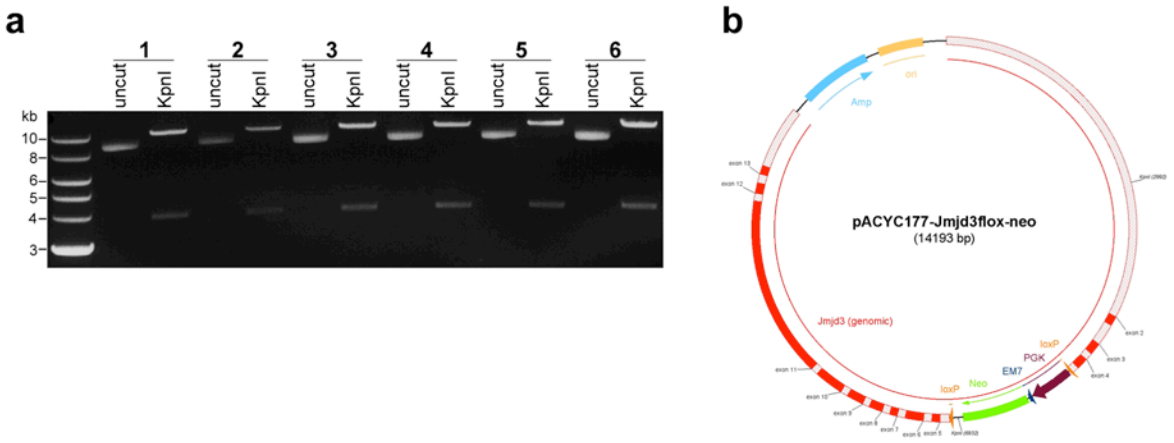

Figure 50. Insertion of the floxed selectable marker cassette into intron four of Jmjd3 using Red/ET recombination. (a) Digestion with KpnI shows for all six colonies the correct restriction pattern with two fragments of 10253 bp and 3940 bp, respectively. **(b)** Map of the recombined targeting vector containing the loxP flanked selectable marker cassette in intron four of Jmjd3. *E. coli* cells carrying the recombined plasmid were identified by double selection for kanamycin and ampicillin resistance.

Removal of the selection marker was achieved through Cre-mediated recombination using a well established construct driving Cre expression in *E. coli* [131] (Figure 51). The 705-Cre plasmid has a temperature-sensitive pSC101 origin that permits replication only at 30 °C. The expression of Cre recombinase is driven by the thermosensitive promoter cI857, which induces Cre expression between 37-42 °C.

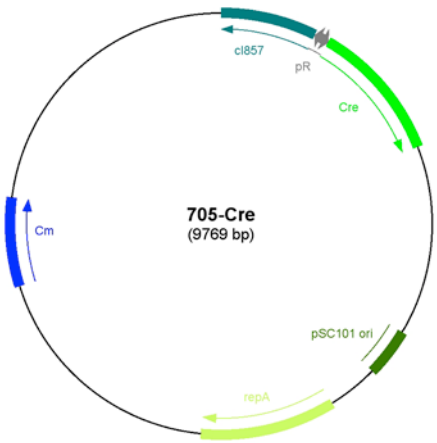

Figure 51. Map of the 705-Cre expression plasmid. Expression of the Cre recombinase is regulated by the cI857 temperature-sensitive λ-repressor, which induces expression between 37-42 °C. The pSC101 origin allows replication only at 30 °C. The plasmid confers chloramphenicol resistance.

The Cre expression plasmid was transformed into *E. coli* cells containing the target plasmid pACYC177-Jmjd3flox-neo with the loxP flanked selection marker. After electroporation, cells were incubated on plates containing chloramphenicol and ampicillin for 24 h at 30 °C. Eight single colonies were picked, grown in LB ampicillin selective medium at 30 °C for 3 h, and then incubated at 37 °C overnight to induce transient Cre expression. Plasmid DNA was isolated and retransformed to eliminate the unrecombined plasmid. Restriction digest with SacI on two colonies verified the Cre-mediated excision of the selection marker, yielding four fragments with sizes of 5835 bp, 2442 bp, 2198 bp and 2160 bp (pACYC177-Jmjd3loxP, Figure 52). The two smallest fragments were not clearly separated by gel electrophoresis, because the difference between their sizes was too small.

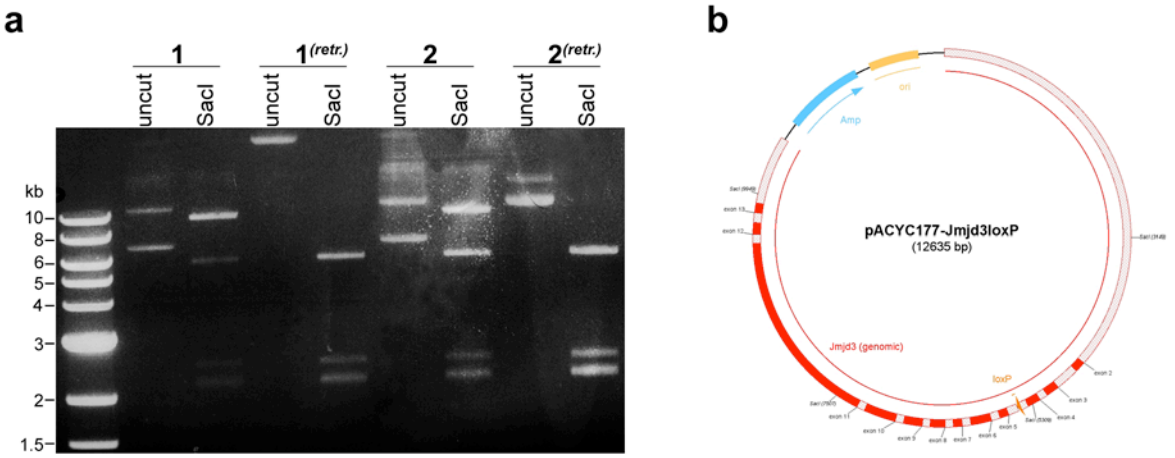

Figure 52. Cre-mediated removal of the selection marker leaving behind the loxP site. (a) Digestion with SacI shows that the two colonies are mixed before retransformation, whereas they contain the pure recombined plasmid after retransformation (retr.). The correct restriction pattern for the recombined plasmid consists of four fragments (5835 bp, 2442 bp, 2198 bp, 2160 bp). **(b)** Map of the recombined targeting vector containing a single loxP site in intron four of Jmjd3.

The last step involved the placement of the βgeok cassette in the first intron of Jmjd3 by Red/ET recombination. The βgeok cassette, flanked by FRT sites and a single loxP site on the 3' end, comprised a splice acceptor site from *engrailed-2* (sA), an internal ribosomal entry site (IRES) and the lacZ-neomycin phosphotransferase fusion (βgeok) followed by the simian virus-40 polyadenylation signal (pA). The splice acceptor and the polyadenylation signal serve to trap and truncate, respectively, the nascent Jmjd3 transcript in targeted ESCs. The IRES enables translation of the lacZ-neo fusion for selection and reporting gene expression. Thereby, the dual selectable marker *neo* allows, in *E. coli* selection for kanamycin resistance to identify integrations of the βgeok cassette in the targeting vector, and in ESCs selection for G418 resistance to identify homologous recombinant clones. The expression of *neo* in *E. coli* is driven by the prokaryotic promoter Tn903, which was integrated into the linker region in frame between the *lacZ* and *neo* genes [57]. Before the βgeok cassette could be placed in the targeting construct, two homology arms plus the FRT and loxP sites had to be inserted upstream and downstream of the cassette. The 3' and 5' homology arms with sequence identity to the intended

insertion site in the targeting vector pACYC177-Jmjd3loxP were generated by PCR using the oligonucleotides listed in Table 15.

Table 15. Oligonucleotides used for PCR amplification of the homology arms. Primer pair HA3 was used to generate the 3' homology and primer pair HA5 was used to amplify the 5' homology arm. The loxP site is shown in blue and the FRT sites are shown in red. The inserted restriction sites are indicated in italics: PmeI in HA3-F, NotI in HA3-R, AscI in HA5-F and PacI in HA5-R. The residues which anneal in the PCR reaction to the template are shown in bold.

Name		Sequence (5'-3')
HA3	*F:*	CCCTATC*GTTTAAAC*GAAGTTCCTATTCTCTAGAAAGTATAGGAACTTCCTCGAG TGCGTATAACTTCGTATAATGTATGCTATACGAAGTTATGGCCGGCCATG**GCG GGAGGGCCTGGGTGCTGG**
	R:	AAATTAA*GCGGCCGC***CATCCACCGAACTGGCAATGGT**
HA5	*F:*	TTTGTTT*GGCGCGCC***GCACAGAGGATACAGGAGCCAC**
	R:	CCCTGAG*TTAATTAA*GTGCACGAAGTTCCTATACTTTCTAGAGAATAGGAACTTC CTGCAG**GCGCCTCTATCAGAATGCTCCAC**

The two PCR products carried, besides the respective ~200 bp homology regions to intron one, the relevant site-specific recombination target sites (FRT and loxP) and unique restriction sites for further cloning. Following digestion with PmeI/NotI for the 3' homology arm and with AscI/PacI for the 5' homology arm, the PCR products were inserted by ligation into the plasmid pPUX4-βgeok upstream and downstream of the βgeok cassette (Figure 53). Correct insertions were verified by restriction analysis and sequencing.

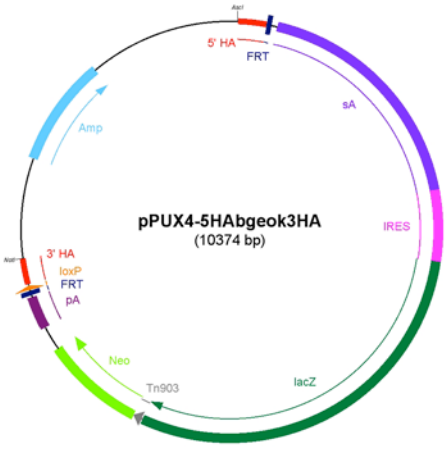

Figure 53. Insertion of the homology arms upstream and downstream, respectively of the βgeok cassette. The 221 bp 5' homology arm including one FRT site was cloned upstream of the splice acceptor (sA) and the 206 bp 3' homology arm containing a loxP and FRT site was inserted downstream of the polyadenylation signal (pA).

Next, the βgeok cassette flanked by an FRT site on the 5' end and by an FRT and a loxP site on the 3' end, was excised from the plasmid with AscI/NotI and cloned into the targeting vector by Red/ET recombination. Recombinant colonies were identified by kanamycin selection. Ten colonies were picked and digested with AccI to confirm the presence of the recombined targeting vector (pACYC177-Jmjd3-FRTbgeok-flox). As shown for three representative colonies in Figure 54a, all colonies yielded the correct restriction pattern, consisting of seven fragments with sizes of 6539 bp, 5441 bp, 2590 bp, 2460 bp, 1361 bp, 1200 bp and 99 bp. The smallest fragment was not visible for technical limitations. Moreover, the absence of the unrecombined plasmid indicated a very high recombination efficiency.

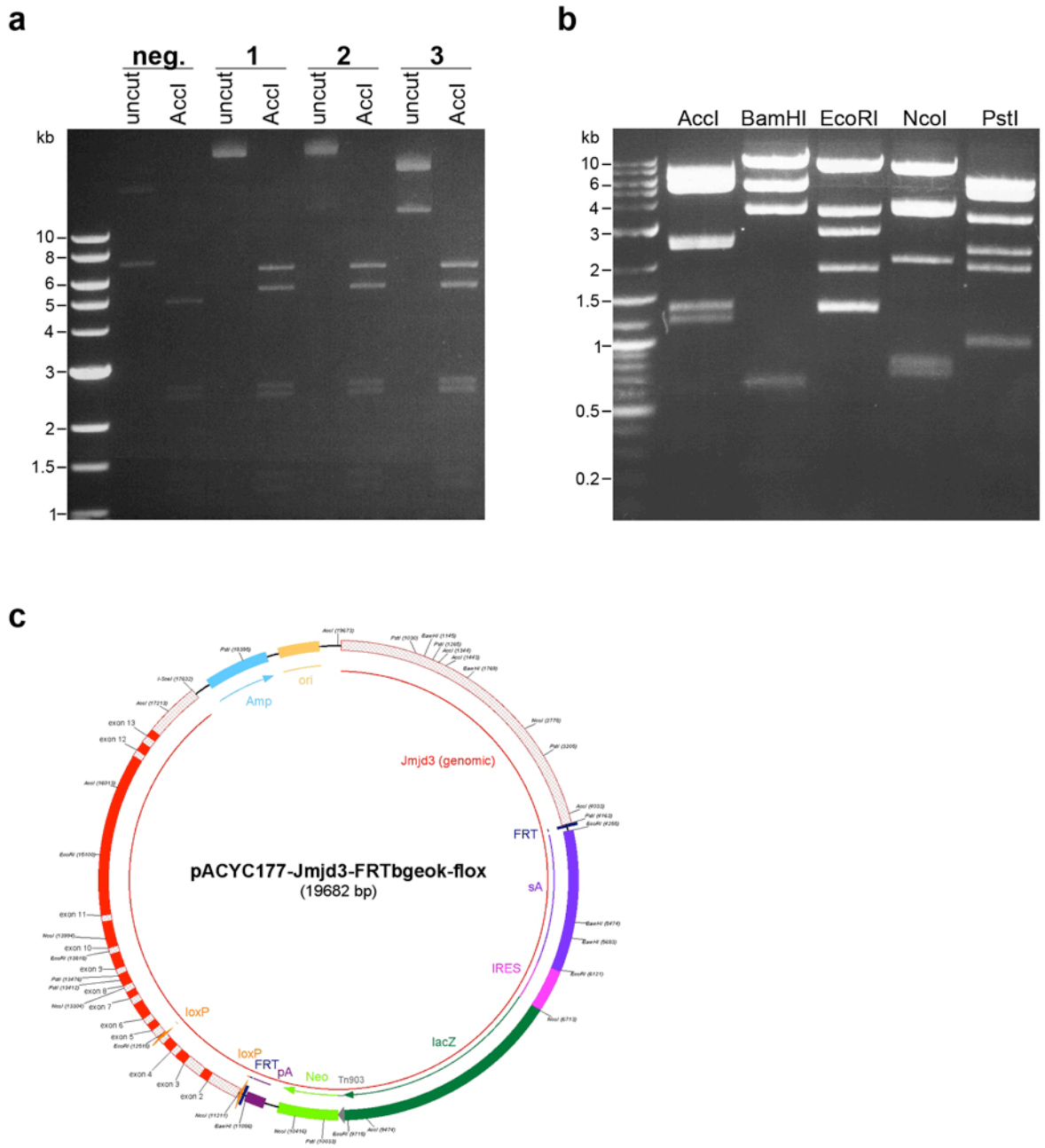

Figure 54. Insertion of the βgeok cassette in the final targeting vector by ET cloning. (a) AccI digest shows for all colonies the correct restriction pattern. The targeting vector before the recombination step served as control for the unrecombined plasmid (neg.). **(b)** The correct structure of the targeting vector is verified by additional analytical digests with various restriction enzymes. **(c)** Plasmid map of the final targeting vector.

Finally, colony number one was chosen for a more detailed restriction analysis using BamHI, EcoRI, NcoI and PstI in order to confirm that the targeting construct had been correctly assembled (Figure 54b, c). The loxP sites, the FRT sites and the structure of the βgeok cassette were further verified by sequencing.

The final linearized targeting construct had a size of 17.6 kb and was flanked by a 5' homology arm of 4.1 kb and a 3' homology arm of 5.1 kb, respectively.

2.2.2 Targeting of ESCs by homologous recombination

The targeting vector was cut with I-SceI and the linearized construct purified. C57BL/6 ESCs were electroporated with the targeting construct and two days later the selection with G418 was started. After eight days of selection, massive cell death had occurred and drug-resistant ESCs had formed fully grown colonies, which were picked and expanded. Seven electroporations yielded 765 picked colonies of which 295 could be expanded and maintained for extraction of genomic DNA. These clones were screened for homologous recombination on the 5' side of the Jmjd3 locus by Southern blot with a probe external to the targeting construct (Figure 55a). Upon EcoRI digestion, the 5' probe hybridised to a wild-type fragment of 10 kb. In case of correct integration of the targeting construct in the endogenous Jmjd3 locus the probe recognized a 7.6 kb fragment (Figure 55b). The results showed that 24 clones had the correct integration pattern on the 5' side, corresponding to a targeting efficiency of 8% for the Jmjd3 locus with this promoter trap approach. This is a very high targeting frequency, similar to what is reported for most targeting experiments with promoterless trap constructs.

These positively identified clones were then analysed for the correct integration of the 3' homology arm. This Southern strategy was based on DraI digest and an external probe which hybridised to 13.5 kb and 10.4 kb restriction fragments generated from the wild-type and the targeted allele, respectively (Figure 55c).

Furthermore, a probe internal to the targeting construct was used, resulting upon SspI digest in an 11.4 kb band that detected correct genome integration by homologous recombination (Figure 55d). This strategy enabled to distinguish single-copy from multi-

copy integrants, since it has been shown that multiple-copy integration of loxP sites and the presence of Cre recombinase can lead to chromosome loss [132].

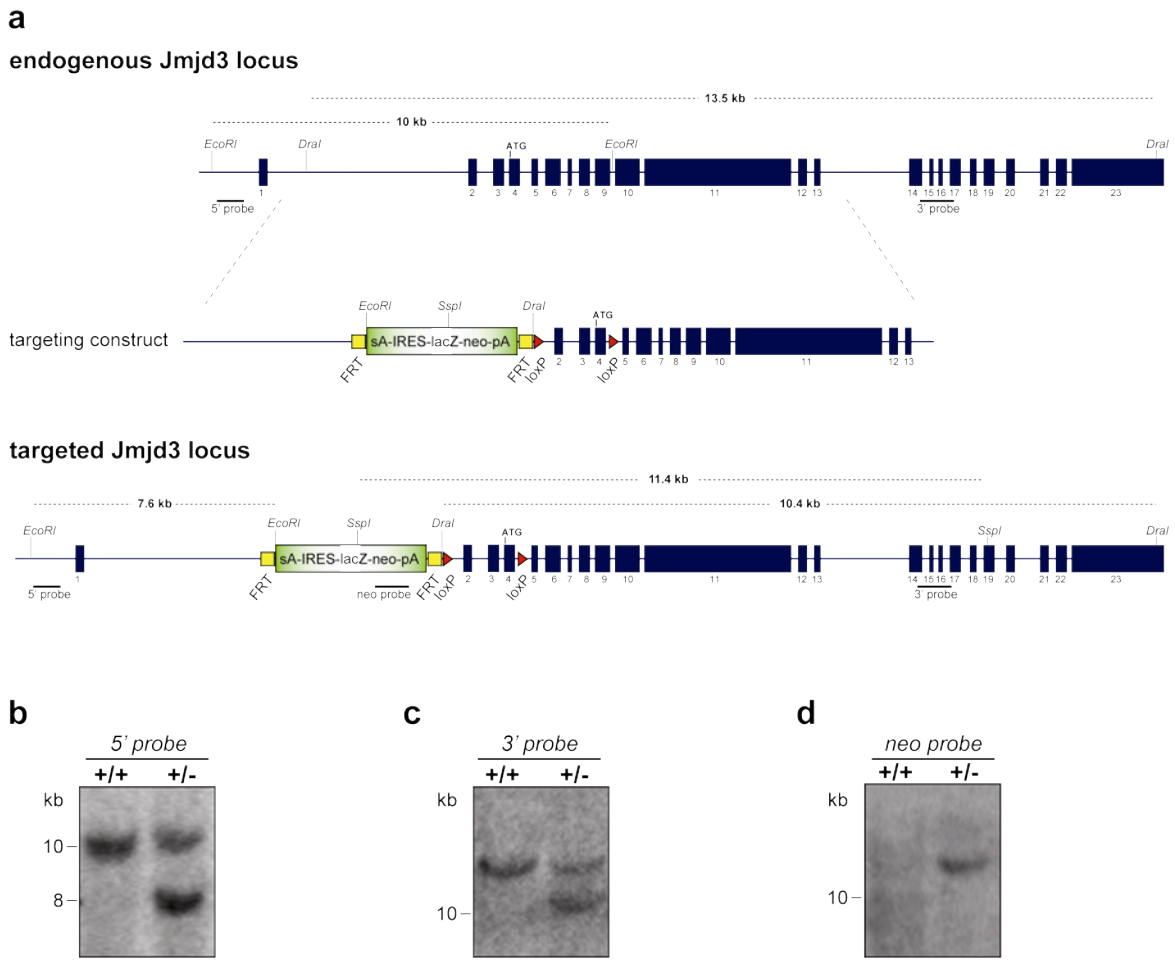

Figure 55. Genetic inactivation of Jmjd3. (a) Schematic structure of the gene targeting strategy, showing the mouse Jmjd3 wild-type locus, the targeting construct and the recombined allele. Exons are depicted along with the positions of the relevant restriction sites and the probes used to identify homologous recombined ESC clones by Southern blot analysis. **(b)** Correct integration of the 5' side was assessed by hybridisation of the 5' flanking probe to EcoRI digested genomic DNA, yielding a 10 kb band for the wild-type allele and a 7.6 kb fragment for the targeted allele. **(c)** Homologous recombination at the 3' end was confirmed by DraI digest hybridised with the 3' flanking probe, showing restriction fragments of 13.5 kb and 10.4 kb for the wild-type and the targeted allele, respectively. **(d)** Single integration of the targeting construct was confirmed on SspI digest with an internal probe hybridising to the *neo* gene. The targeted allele shows a band of 11.4 kb, whereas the probe does not hybridise to the wild-type allele.

As the targeting construct contains between the βgeok cassette and the second loxP site about 1.3 kb of homology to the endogenous Jmjd3 locus, which could cause improper recombination and rupture of the construct, it was important to confirm that the entire 3' homology arm including the second loxP site had been inserted in the targeted allele. First,

the presence of the second loxP site was confirmed by PCR with primers annealing to the endogenous region flanking the loxP site (Table 16).

Table 16. PCR primers to confirm the presence of the second loxP site.

Name	Sequence (5'-3')
loxP-F	AGGCAGGTGAGAATGTGGC
loxP-R	GGAGCTACTGCCATGAGATG

The resulting wild-type PCR product was 264 bp long and the amplicon containing the loxP site was 298 bp long (Figure 56).

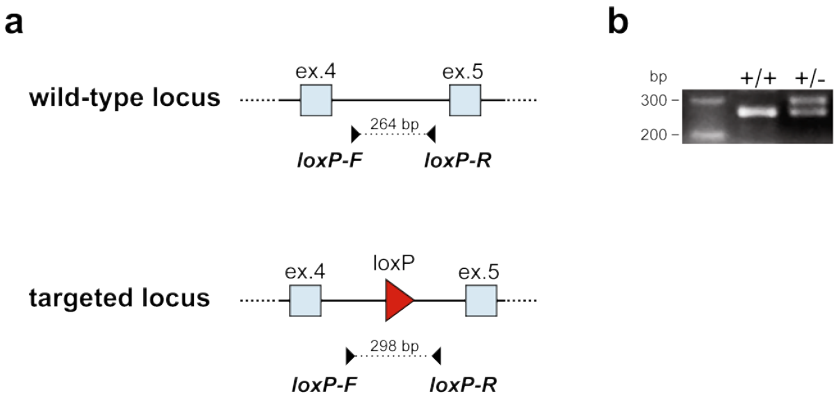

Figure 56. PCR-based strategy to confirm the presence of the second loxP site. (a) Scheme illustrating the PCR strategy used to confirm the presence of the second loxP site. The primer pair annealed in intron four of the endogenous Jmjd3 locus and flanked in the targeted allele the loxP site. The amplified PCR product for the wild-type allele was 264 bp and could be distinguished from the 298 bp amplicon for the targeted allele. **(b)** The presence of the second loxP site in homologous recombined ESC clones was confirmed by PCR.

In order to verify that both loxP sites had been integrated in the same endogenous Jmjd3 allele and to demonstrate their functionality, the targeted ESC clones were treated with Tat-Cre. The Cre recombinase-mediated deletion of the floxed region comprising exons two to four of the targeted allele was assessed by PCR using the primers indicated in Table 17.

Table 17. PCR primers to confirm Cre-mediated recombination of loxP sites flanking exons two to four of the targeted Jmjd3 allele.

Name	Sequence (5'-3')
polyA-F	TCTTATCATGTCTGGATCCGG
loxP-R2	GGAAGAGCAGATGAGACTGG

Successful site-specific recombination of the loxP sites resulted in a PCR product of 182 bp, whereas the unrecombined allele yielded a product of 1.5 kb, confirming the proper insertion of both loxP sites and their functionality (Figure 57).

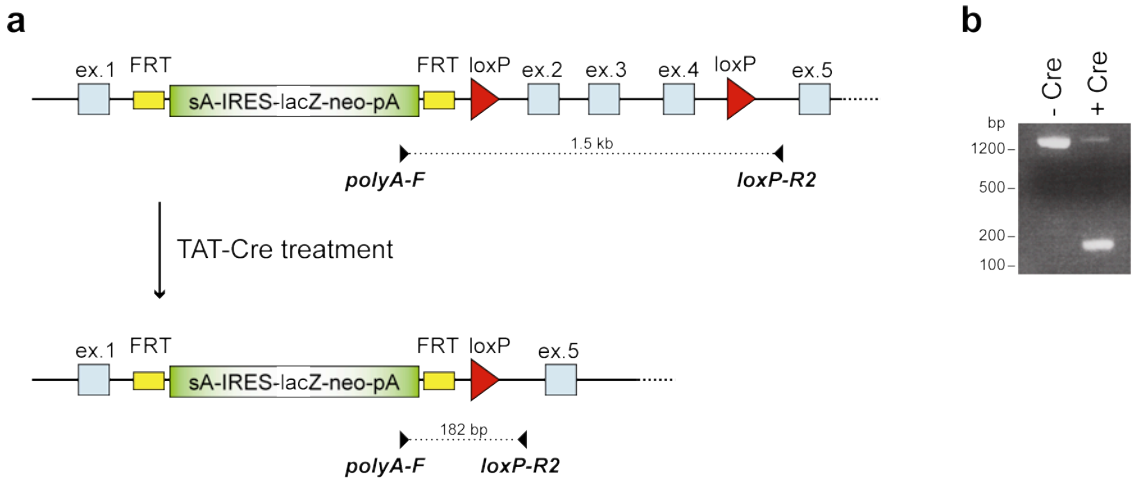

Figure 57. TAT-Cre experiment to confirm the functionality of the two loxP sites. (a) Scheme illustrating the PCR strategy used to detect site-specific Cre recombination. **(b)** The amplified PCR product of the recombined allele after TAT-Cre treatment (+ Cre) was 182 bp and could be distinguished from the 1.5 kb product of the unrecombined allele in non-treated cells (- Cre). The faint band at the height of the unrecombined allele in the treated cells indicates that transfection and recombination efficiencies were not 100%.

The final characterisation step before injection of the targeted clones into mouse blastocysts was the analysis of the karyotype to exclude chromosomal abnormalities (Figure 58). Studies have shown that aneuploidy affects the ability of ESCs to contribute to chimeras and to colonise the germline [133-134].

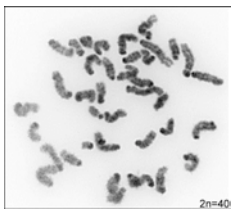

Figure 58. Targeted ESCs have normal karyotype. Reverted image of Dapi banded karyotype with 2n=40.

On the basis of above results two targeted ESC clones were injected into C57BL/6 mouse blastocysts. 11 male chimeras were obtained, which are currently being crossed to C57BL/6 females to transmit the targeted Jmjd3 allele through the germline.

Discussion

The work presented in this thesis shows that Jmjd3 is required for the differentiation of embryonic stem cells (ESCs) into neural stem cells (NSCs) *in vitro* and provides the molecular context for starting to unravel its function. H3K27me3 is the defining mark of Polycomb group (PcG)-mediated epigenetic regulation. Historically, PcG proteins were identified as transcriptional repressors in maintaining the spatial and temporal pattern of homeotic (Hox) gene expression in *Drosophila* and mammals [32,135]. This Hox paradigm has been applied more recently to the issue of stem cell pluripotency, leading to an attractive simple model in which PcG proteins keep ESCs undifferentiated by silencing lineage-specific genes. Genome-wide profiling of PcG protein binding has revealed that indeed many developmental regulators are PcG protein targets and are repressed in ESCs, with many of them 'held-in-check' by H3K4me3/H3K27me3 bivalent chromatin domains that are resolved during differentiation in a lineage-specific manner. But these genome-wide studies have also uncovered a more complex system of regulation, in which a significant number of genes, including those associated with key stem cell pathways like Wnt, Fgf and Hedgehog, are expressed despite being bound by PcG proteins [44-45,47]. And from detailed studies of PcG target sites in both *Drosophila* and mammalian cells it has become clear that the presence of the H3K27me3 mark at promoters is certainly compatible with transcriptional activity [42,45,136-138]. Hence, these divergent observations have led to hypothesise that in stem cells PcG proteins act as a common platform that can prime genes for later activation as well as for later repression. Each mode of PcG regulation clearly requires additional gene- and lineage-specific signals, which may include binding of transcriptional activators or repressors, posttranslational modifications of PcG proteins and DNA methylation when differentiation unfolds [45]. This model

captures the functional nature of histone marks as molecular signals that need not only to be 'written' but also to be 'read' by the appropriate machinery.

Our characterisation of Jmjd3 activity at the onset of neural commitment reflects the complexity of this regulation. It is noteworthy that at the time this thesis work was started current knowledge of global changes in chromatin signatures and gene transcription resulted from a comparison between ESCs and NSCs, which are points of departure and arrival for neural commitment, respectively. In order to assess the mechanisms regulating the dynamic modulation of histone lysine methylation during cell lineage specification it was necessary to look at the intermediate stages about which nothing was known. Therefore we chose to differentiate ESCs into NSCs using the adherent monolayer protocol which is the best characterised system to study neural lineage specification *in vitro* [78,89]. Our focus on the early stages of neural commitment, well before the stable NSC state has been achieved, allowed us to identify Jmjd3 as a gene that is specifically upregulated at the outset of differentiation.

The defect of Jmjd3 knockdown ESCs in neural commitment is reflected at the molecular level in the impaired upregulation of key inducers and markers of neurogenesis, like Pax6, Sox1 and Nestin. The progressive recruitment of Jmjd3 to their promoters indicates that Jmjd3 directly regulates the neurogenic program of gene expression.

Interestingly, the correlation between H3K27me3 and Jmjd3 binding at its target genes points to distinct modes of action that set the stage for further investigations. For some bivalent domain genes, exemplified here by Nestin, loss of H3K27me3 coincides with Jmjd3 occupancy and correlates with transcriptional upregulation. This observation is in agreement with the current paradigm of PcG-mediated silencing of lineage-specific genes. Loss of Jmjd3 resulted in failure of H3K27me3 demethylation, providing evidence for its physiologic role in demethylating this promoter. In agreement with previous reports we noted a modest increase of Nestin expression already at day four of differentiation (data

not shown) [78], when Jmjd3 is not yet detectable at the Nestin promoter. Although a trivial explanation is that the low sensitivity of the Jmjd3 ChIP hinders the detection of low levels of Jmjd3 in the initial phase of Nestin activation. An alternative possibility is that gene expression is induced by other mechanisms, for example recruitment of H3K4 methyltransferases of the Trithorax group (TrxG) protein family or displacement of PcG proteins from their binding site, with H3K27me3 demethylation following to either potentiate or maintain the induction.

For other bivalent domain genes, exemplified by Pax6, Jmjd3 binding correlates with transcriptional upregulation but apparently its H3K27me3 demethylation activity sets in only later, likely to enable stable activation in NSCs. Our results show that the upregulation of Pax6 expression is severely impaired in Jmjd3 knockdown cells at day seven of differentiation when demethylation has not yet occurred but Jmjd3 is already recruited to Pax6. Possible explanations are that either Jmjd3 first contributes to Pax6 activation through mechanisms that are independent of its H3K27me3 demethylase activity or that the initial effects of Jmjd3 knockdown on Pax6 expression are mediated by indirect mechanisms. The observation that the upregulation of Pax6 coincides with an increase in H3K27me3 at its regulatory regions expands previous findings from both flies and mammals [136,138]. It further reveals that the presence or even an increase in H3K27me3 is compatible not simply with basal transcription but also with upregulation of transcriptional activity, suggesting that the H3K27 methylation status may fulfil different regulatory functions at different genes and in different cellular contexts. In addition, it would be certainly worth investigating the status of other histone modifications as it has been proposed that they can cross-talk and function cooperatively to regulate gene expression [139].

Finally, Jmjd3 is also recruited to developmental regulators that retain bivalent domains, like Sox1. Also in this case, the presence of the H3K27me3 mark at the promoter region is

compatible with a pronounced transcriptional upregulation. As Sox1 is repressed in NSCs, when its H3K27me3 levels peak, it is possible that Jmj3 binding at day eight of differentiation may prevent or alleviate an increase in H3K27me3 thereby allowing unrestrained activation mediated by other cofactors. Interestingly, also other histone lysine demethylases localise at promoters enriched in the methylation mark that they are competent to erase, as in the case of Utx and Jarid1a (also known as Rbp2 and Kdm5a) that occupy a subset of H3K27me3 and H3K4me3-enriched promoters, respectively [140-141]. Hence, our data on Jmjd3 expand the findings of these studies and further strengthen the model in which histone lysine demethylases operate also, if not primarily, in the modulation rather than the simple removal of histone lysine methylation marks. Furthermore, the notion that Jmjd3 contributes in activated macrophages to the transcriptional control of target gene expression in an H3K27me3 demethylation-independent manner encourages to consider the possibility that histone demethylases may demethylate non-histone substrates and/or may catalyse other biochemical reactions than the demethylation of histones or may even have alternative functions besides their enzymatic activity [142-143]. Current knowledge of the substrate specificity of JmjC proteins is biased toward methylated histones, however, JmjC proteins are members of the Fe(II)- and α-ketoglutarate-dependent family of dioxygenases, which have generally low substrate specificity and catalyse a number of oxidation reactions. In fact, the Jumonji domain-2 (Jmjd2) family has been shown to demethylate non-histone proteins in addition to its known substrate H3K9me3 [144] and Jmjd6 has been demonstrated to hydroxylate lysine residues on U2AF65, a splicing factor [145]. In addition, the histone demethylase LSD1 has been shown to demethylate non-histone proteins such as p53 and DNA methyltransferase 1 (DNMT1) [146-147].

Our findings showed for the first time that Jmjd3 regulates key neural genes at the onset of neural differentiation of ESCs, by binding to their promoters and resolving their bivalent

states. Interestingly, it has been reported that the developmental potential of multipotent neural progenitors is defined, similar to that of pluripotent ESCs, by the establishment of PcG-mediated poised states of developmental genes [46]. Using a cellular differentiation model that progresses from ESCs to neural progenitors to terminally differentiated neurons this study showed that PcG-mediated H3K27me3 is highly dynamic and stage specific. In contrast, DNA methylation occurs primarily during the transition from ESCs to lineage-committed progenitors thereby contributing to their fate restriction through silencing of pluripotency-related genes. Strikingly, a subset of neuron-specific genes that function in terminally differentiated neurons becomes poised for expression only in neural progenitors by acquiring a *de novo* bivalent domain signature. Upon terminal differentiation, these genes lose the H3K27me3 mark and thus become activated, a process that strongly speaks for a possible functional involvement of Jmjd3. In line with this observation, Jmjd3 was identified also as a target of SMRT-mediated repression in neural stem cells, and its overexpression in transformed human embryonic kidney cells (HEK cells) resulted in the upregulation of neural genes, suggesting a possible function in the retinoic acid (RA)-dependent neural differentiation [148]. Our findings expand this model and suggest that Jmjd3 fulfils a biphasic role in neurogenesis, regulating the neurogenic program both in the transition from ESCs to NSCs and in the further differentiation of NSCs down the neuronal lineage. Further evidence for the importance of Jmjd3 in neural development is provided by our *in vivo* expression analysis, revealing a strong increase in Jmjd3 expression during the development of the central nervous system, and our loss-of-function study in the mouse.

Although Jmjd3 has been reported to play a key role in several cellular processes, such as neuronal differentiation [148], differentiation of macrophages in response to inflammatory stimuli [149], epidermal differentiation of human keratinocytes [150] and cellular senescence [151-152] its biological function in the context of an animal model, was still

lacking. In the present work we have described the first mutant mouse model for Jmjd3 and demonstrated that Jmjd3 is crucial for the late maturation of the neural network generating respiratory rhythm. In order to dissect the role of Jmjd3 *in vivo* we inactivated Jmjd3 genetically by gene trap mutagenesis. Based on our *in vitro* data demonstrating that Jmjd3 is required for early cell fate decisions and studies by others that implicate the dynamic regulation of the H3K27me3 mark during early embryonic processes, such as initial cell lineage segregation in the blastocyst [153], X-inactivation [154] and gastrulation [155] we assumed that the disruption of Jmjd3 would severely impair embryonic development at early stages. Surprisingly, mice homozygous for the Jmjd3 trap allele did not display any apparent morphological abnormalities during embryonic development, but died perinatally due to the inability to breathe. The detailed characterisation of the Jmjd3 trap allele revealed that the insertion of the trap cassette did not result in a null allele, but rather in a strong hypomorphic allele. In fact, in Jmjd3$^{-/-}$ ESCs we derived from this mutant line, we found only a moderate decrease in the Jmjd3 protein level. We therefore performed a systematic analysis at the transcript level and demonstrated the existence of an alternative transcription start site which is downstream of the inserted trap cassette and retains Jmjd3 expression in Jmjd3$^{-/-}$ ESCs, although at a reduced level. It would certainly be important to investigate the expression of Jmjd3 during early embryonic development, such as the blastocyst stage, in the mutant to assess whether residual levels of Jmjd3 can also be observed *in vivo*. At later stages of development starting from E16.5 however, expression analysis in mutant embryos by RNA *in situ* hybridisation revealed that Jmjd3 expression was overall drastically reduced and almost undetectable, even in regions in which we observed the highest expression of Jmjd3, such as the developing cortex. In macrophages obtained from fetal livers of Jmjd3$^{-/-}$ mice the trap allele behaves like a null allele, as they are completely devoid of Jmjd3 mRNA and protein [142]. Taken together, these findings suggest that Jmjd3 expression is differentially and tightly regulated, most likely by the

action of different transcription start sites, in a cell type-specific manner. In agreement with this view, Jmjd3 has been shown to be the target gene of a range of transcriptional regulators depending on the cellular context: SMAD in ESCs [156], NF-κB in macrophages [149] and SMRT in NSCs [148]. This hypomorph enabled us to begin to unravel the intricate and complex mechanisms regulating the expression of Jmjd3.

In order to determine the cause of the perinatal lethal phenotype we carried out a systematic histological and physiological analysis. When exteriorised at E18.5, Jmjd3$^{-/-}$ embryos did not produce breathing movements *in vivo* and the central respiratory network isolated in en bloc brainstem preparations did not show any respiratory activity *in vitro*. Our findings suggest that the failure of mutant mice to breathe is due to the specific inability of the respiratory network of the preBötC to generate a rhythmic respiratory drive, as we show that, 1) the synapses of the output pathways from the medullary respiratory centres to the phrenic motoneurons are functional, 2) chest muscles are able to contract and 3) mutant mice have normal cardiac activity *in utero*, thereby excluding peripheral causes of the perinatal lethality. However, the observation that at E16.5, one day after the preBötC initiates its activity, some of the Jmjd3 mutants produce breathing movements *in vivo* and show rhythmic respiratory activity *in vitro*, leads us to conclude that the loss of Jmjd3 does not impair the early formation and initial activity of the preBötC but is mainly required for its maturation and ongoing function. These electrophysiological results are supported by the histological analysis we performed of the neural respiratory network in the ventrolateral medulla. This demonstrated that Jmjd3 is normally expressed in the preBötC and that in Jmjd3 mutants the preBötC presents anatomical alterations with a partial loss of neurons expressing the marker NK1R. PreBötC neurons expressing NK1R are functionally heterogeneous and NK1R per se is not critical for breathing, since mice lacking NK1R continue to breathe [157-158], rather NK1R marks preBötC neurons that are necessary for normal rhythm generation. Since other NK1R-expressing regions do not seem to be

affected in mutant brainstems we do not expect NK1R to be a direct target of Jmjd3 and thus the loss of NK1R expression can be attributed with confidence to the absence of a specific subpopulation of neurons rather than to the downregulation of NK1R per se. It is remarkable, that the almost complete loss of Jmjd3, in particular the absence of detectable levels of mRNA comprising the coding region for the functional JmjC domain, does not lead to apparent morphological abnormalities in the development of the embryo but rather perturbs a specific neuronal circuit that becomes functionally relevant only at birth. The most trivial explanation is that the overall residual levels of Jmjd3 in Jmjd3$^{-/-}$ mice are still compatible with normal embryonic development, but that the expression of Jmjd3 in the neurons of the preBötC depends exclusively on the trapped transcript. However, the only way to address this issue is by analysing Jmjd3 expression at the protein level, which could not be done during the present study due to the lack of an antibody working in immunohistochemistry. Taken together, these findings implicate a role for Jmjd3 in the functional maturation of the preBötC during late gestational stages. Recent advances in mouse genetics enabled to gain insight into the cellular and molecular mechanisms involved in the development and specification of neuronal populations constituting the respiratory rhythm-generating circuits. Loss-of-function studies in mutant mice have identified several developmental genes encoding transcription factors that are required for normal maturation and/or function of the respiratory network. For instance, MafB is crucial for normal rhythm generation by the preBötC oscillator [159], Dbx1 for the coupling between RTN/pFRG and preBötC [160], Phox2b for the CO_2 chemosensitivity of the RTN/pFRG region [130,161] and Tshz3 plays an important role in the development of upper airway motoneurons as well as the functional emergence of the embryonic parafacial respiratory group (e-pF) [162]. Mutations of these transcription factors resulted in abnormal respiratory rhythmogenesis, impaired normal lung ventilation and compromised survival at birth. However, the deletion of none of these genes completely abolished the

RRG function as observed for Jmjd3 mutants, indicating the complexity that underlies the functional respiratory network in the hindbrain.

Despite the fact that several characteristics of the respiratory neural network are already established at E16.5, it is believed that this network undergoes additional changes, for instance in synaptic interactions and voltage-dependent membrane properties, at late fetal stages which are required for the network to become functionally mature and developmentally comparable with that of neonates [122,163]. Our results suggest strongly that Jmjd3 is required in this terminal maturation of respiratory neurons and it is tempting to speculate that Jmjd3, in this context, operates by removing the repressive H3K27me3 mark and thereby activating genes that are involved in neuronal maturation and/or function, such as those encoding neurotransmitters or ion-channels. The next step, which is already part of the ongoing work, will be the identification of theses target genes in order to dissect the molecular mechanisms underlying the establishment and function of the respiratory neural network. These findings will provide valuable information about the general principles of the vital motor behaviour of breathing and enable to gain insight into the pathogenesis of respiratory disorders, such as congenital central hypoventilation syndrome (CCHS) and sudden infant death syndrome (SIDS).

Moreover, our results indicate a possible involvement of Jmjd3 in the formation and functional maturation of other neuronal networks. The observation that Jmjd3 is highly expressed in the developing cortex suggests a role for Jmjd3 during cortical neurogenesis. In line with this hypothesis, it has been reported that PcG proteins restrict the neurogenic potential of neural precursors in the late stage of neocortical development and promote the fate switch in neural precursor differentiation from neurogenic to astrogenic [164]. This model has been expanded recently, by showing that Ezh2 controls the balance between self-renewal and differentiation in cortical progenitor cells even before the onset of neurogenesis [165]. These rapid changes in the H3K27me3 methylation state posit the

dynamic involvement of an antagonist of PcG-mediated methylation of H3K27, and Jmjd3 is a good candidate. As the respiratory network is the first one that needs to be active at birth, possible functional defects in other neuronal circuits could not be revealed with this mouse model. Thus, a detailed analysis of the cortex in Jmjd3$^{-/-}$ embryos will be object of further investigations with the Jmjd3 conditional knockout allele we generated. This is a versatile tool to further characterise the role of Jmjd3 at each stage of neural development and to dissect the epigenetic mechanisms that underlie the establishment and regulation of developmental competence during neurogenesis.

In conclusion, our findings establish Jmjd3 as a H3K27me3 demethylase required for neural commitment. The dynamics of H3K27me3 demethylation and its correlation to transcriptional output appear to follow distinct gene-specific patterns and prompt further investigations into the changes of this chromatin mark at the onset of differentiation. Furthermore, we have shown in this study that the expression of Jmjd3 is regulated during neurogenesis *in vivo* and its loss of function results in a complex lethal neurodevelopmental phenotype. Hence, we propose that Jmjd3 is not only involved in the major developmental transitions in neural progenitor cells, but it is likely to be important also in the terminal differentiation leading to neural cell type specification.

References

1. Shen Q, Wang Y, Dimos JT, Fasano CA, Phoenix TN, et al. (2006) The timing of cortical neurogenesis is encoded within lineages of individual progenitor cells. Nat Neurosci 9: 743-751.
2. Waddington CH (1942) The epigenotype. Endeavour 1: 18-20.
3. Wigler M, Levy D, Perucho M (1981) The somatic replication of DNA methylation. Cell 24: 33-40.
4. Hansen KH, Bracken AP, Pasini D, Dietrich N, Gehani SS, et al. (2008) A model for transmission of the H3K27me3 epigenetic mark. Nat Cell Biol 10: 1291-1300.
5. Margueron R, Justin N, Ohno K, Sharpe ML, Son J, et al. (2009) Role of the polycomb protein EED in the propagation of repressive histone marks. Nature 461: 762-767.
6. Strahl BD, Allis CD (2000) The language of covalent histone modifications. Nature 403: 41-45.
7. Jenuwein T, Allis CD (2001) Translating the Histone Code. Science 293: 1074-1080.
8. Rogakou EP, Pilch DR, Orr AH, Ivanova VS, Bonner WM (1998) DNA double-stranded breaks induce histone H2AX phosphorylation on serine 139. J Biol Chem 273: 5858-5868.
9. Huyen Y, Zgheib O, DiTullio Jr RA, Gorgoulis VG, Zacharatos P, et al. (2004) Methylated lysine 79 of histone H3 targets 53BP1 to DNA double-strand breaks. Nature 432: 406-411.
10. Bhaumik SR, Smith E, Shilatifard A (2007) Covalent modifications of histones during development and disease pathogenesis. Nat Struct Mol Biol 14: 1008-1016.
11. Lachner M, O'Carroll D, Rea S, Mechtler K, Jenuwein T (2001) Methylation of histone H3 lysine 9 creates a binding site for HP1 proteins. Nature 410: 116-120.
12. Bannister AJ, Zegerman P, Partridge JF, Miska EA, Thomas JO, et al. (2001) Selective recognition of methylated lysine 9 on histone H3 by the HP1 chromo domain. Nature 410: 120-124.
13. Fischle W, Wang Y, Jacobs SA, Kim Y, Allis CD, et al. (2003) Molecular basis for the discrimination of repressive methyl-lysine marks in histone H3 by Polycomb and HP1 chromodomains. Genes & Development 17: 1870-1881.
14. Bernstein E, Duncan EM, Masui O, Gil J, Heard E, et al. (2006) Mouse Polycomb Proteins Bind Differentially to Methylated Histone H3 and RNA and Are Enriched in Facultative Heterochromatin. Mol Cell Biol 26: 2560-2569.
15. Vakoc CR, Mandat SA, Olenchock BA, Blobel GA (2005) Histone H3 lysine 9 methylation and HP1gamma are associated with transcription elongation through mammalian chromatin. Mol Cell 19: 381-391.
16. Barski A, Cuddapah S, Cui K, Roh T-Y, Schones DE, et al. (2007) High-Resolution Profiling of Histone Methylations in the Human Genome. Cell 129: 823-837.
17. Byvoet P, Shepherd GR, Hardin JM, Noland BJ (1972) The distribution and turnover of labeled methyl groups in histone fractions of cultured mammalian cells. Arch Biochem Biophys 148: 558-567.
18. Saccani S, Natoli G (2002) Dynamic changes in histone H3 Lys 9 methylation occurring at tightly regulated inducible inflammatory genes. Genes & Development 16: 2219-2224.
19. Ahmad K, Henikoff S (2002) The Histone Variant H3.3 Marks Active Chromatin by Replication-Independent Nucleosome Assembly. Molecular Cell 9: 1191-1200.

20. Allis CD, Bowen JK, Abraham GN, Glover CVC, Gorovsky MA (1980) Proteolytic processing of histone H3 in chromatin: a physiologically regulated event in tetrahymena micronuclei. Cell 20: 55-64.
21. Lin R, Cook RG, Allis CD (1991) Proteolytic removal of core histone amino termini and dephosphorylation of histone H1 correlate with the formation of condensed chromatin and transcriptional silencing during Tetrahymena macronuclear development. Genes & Development 5: 1601-1610.
22. Duncan EM, Muratore-Schroeder TL, Cook RG, Garcia BA, Shabanowitz J, et al. (2008) Cathepsin L proteolytically processes histone H3 during mouse embryonic stem cell differentiation. Cell 135: 284-294.
23. Shi Y, Lan F, Matson C, Mulligan P, Whetstine JR, et al. (2004) Histone demethylation mediated by the nuclear amine oxidase homolog LSD1. Cell 119: 941-953.
24. Metzger E, Wissmann M, Yin N, Muller JM, Schneider R, et al. (2005) LSD1 demethylates repressive histone marks to promote androgen-receptor-dependent transcription. Nature 437: 436-439.
25. Trewick SC, McLaughlin PJ, Allshire RC (2005) Methylation: lost in hydroxylation? EMBO Rep 6: 315-320.
26. Falnes PO, Johansen RF, Seeberg E (2002) AlkB-mediated oxidative demethylation reverses DNA damage in Escherichia coli. Nature 419: 178-182.
27. Trewick SC, Henshaw TF, Hausinger RP, Lindahl T, Sedgwick B (2002) Oxidative demethylation by Escherichia coli AlkB directly reverts DNA base damage. Nature 419: 174-178.
28. Tsukada Y, Fang J, Erdjument-Bromage H, Warren ME, Borchers CH, et al. (2006) Histone demethylation by a family of JmjC domain-containing proteins. Nature 439: 811-816.
29. Azuara V, Perry P, Sauer S, Spivakov M, Jorgensen HF, et al. (2006) Chromatin signatures of pluripotent cell lines. Nat Cell Biol 8: 532-538.
30. Bernstein BE, Mikkelsen TS, Xie X, Kamal M, Huebert DJ, et al. (2006) A bivalent chromatin structure marks key developmental genes in embryonic stem cells. Cell 125: 315-326.
31. Lewis EB (1978) A gene complex controlling segmentation in Drosophila. Nature 276: 565-570.
32. Struhl G (1981) A gene product required for correct initiation of segmental determination in Drosophila. Nature 293: 36-41.
33. Jurgens G (1985) A group of genes controlling the spatial expression of the bithorax complex in Drosophila. Nature 316: 153-155.
34. Chan CS, Rastelli L, Pirrotta V (1994) A Polycomb response element in the Ubx gene that determines an epigenetically inherited state of repression. EMBO J 13: 2553-2564.
35. Pirrotta V (1997) Chromatin-silencing mechanisms in Drosophila maintain patterns of gene expression. Trends in Genetics 13: 314-318.
36. Beuchle D, Struhl G, Muller J (2001) Polycomb group proteins and heritable silencing of Drosophila Hox genes. Development 128: 993-1004.
37. Cao R, Wang L, Wang H, Xia L, Erdjument-Bromage H, et al. (2002) Role of Histone H3 Lysine 27 Methylation in Polycomb-Group Silencing. Science 298: 1039-1043.
38. Kuzmichev A, Nishioka K, Erdjument-Bromage H, Tempst P, Reinberg D (2002) Histone methyltransferase activity associated with a human multiprotein complex containing the Enhancer of Zeste protein. Genes & Development 16: 2893-2905.

39. Czermin B, Melfi R, McCabe D, Seitz V, Imhof A, et al. (2002) Drosophila Enhancer of Zeste/ESC Complexes Have a Histone H3 Methyltransferase Activity that Marks Chromosomal Polycomb Sites. Cell 111: 185-196.
40. Müller J, Hart CM, Francis NJ, Vargas ML, Sengupta A, et al. (2002) Histone Methyltransferase Activity of a Drosophila Polycomb Group Repressor Complex. Cell 111: 197-208.
41. Tolhuis B, Muijrers I, de Wit E, Teunissen H, Talhout W, et al. (2006) Genome-wide profiling of PRC1 and PRC2 Polycomb chromatin binding in Drosophila melanogaster. Nat Genet 38: 694-699.
42. Schwartz YB, Kahn TG, Nix DA, Li X-Y, Bourgon R, et al. (2006) Genome-wide analysis of Polycomb targets in Drosophila melanogaster. Nat Genet 38: 700-705.
43. Nègre N, Hennetin J, Sun LV, Lavrov S, Bellis M, et al. (2006) Chromosomal Distribution of PcG Proteins during Drosophila Development. PLoS Biol 4: e170.
44. Boyer LA, Plath K, Zeitlinger J, Brambrink T, Medeiros LA, et al. (2006) Polycomb complexes repress developmental regulators in murine embryonic stem cells. Nature 441: 349-353.
45. Bracken AP, Dietrich N, Pasini D, Hansen KH, Helin K (2006) Genome-wide mapping of Polycomb target genes unravels their roles in cell fate transitions. Genes & Development 20: 1123-1136.
46. Mohn F, Weber M, Rebhan M, Roloff TC, Richter J, et al. (2008) Lineage-specific polycomb targets and de novo DNA methylation define restriction and potential of neuronal progenitors. Mol Cell 30: 755-766.
47. Lee TI, Jenner RG, Boyer LA, Guenther MG, Levine SS, et al. (2006) Control of Developmental Regulators by Polycomb in Human Embryonic Stem Cells. Cell 125: 301-313.
48. Mikkelsen TS, Ku M, Jaffe DB, Issac B, Lieberman E, et al. (2007) Genome-wide maps of chromatin state in pluripotent and lineage-committed cells. Nature 448: 553-560.
49. MGSC (2002) Initial sequencing and comparative analysis of the mouse genome. Nature 420: 520-562.
50. Gossler A, Joyner AL, Rossant J, Skarnes WC (1989) Mouse embryonic stem cells and reporter constructs to detect developmentally regulated genes. Science 244: 463-465.
51. Doetschman T, Gregg RG, Maeda N, Hooper ML, Melton DW, et al. (1987) Targetted correction of a mutant HPRT gene in mouse embryonic stem cells. Nature 330: 576-578.
52. Thomas KR, Capecchi MR (1987) Site-directed mutagenesis by gene targeting in mouse embryo-derived stem cells. Cell 51: 503-512.
53. Lakso M, Sauer B, Mosinger B, Lee EJ, Manning RW, et al. (1992) Targeted oncogene activation by site-specific recombination in transgenic mice. Proc Natl Acad Sci U S A 89: 6232-6236.
54. Gu H, Marth J, Orban P, Mossmann H, Rajewsky K (1994) Deletion of a DNA polymerase beta gene segment in T cells using cell type-specific gene targeting. Science 265: 103-106.
55. Rodriguez CI, Buchholz F, Galloway J, Sequerra R, Kasper J, et al. (2000) High-efficiency deleter mice show that FLPe is an alternative to Cre-loxP. Nat Genet 25: 139-140.
56. Testa G, Zhang Y, Vintersten K, Benes V, Pijnappel WW, et al. (2003) Engineering the mouse genome with bacterial artificial chromosomes to create multipurpose alleles. Nat Biotechnol 21: 443-447.

57. Testa G, Schaft J, van der Hoeven F, Glaser S, Anastassiadis K, et al. (2004) A reliable lacZ expression reporter cassette for multipurpose, knockout-first alleles. Genesis 38: 151-158.
58. Kunath T, Gish G, Lickert H, Jones N, Pawson T, et al. (2003) Transgenic RNA interference in ES cell-derived embryos recapitulates a genetic null phenotype. Nat Biotechnol 21: 559-561.
59. Fire A, Xu S, Montgomery MK, Kostas SA, Driver SE, et al. (1998) Potent and specific genetic interference by double-stranded RNA in Caenorhabditis elegans. Nature 391: 806-811.
60. Zamore PD, Tuschl T, Sharp PA, Bartel DP (2000) RNAi: double-stranded RNA directs the ATP-dependent cleavage of mRNA at 21 to 23 nucleotide intervals. Cell 101: 25-33.
61. Bernstein E, Caudy AA, Hammond SM, Hannon GJ (2001) Role for a bidentate ribonuclease in the initiation step of RNA interference. Nature 409: 363-366.
62. Elbashir SM, Lendeckel W, Tuschl T (2001) RNA interference is mediated by 21- and 22-nucleotide RNAs. Genes Dev 15: 188-200.
63. Hammond SM, Bernstein E, Beach D, Hannon GJ (2000) An RNA-directed nuclease mediates post-transcriptional gene silencing in Drosophila cells. Nature 404: 293-296.
64. Kasschau KD, Carrington JC (1998) A counterdefensive strategy of plant viruses: suppression of posttranscriptional gene silencing. Cell 95: 461-470.
65. Jensen S, Gassama MP, Heidmann T (1999) Taming of transposable elements by homology-dependent gene silencing. Nat Genet 21: 209-212.
66. Ratcliff FG, MacFarlane SA, Baulcombe DC (1999) Gene silencing without DNA. rna-mediated cross-protection between viruses. Plant Cell 11: 1207-1216.
67. Tabara H, Sarkissian M, Kelly WG, Fleenor J, Grishok A, et al. (1999) The rde-1 gene, RNA interference, and transposon silencing in C. elegans. Cell 99: 123-132.
68. Elbashir SM, Harborth J, Lendeckel W, Yalcin A, Weber K, et al. (2001) Duplexes of 21-nucleotide RNAs mediate RNA interference in cultured mammalian cells. Nature 411: 494-498.
69. Brummelkamp TR, Bernards R, Agami R (2002) A system for stable expression of short interfering RNAs in mammalian cells. Science 296: 550-553.
70. Paddison PJ, Caudy AA, Bernstein E, Hannon GJ, Conklin DS (2002) Short hairpin RNAs (shRNAs) induce sequence-specific silencing in mammalian cells. Genes Dev 16: 948-958.
71. Paul CP, Good PD, Winer I, Engelke DR (2002) Effective expression of small interfering RNA in human cells. Nat Biotechnol 20: 505-508.
72. Rubinson DA, Dillon CP, Kwiatkowski AV, Sievers C, Yang L, et al. (2003) A lentivirus-based system to functionally silence genes in primary mammalian cells, stem cells and transgenic mice by RNA interference. Nat Genet 33: 401-406.
73. Dickins RA, Hemann MT, Zilfou JT, Simpson DR, Ibarra I, et al. (2005) Probing tumor phenotypes using stable and regulated synthetic microRNA precursors. Nat Genet 37: 1289-1295.
74. Jackson AL, Bartz SR, Schelter J, Kobayashi SV, Burchard J, et al. (2003) Expression profiling reveals off-target gene regulation by RNAi. Nat Biotechnol 21: 635-637.
75. Zhang Y, Buchholz F, Muyrers JP, Stewart AF (1998) A new logic for DNA engineering using recombination in Escherichia coli. Nat Genet 20: 123-128.
76. Zhang Y, Muyrers JP, Testa G, Stewart AF (2000) DNA cloning by homologous recombination in Escherichia coli. Nat Biotechnol 18: 1314-1317.

77. Muyrers JPP, Zhang Y, Testa G, Stewart AF (1999) Rapid modification of bacterial artificial chromosomes by ET-recombination. Nucleic Acids Research 27: 1555-1557.
78. Ying QL, Stavridis M, Griffiths D, Li M, Smith A (2003) Conversion of embryonic stem cells into neuroectodermal precursors in adherent monoculture. Nat Biotechnol 21: 183-186.
79. Ying QL, Wray J, Nichols J, Batlle-Morera L, Doble B, et al. (2008) The ground state of embryonic stem cell self-renewal. Nature 453: 519-523.
80. Burdon T, Chambers I, Stracey C, Niwa H, Smith A (1999) Signaling mechanisms regulating self-renewal and differentiation of pluripotent embryonic stem cells. Cells Tissues Organs 165: 131-143.
81. Buehr M, Smith A (2003) Genesis of embryonic stem cells. Philos Trans R Soc Lond B Biol Sci 358: 1397-1402; discussion 1402.
82. Ying QL, Smith AG (2003) Defined conditions for neural commitment and differentiation. Methods Enzymol 365: 327-341.
83. Conti L, Pollard SM, Gorba T, Reitano E, Toselli M, et al. (2005) Niche-independent symmetrical self-renewal of a mammalian tissue stem cell. PLoS Biol 3: e283.
84. Pfeifer A, Ikawa M, Dayn Y, Verma IM (2002) Transgenesis by lentiviral vectors: lack of gene silencing in mammalian embryonic stem cells and preimplantation embryos. Proc Natl Acad Sci U S A 99: 2140-2145.
85. Ventura A, Meissner A, Dillon CP, McManus M, Sharp PA, et al. (2004) Cre-lox-regulated conditional RNA interference from transgenes. Proc Natl Acad Sci U S A 101: 10380-10385.
86. Dull T, Zufferey R, Kelly M, Mandel RJ, Nguyen M, et al. (1998) A third-generation lentivirus vector with a conditional packaging system. J Virol 72: 8463-8471.
87. Peitz M, Pfannkuche K, Rajewsky K, Edenhofer F (2002) Ability of the hydrophobic FGF and basic TAT peptides to promote cellular uptake of recombinant Cre recombinase: A tool for efficient genetic engineering of mammalian genomes. Proc Natl Acad Sci U S A 99: 4489-4494.
88. Zhang Y, Buchholz F, Muyrers JPP, Stewart AF (1998) A new logic for DNA engineering using recombination in Escherichia coli. Nat Genet 20: 123-128.
89. Abranches E, Silva M, Pradier L, Schulz H, Hummel O, et al. (2009) Neural differentiation of embryonic stem cells in vitro: a road map to neurogenesis in the embryo. PLoS One 4: e6286.
90. Glaser T, Pollard SM, Smith A, Brustle O (2007) Tripotential differentiation of adherently expandable neural stem (NS) cells. PLoS One 2: e298.
91. Hayashi K, Lopes SM, Tang F, Surani MA (2008) Dynamic equilibrium and heterogeneity of mouse pluripotent stem cells with distinct functional and epigenetic states. Cell Stem Cell 3: 391-401.
92. Toyooka Y, Shimosato D, Murakami K, Takahashi K, Niwa H (2008) Identification and characterization of subpopulations in undifferentiated ES cell culture. Development 135: 909-918.
93. Niwa H, Miyazaki J, Smith AG (2000) Quantitative expression of Oct-3/4 defines differentiation, dedifferentiation or self-renewal of ES cells. Nat Genet 24: 372-376.
94. Götz M, Stoykova A, Gruss P (1998) Pax6 controls radial glia differentiation in the cerebral cortex. Neuron 21: 1031-1044.
95. Lendahl U, Zimmerman LB, McKay RD (1990) CNS stem cells express a new class of intermediate filament protein. Cell 60: 585-595.

96. Pevny LH, Sockanathan S, Placzek M, Lovell-Badge R (1998) A role for SOX1 in neural determination. Development 125: 1967-1978.
97. Skarnes WC, Moss JE, Hurtley SM, Beddington RS (1995) Capturing genes encoding membrane and secreted proteins important for mouse development. Proc Natl Acad Sci U S A 92: 6592-6596.
98. Leighton PA, Mitchell KJ, Goodrich LV, Lu X, Pinson K, et al. (2001) Defining brain wiring patterns and mechanisms through gene trapping in mice. Nature 410: 174-179.
99. Mitchell KJ, Pinson KI, Kelly OG, Brennan J, Zupicich J, et al. (2001) Functional analysis of secreted and transmembrane proteins critical to mouse development. Nat Genet 28: 241-249.
100. Wang N, Finegold M, Bradley A, Ou C, Abdelsayed S, et al. (1995) Impaired energy homeostasis in C/EBP alpha knockout mice. Science 269: 1108-1112.
101. She P, Shiota M, Shelton KD, Chalkley R, Postic C, et al. (2000) Phosphoenolpyruvate carboxykinase is necessary for the integration of hepatic energy metabolism. Mol Cell Biol 20: 6508-6517.
102. Pasquale ED, Monteau R, Hilaire G (1992) In vitro study of central respiratory-like activity of the fetal rat. Experimental Brain Research 89: 459-464.
103. Greer JJ, Smith JC, Feldman JL (1992) Respiratory and locomotor patterns generated in the fetal rat brain stem-spinal cord in vitro. J Neurophysiol 67: 996-999.
104. Greer JJ, Funk GD, Ballanyi K (2006) Preparing for the first breath: prenatal maturation of respiratory neural control. The Journal of Physiology 570: 437-444.
105. Cosmi EV, Anceschi MM, Cosmi E, Piazze JJ, La Torre R (2003) Ultrasonographic patterns of fetal breathing movements in normal pregnancy. International Journal of Gynecology & Obstetrics 80: 285-290.
106. Blanco CE (1994) Maturation of fetal breathing activity. Biol Neonate 65: 182-188.
107. Smith JC, Ellenberger HH, Ballanyi K, Richter DW, Feldman JL (1991) Pre-Botzinger complex: a brainstem region that may generate respiratory rhythm in mammals. Science 254: 726-729.
108. Smith JC, Morrison DE, Ellenberger HH, Otto MR, Feldman JL (1989) Brainstem projections to the major respiratory neuron populations in the medulla of the cat. J Comp Neurol 281: 69-96.
109. Pearce RA, Stornetta RL, Guyenet PG (1989) Retrotrapezoid nucleus in the rat. Neuroscience Letters 101: 138-142.
110. Onimaru H, Homma I (2003) A Novel Functional Neuron Group for Respiratory Rhythm Generation in the Ventral Medulla. J Neurosci 23: 1478-1486.
111. Mulkey DK, Stornetta RL, Weston MC, Simmons JR, Parker A, et al. (2004) Respiratory control by ventral surface chemoreceptor neurons in rats. Nat Neurosci 7: 1360-1369.
112. Nattie EE, Li A (2002) Substance P–saporin lesion of neurons with NK1 receptors in one chemoreceptor site in rats decreases ventilation and chemosensitivity. The Journal of Physiology 544: 603-616.
113. Thoby-Brisson M, Karlen M, Wu N, Charnay P, Champagnat J, et al. (2009) Genetic identification of an embryonic parafacial oscillator coupling to the preBotzinger complex. Nat Neurosci 12: 1028-1035.
114. Stornetta RL, Rosin DL, Wang H, Sevigny CP, Weston MC, et al. (2003) A group of glutamatergic interneurons expressing high levels of both neurokinin-1 receptors and somatostatin identifies the region of the pre-Botzinger complex. J Comp Neurol 455: 499-512.
115. Wallen-Mackenzie A, Gezelius H, Thoby-Brisson M, Nygard A, Enjin A, et al. (2006) Vesicular glutamate transporter 2 is required for central respiratory rhythm

generation but not for locomotor central pattern generation. J Neurosci 26: 12294-12307.
116. Gray PA, Rekling JC, Bocchiaro CM, Feldman JL (1999) Modulation of Respiratory Frequency by Peptidergic Input to Rhythmogenic Neurons in the PreBötzinger Complex. Science 286: 1566-1568.
117. Gray PA, Janczewski WA, Mellen N, McCrimmon DR, Feldman JL (2001) Normal breathing requires preBotzinger complex neurokinin-1 receptor-expressing neurons. Nat Neurosci 4: 927-930.
118. Johnson SM, Smith JC, Funk GD, Feldman JL (1994) Pacemaker behavior of respiratory neurons in medullary slices from neonatal rat. J Neurophysiol 72: 2598-2608.
119. Koshiya N, Smith JC (1999) Neuronal pacemaker for breathing visualized in vitro. Nature 400: 360-363.
120. Thoby-Brisson M, Ramirez J-M (2001) Identification of Two Types of Inspiratory Pacemaker Neurons in the Isolated Respiratory Neural Network of Mice. J Neurophysiol 86: 104-112.
121. Feldman JL, Del Negro CA (2006) Looking for inspiration: new perspectives on respiratory rhythm. Nat Rev Neurosci 7: 232-242.
122. Thoby-Brisson M, Trinh JB, Champagnat J, Fortin G (2005) Emergence of the pre-Botzinger respiratory rhythm generator in the mouse embryo. J Neurosci 25: 4307-4318.
123. Dean JB, Lawing WL, Millhorn DE (1989) CO_2 decreases membrane conductance and depolarizes neurons in the nucleus tractus solitarii. Experimental Brain Research 76: 656-661.
124. Al-Zubaidy Z, Erickson R, Greer J (1996) Serotonergic and noradrenergic effects on respiratory neural discharge in the medullary slice preparation of neonatal rats. Pflügers Archiv European Journal of Physiology 431: 942-949.
125. Errchidi S, Monteau R, Hilaire G (1991) Noradrenergic modulation of the medullary respiratory rhythm generator in the newborn rat: an in vitro study. The Journal of Physiology 443: 477-498.
126. Schwarzacher SW, Pestean A, Günther S, Ballanyi K (2002) Serotonergic modulation of respiratory motoneurons and interneurons in brainstem slices of perinatal rats. Neuroscience 115: 1247-1259.
127. Spyer KM (2009) To breathe or not to breathe? That is the question. Exp Physiol 94: 1-10.
128. Hilaire G, Bou C, Monteau R (1997) Rostral ventrolateral medulla and respiratory rhythmogenesis in mice. Neuroscience Letters 224: 13-16.
129. Hilaire G, Duron B (1999) Maturation of the Mammalian Respiratory System. Physiol Rev 79: 325-360.
130. Dubreuil V, Ramanantsoa N, Trochet D, Vaubourg V, Amiel J, et al. (2008) A human mutation in Phox2b causes lack of CO2 chemosensitivity, fatal central apnea, and specific loss of parafacial neurons. Proc Natl Acad Sci U S A 105: 1067-1072.
131. Buchholz F, Angrand PO, Stewart AF (1996) A simple assay to determine the functionality of Cre or FLP recombination targets in genomic manipulation constructs. Nucleic Acids Res 24: 3118-3119.
132. Lewandoski M, Martin GR (1997) Cre-mediated chromosome loss in mice. Nat Genet 17: 223-225.
133. Liu X, Wu H, Loring J, Hormuzdi S, Disteche CM, et al. (1997) Trisomy eight in ES cells is a common potential problem in gene targeting and interferes with germ line transmission. Dev Dyn 209: 85-91.

134. Longo L, Bygrave A, Grosveld FG, Pandolfi PP (1997) The chromosome make-up of mouse embryonic stem cells is predictive of somatic and germ cell chimaerism. Transgenic Res 6: 321-328.
135. van der Lugt NM, Domen J, Linders K, van Roon M, Robanus-Maandag E, et al. (1994) Posterior transformation, neurological abnormalities, and severe hematopoietic defects in mice with a targeted deletion of the bmi-1 proto-oncogene. Genes & Development 8: 757-769.
136. Ringrose L, Ehret H, Paro R (2004) Distinct Contributions of Histone H3 Lysine 9 and 27 Methylation to Locus-Specific Stability of Polycomb Complexes. Molecular Cell 16: 641-653.
137. Papp B, Muller J (2006) Histone trimethylation and the maintenance of transcriptional ON and OFF states by trxG and PcG proteins. Genes Dev 20: 2041-2054.
138. Pasini D, Bracken AP, Hansen JB, Capillo M, Helin K (2007) The Polycomb Group Protein Suz12 Is Required for Embryonic Stem Cell Differentiation. Mol Cell Biol 27: 3769-3779.
139. Wang Z, Zang C, Rosenfeld JA, Schones DE, Barski A, et al. (2008) Combinatorial patterns of histone acetylations and methylations in the human genome. Nat Genet 40: 897-903.
140. Agger K, Cloos PA, Christensen J, Pasini D, Rose S, et al. (2007) UTX and JMJD3 are histone H3K27 demethylases involved in HOX gene regulation and development. Nature 449: 731-734.
141. Pasini D, Hansen KH, Christensen J, Agger K, Cloos PA, et al. (2008) Coordinated regulation of transcriptional repression by the RBP2 H3K4 demethylase and Polycomb-Repressive Complex 2. Genes Dev 22: 1345-1355.
142. De Santa F, Narang V, Yap ZH, Tusi BK, Burgold T, et al. (2009) Jmjd3 contributes to the control of gene expression in LPS-activated macrophages. EMBO J 28: 3341-3352.
143. Huang J, Berger SL (2008) The emerging field of dynamic lysine methylation of non-histone proteins. Current Opinion in Genetics & Development 18: 152-158.
144. Ponnaluri VKC, Vavilala DT, Putty S, Gutheil WG, Mukherji M (2009) Identification of non-histone substrates for JMJD2A-C histone demethylases. Biochemical and Biophysical Research Communications 390: 280-284.
145. Webby CJ, Wolf A, Gromak N, Dreger M, Kramer H, et al. (2009) Jmjd6 Catalyses Lysyl-Hydroxylation of U2AF65, a Protein Associated with RNA Splicing. Science 325: 90-93.
146. Huang J, Sengupta R, Espejo AB, Lee MG, Dorsey JA, et al. (2007) p53 is regulated by the lysine demethylase LSD1. Nature 449: 105-108.
147. Wang J, Hevi S, Kurash JK, Lei H, Gay F, et al. (2009) The lysine demethylase LSD1 (KDM1) is required for maintenance of global DNA methylation. Nat Genet 41: 125-129.
148. Jepsen K, Solum D, Zhou T, McEvilly RJ, Kim HJ, et al. (2007) SMRT-mediated repression of an H3K27 demethylase in progression from neural stem cell to neuron. Nature 450: 415-419.
149. De Santa F, Totaro MG, Prosperini E, Notarbartolo S, Testa G, et al. (2007) The histone H3 lysine-27 demethylase Jmjd3 links inflammation to inhibition of polycomb-mediated gene silencing. Cell 130: 1083-1094.
150. Sen GL, Webster DE, Barragan DI, Chang HY, Khavari PA (2008) Control of differentiation in a self-renewing mammalian tissue by the histone demethylase JMJD3. Genes Dev 22: 1865-1870.
151. Agger K, Cloos PA, Rudkjaer L, Williams K, Andersen G, et al. (2009) The H3K27me3 demethylase JMJD3 contributes to the activation of the INK4A-ARF

locus in response to oncogene- and stress-induced senescence. Genes Dev 23: 1171-1176.
152. Barradas M, Anderton E, Acosta JC, Li S, Banito A, et al. (2009) Histone demethylase JMJD3 contributes to epigenetic control of INK4a/ARF by oncogenic RAS. Genes Dev 23: 1177-1182.
153. Gao Y, Hyttel P, Hall VJ (2010) Regulation of H3K27me3 and H3K4me3 during early porcine embryonic development. Molecular Reproduction and Development 77: 540-549.
154. Wang J, Mager J, Chen Y, Schneider E, Cross JC, et al. (2001) Imprinted X inactivation maintained by a mouse Polycomb group gene. Nat Genet 28: 371-375.
155. O'Carroll D, Erhardt S, Pagani M, Barton SC, Surani MA, et al. (2001) The polycomb-group gene Ezh2 is required for early mouse development. Mol Cell Biol 21: 4330-4336.
156. Fei T, Xia K, Li Z, Zhou B, Zhu S, et al. (2009) Genome-wide mapping of SMAD target genes reveals the role of BMP signaling in embryonic stem cell fate determination. Genome Res.
157. Felipe CD, Herrero JF, O'Brien JA, Palmer JA, Doyle CA, et al. (1998) Altered nociception, analgesia and aggression in mice lacking the receptor for substance P. Nature 392: 394-397.
158. Guyenet PG, Sevigny CP, Weston MC, Stornetta RL (2002) Neurokinin-1 Receptor-Expressing Cells of the Ventral Respiratory Group Are Functionally Heterogeneous and Predominantly Glutamatergic. J Neurosci 22: 3806-3816.
159. Blanchi B, Kelly LM, Viemari JC, Lafon I, Burnet H, et al. (2003) MafB deficiency causes defective respiratory rhythmogenesis and fatal central apnea at birth. Nat Neurosci 6: 1091-1100.
160. Bouvier J, Thoby-Brisson M, Renier N, Dubreuil V, Ericson J, et al. (2010) Hindbrain interneurons and axon guidance signaling critical for breathing. Nat Neurosci advance online publication.
161. Dauger S, Pattyn A, Lofaso F, Gaultier C, Goridis C, et al. (2003) Phox2b controls the development of peripheral chemoreceptors and afferent visceral pathways. Development 130: 6635-6642.
162. Caubit X, Thoby-Brisson M, Voituron N, Filippi P, Bevengut M, et al. (2010) Teashirt 3 regulates development of neurons involved in both respiratory rhythm and airflow control. J Neurosci 30: 9465-9476.
163. Onimaru H, Homma I (2002) Development of the rat respiratory neuron network during the late fetal period. Neuroscience Research 42: 209-218.
164. Hirabayashi Y, Suzki N, Tsuboi M, Endo TA, Toyoda T, et al. (2009) Polycomb limits the neurogenic competence of neural precursor cells to promote astrogenic fate transition. Neuron 63: 600-613.
165. Pereira JD, Sansom SN, Smith J, Dobenecker M-W, Tarakhovsky A, et al. (2010) Ezh2, the histone methyltransferase of PRC2, regulates the balance between self-renewal and differentiation in the cerebral cortex. Proceedings of the National Academy of Sciences 107: 15957-15962.

Acknowledgements

First and foremost, I would like to thank Giuseppe Testa for giving me the opportunity to work with him, for setting the highest standards to strive towards, and for expertly guiding me in my continuing development as an inquiring student over the last five years. His support, stimulating suggestions and encouragement always helped me throughout my PhD.

Furthermore, I would like to thank the members of our group, in particular Aga, Sere and Ele. It was a pleasure for me to work with you and we were a great team in our daily fight with the mysteries and challenges of science. I wish you all the best for your future and I hope we will meet again, no matter where our paths will lead us.

A special thanks goes to Fabio for disclosing and teaching me all the strategies and small tricks that made the survival in the lab easier and for being a friend.

I am extremely grateful to the respiration-team Gérard Hilaire, Nicolas and Clément for their indispensable contribution to this project and insightful discussions.

A big thanks to Sigi for her constant support and keeping my Müsli stock filled.

Life outside the lab has been a great pleasure together with Teo my mountain guide of alpine paths, and Lucy, Rachel and Rodri with which I enjoyed hunting bohnenfressende Werwölfe over delicious dinners. I am truly grateful for your friendship and all the memorable moments.

Ich danke von ganzem Herzen meiner Familie und besonders Margherita, sowie all meinen Freunden für ihre Unterstützung und unerschütterlichen Glauben an mich.

Thomas